KAUNAS UNIVERSITY OF TECHNOLOGY

MECHANICAL ENGINEERING & DESIGN FACULTY

SHARATH PEETHAMBARAN SUBADRA

STUDY OF ACOUSTIC EMISSION SIGNALS DURING CRACK PROPAGATION IN NANO CARBON FIBRE COMPOSITES

Master's Degree Final Project

Supervisor

Assoc. prof. Dr. Paulius Griškevičius

Assisstant supervior

doc. dr. Tomaž Kek (University of Ljubljana)

KAUNAS, 2016

KAUNAS UNIVERSITY OF TECHNOLOGY
MECHANICAL ENGINEERING AND DESIGN FACULTY

I APPROVE

Head of Department

Assoc.Prof.Dr. Vytautas Grigas

(Signature)

(Date)

STUDY OF ACOUSTIC EMISSION SIGNALS DURING CRACK PROPAGATION IN NANO CARBON FIBRE COMPOSITES

Final Project for Master degree

Master's in Mechanical Engineering (621H30001)

Supervisor

Assoc. Prof. Dr. Paulius Griškevičius

(Signature)

(Date)

Project made by

Sharath Peethambaran Subadra

(Signature)

(Date)

Reviewer

Assoc.Prof.Dr. Rūta Rimašauskienė

(Signature)

(Date)

Kaunas 2016

KAUNAS UNIVERSITY OF TECHNOLOGY

Mechanical Engineering & Design Faculty

SHARATH PEETHAMBARN SUBADRA

Mechanical Engineering (621H30001)

STUDY OF ACOUSTIC EMISSION SIGNALS DURING CRACK PROPAGATION IN NANO CARBON FIBRE COMPOSITES

DECLARATION OF ACADEMIC INTEGRITY

June 2016

Kaunas

I confirm that the final project of mine, **SHARATH PEETHAMBARN SUBADRA**, on the subject "Acoustic emission signals during crack propagation in carbon nanotubes/carbon fibre reinforced composites" is written completely by myself; all the provided data and research results are correct and have been obtained honestly. None of the parts of this thesis have been plagiarized from any printed, Internet-based or otherwise recorded sources. All direct and indirect quotations from external resources are indicated in the list of references. No monetary funds (unless required by law) have been paid to anyone for any contribution to this thesis.

I fully and completely understand that any discovery of any manifestations/case/facts of dishonesty inevitably results in me incurring a penalty according to the procedure(s) effective at Kaunas University of Technology.

(name and surname filled in by hand) *(signature)*

KAUNAS UN IVERSITY OF TECHNOLOGY
FACULTY OF MECHANICAL ENGINEERING AND DESIGN

Approved:
Head of Mechanical Engineering Department

(Signature, date)

Vytautas Grigas

(Name, Surname)

Head of Study Programmes in the Field of Mechanical Engineering

(Signature, date)

Kęstutis Pilkauskas

(Name, Surname)

BACHELOR STUDIES FINAL PROJECT TASK ASSIGNMENT
Study programme MECHANICAL ENGINERING - 612H30001

Approved by the Dean's Order No.V25-11-6 of May 3rd , 2016 y

Assigned to the student: SHARATH PEETHAMBARAN SUBADRA

(Name, surname)

1. Title of the Project

STUDY OF ACOUSTIC EMISSION SIGNALS DURING CRACK PROPAGATION IN MULTISCALE

2. Aim of the project

To understand the influence of carbon nanotubes on the mechanical properties of carbon fiber reinforced composites and to register acoustic emission signals during mode-I crack propagation in the material and to classify the signals according to the fracture mechanism using modal acoustic emission analysis.

3. Tasks of the project

Selection of appropriate standard for making specimens and conducting experiments, material selection, selection of method to make specimen, design of experiments, determination of inter-laminar fracture toughness energy, generation of necessary plots, determining the positive/negative influence of CNT, obtaining SEM images, generating wavelet transforms using appropriate solver, carrying out modal acoustic emission analysis to determine the fracture mechanism.

4. Specific Requirements

-Determination of inter-laminar fracture toughness of the composite material during crack propagation.

-Classification of acoustic signals based on the fracture mechanism in the composite material.

5. This task assignment is an integral part of the final project

6. Project submission deadline: 2016 May 20th .

Task Assignment received SHARATH PEETHAMBARAN SUBADRA _____
(*Name, Surname of the Student*) (*Signature,date*)

Supervisor Assoc. Prof. Dr. PAULIUS GRIŠKEVIČIUS _____
(*Position, Name, Surname*) (*Signature,date*)

Sharath Peethambaran Subadra. Akustinės emisijos signalų tyrimas plyšiui plintant nano anglies pluošto kompozituose. Magistro baigiamasis projektas / vadovas doc. dr. Paulius Griškevičius; Kauno technologijos universitetas, Mechanikos inžinerijos ir dizaino fakultetas.

Mokslo kryptis ir sritis:

Reikšminiai žodžiai: anglies pluoštas, anglies nano vamzdeliai, akustinė emisija, modalinė analizė, tarpsluoksninio irimo tąsumas.

Kaunas, 2016. 1-101 psl.

SANTRAUKA

Anglies pluoštu armuoti kompozitai dėl didelio standumo ir stiprumo yra plačiai naudojami pramonėje. Tačiau kaip ir kitų medžiagų, jų atsparumas irimui nėra idealus. Kompozitinės medžiagos turi specifinius irimo mechanizmus: pluošto irimas, matricos irimas, pluošto-matricos atplyšimas, atsisluoksniavimas esant sluoksniuotiems kompozitams. Kartais atsisluoksniavimas gali būti kaip pasekmė kitų irimo mechanizmų, t.y. pluošto ar matricos irimo arba pluošto nuo matricos atplyšimo, todėl atsisluoksniavimas laikomas vienu iš svarbiausių defektų kompozitų konstrukcijose. Faktoriai įtakojantys atsisluoksniavimą yra silpna pluošto-dervos sąsaja arba trapi derva. Tyrimai parodė, kad atsisluoksniavimo problema gali būti sumažinta pakeičiant vidinę kompozitų medžiagos struktūrą, pvz. panaudojant anglies nano vamzdelius sukuriama kliūtis plyšio vystymuisi.

Atliekant šį darbą buvo pagaminti šeši gembiniai kompozitiniai irimo bandiniai (ASTM 5528). Pirmi trys t.y. 1.n (n=1, 2, 3) buvo be nano vamzdelių, o likę trys $2.n\ (n = 1,2,3)$ *su nano vamzdeliais epoksidinėje terpėje. Nano vamzdeliai buvo dagiasienio tipo be funkcionalumo savybių. Fiksuotas 0.3% nano vamzdelių kiekis buvo išsklaidytas dervoje maišant mažoje vakuuminėje kameroje. Atsisluoksniavimo procesas buvo inicijuotas naudojant dvigubą gembę su pradiniu plyšiu (moda I), bandiniai buvo sujungti su akustinės emisijos signalų registravimo sistema. Po eksperimento 1.3 ir 2.3 bandiniai buvo analizuojami su SEM (Skenuojančiu elektroniniu mikroskopu). Buvo tiriama nano vamzdelių įtaka tarpsluoksniniam irimo tąsumui. Naudojant AGU-Vallen programinę įrangą buvo atliekama akustinės emisijos signalų analizė bangų transformacijų principu. Dvi pagrindinės modos A0 (asimetrinė arba lenkimo moda) ir S0 (simetrinė arba tempimo moda) buvo tiriamos ir sugretinamos su tipiniais irimo mechanizmais kompozituose. Klasė A signalai reiškiantys matricos irimą, klasė B – pluošto irimas ir klasė C – priskiriama pluošto/matricos atplyšimui. Be to buvo atliktos dvi papildomos klasifikacijos su nežymiai besiskiriančiomis signalų formomis, tai klasė AA – matricos irimas ir klasė BB pluošto irimas.*

Rezultatai parodė, kad naudojant anglies nano vamzdelius gaunamas ženklus tarpsluoksninio irimo tąsumo G_{Ic} *padidėjimas, tačiau kritinė jėga liko nežymiai mažesnė. Defektų klasifikavimui akustinės emisijos modalinė signalų analizė labiau tinkama, nei dažninė analizė naudojant Furje transformacijas.*

Sharath Peethambaran Subadra. ACOUTIC EMISSION SIGNALS DURING CRACK PROPAGATION IN CARBON NANOTUBES/CARBON FIBRE REINFORCED COMPOSITES. *Master's* Final Project / supervisor assoc. prof. Dr. Paulius Griškevičius; Faculty of Mechanical Engineering & Design, Kaunas University of Technology.

Research field and area: Carbon fibre reinforced composites, nano-materials, acoustics

Keywords: *Carbon fibre, carbon nanotubes, acoustic emission signals, modal analysis, inter-laminar fracture toughness.*

Kaunas, 2016. 1-101 p.

SUMMARY

Carbon fibre reinforced composites are widely used in industries for their high in-plane specific stiffness and specific strength. But these materials like other materials are prone to damages. These damage mechanisms are unique in the case of these materials and they are fibre breakage, matrix cracking, fibre-matrix de-bonding and delamination in case of laminated composites. De-lamination could be considered as a contribution from other damage mechanisms like matrix cracking, fibre fracture and de-bonding, hence de-lamination is a serious issue in composites. Factors leading to de-lamination are weak fibre/matrix interface and brittle nature of the resins. Researches have revealed that the de-lamination problem could be reduced to some extend by altering the internal structure of a composite material. Introduction of carbon nanotubes is one widely used approach. It has been shown that CNTs bridge crack front thereby resisting crack formation.

In this work, we made six double cantilever beam specimens (ASTM 5528). The first three i.e. $1.n\ (n = 1,2,3)$ *were without nanotubes, while the other three,* $2.n\ (n = 1,2,3)$ *were with nanotubes in the epoxy system, the carbon nanotubes were of multi-wall type with no functionalisation. A fixed amount of 0.3% carbon nanotubes were dispersed in the matrix by stirring in a small vacuum chamber. De-lamination process was simulated using a double cantilever beam in the opening mode (mode I), coupled with acoustic emission (AE) signal registration. Post experiment specimen 1.3 and 2.3 were analysed under SEM. The influence of carbon nanotubes on the inter-laminar fracture toughness was studied. Latter modal acoustic emission analysis was carried out by generating wavelet transforms using the AGU-Vallen wavelet solver. The two main modes A0 (anti-symmetric or flexural mode) and S0 (symmetric or extensional mode) were studied and a classification was tried on the basis of fracture mechanism prevalent in composite materials. Class A signals signified matrix cracking, Class B that of fibre fracture and Class C was synonymous with fibre/matrix de-bonding. Additionally two more classifications were carried out, with signals with slightly different waveform pattern, and hence Class AA was for matrix cracking and Class BB for fibre fracture.*

The results showed a tremendous increase in inter-laminar fracture toughness G_{Ic}*, but at the expense of a reduced load bearing capacity. While classification of signals by carrying out a modal acoustic emission analysis was found to be more promising than conducting a peak frequency analysis.*

TABLE OF CONTENTS

LIST OF TABLES

1. INTRODUCTION

MOTIVATION AND BACKGROUND

COMPOSITE materials have emerged as an important material in the field of aerospace engineering, sports and the automobile engineering. One reason for this shift is their light weight. According to a research published by NASA these materials have emerged as the choice for increasing performance and reducing the weight and cost of military aircraft, general aviation aircraft, and space launch vehicles. This is evident from the efforts made by Boeing and Airbus to incorporate composites into primary load carrying structures of large commercial transports and to certify the airworthiness of these structures is evidence of the significant advancements made in the understanding and the use of these materials in the real world of aircrafts. For instance the weight fraction of the structure made with composites is 50% for Boeing 787. [1] Composites comprise more than 20% of Airbus 380's frame. An example of a car made with all carbon body is the McLaren 570S, the structural panels and body frame are made of carbon laminates.

Presently there are a number of non-destructive methods available which includes the X-ray, ultrasonic and acoustic emission inspection which are being increasingly applied in researches to analyse the failure mechanism of composite materials. All of these methods show high sensitivity, rapid response speed and high precision. But what makes the acoustic emission test method to stand out among others is that the acoustic emission can acquire the evolution information of defects dynamically. The basic principle of the acoustic emission technique is the conversion of the mechanical vibration into electrical signals and the analysis of the acoustic response in terms of the evolvement of the energy, counting and amplitude. [2]

In this work we have used multi-walled carbon nanotubes (MWCNTs) as nano-fillers in the composite matrix material. These composite materials are termed as multiscale nanocomposites i.e. composites with nanotubes, carbon fibres and matrix material. It has been reported in literature that the use of nanotubes in polymers increases the toughness of the same. One important finding reported in many researches has been the tremendous influence that this material has on crack propagation in case of fibre reinforced composite materials. It has been shown that these materials could arrest the growth of cracks in composites when they are for loaded. For instance in one research it was found that composites which uses nano-reinforcements together with micro-reinforcements (frequently

referred in literature as multi-scale, three phase or nano-engineered fibre reinforcement composites-nFRC) an increase of 8.5% in stiffness was observed in comparison with virgin composites (without nano-fillers). [3] In another finding attributed to Ashish Warrier et.al (Ashish Warrier et.al)[4] it was found that the crack initiation value of G_{Ic} -which is defined as the point of sudden decrease in load- increased by 10% when CNTs are present in the sizing and much higher of 25% when they are present in the matrix material. In the former it was due to increased interaction between the fibre surface and matrix, while in the latter it was due to localised failure mechanisms like fibre bridging. Thus we intend to use this very novel material i.e. carbon nanotubes in this work. The aim is to use a different dispersion technique in contrast to the techniques used in literature like sonication, calendaring etc. We intend to incorporate CNTs in the matrix material by stirring the mixture of epoxy system and CNTs in a small vacuum chamber, vacuum ensures no air bubbles are formed. We also study internal fracture mechanisms like matrix cracking, fibre breakage and fibre/matrix de-bonding during crack propagation indirectly with AE registration and understand the feasibility of this non-destructive technique in composite damage mechanism (crack propagation). The modal acoustic emission analysis would be used to study the signals and latter classified according to the fracture mechanisms.

OBJECTIVES

The research work carried out in this thesis was mainly inspired by the novelty of fibre reinforced composites and enhancement of its mechanical properties by introducing carbon nanotubes, the use of AE to study its failure mechanisms also forms part of this inspiration. The objective of this work is threefold, one to study the strengthening effect of the carbon nanotubes in fibre reinforced composites by using a different dispersion technique, two, to understand the feasibility of using AE in the damage mechanism and third to provide another source as a literature in the field of acoustic emission analysis of failure mechanism in multiscale composites. To fulfil this objective I try to address the following tasks in this thesis;

- Understanding the mechanism of the failure when carbon nanotubes are present in the matrix material
- Experimental determination of inter-laminar fracture toughness as per ASTM D5528-01.
- Registering AE signals during crack propagation.
- Performing wavelet transforms of the signals using AGU-Vallen wavelet solver, and performing modal acoustic emission analysis.

- Trying to classify the signals based on the fracture mechanisms, and make a comparison with peak frequency analysis. The data for the peak frequency analysis would be obtained from literature.

LAYOUT OF THE THESIS

The thesis is divided into five main topics including this. The second topic is a detailed literature review on the thesis topic. This topic is further divided into three sub-topics. The first part forms a very small section and deals with fibre reinforced composites in general. The second part deals with multiscale-composites, this part elaborates extensively on the effect of nanotubes in failure mechanism in fibre reinforced composites. The general failure mechanism in any composite is also dealt with briefly, as the failure mechanism in composites is well documented in literature. The bridging mechanism of nanotubes in composites is explained in detail. The third part is on acoustic waves and acoustic equipment. A detailed introduction on the feasibility of this method is given. Latter the Kaiser effect is elaborated and followed by characteristics of acoustic wave. Mathematical formulations for Fourier transforms and wavelet transforms are elaborated. Modal acoustic emission analysis is also explained.

The third topic deals with design of experiments. Materials used in the experiment are elaborated along with their properties. The method used in the preparation of the composite panel is mentioned. A few references are quoted in this chapter to make the reader acquainted with reason for the selection of some particular processes. The reader would come across the standard used in this thesis. The fourth topic is on results and conclusions and the fifth is on possible future works.

2. BACKGROUND

2.1 FIBRE REINFORCED COMPOSITES DEFINITION

Fibre-reinforced composite materials consists of fibres of high strength and modulus embedded in a matrix material. In this way each of the individual material (fibre and matrix) retains its physical and chemical properties, and they provide a combination of properties which wouldn't be possible if they were to be used alone. Here the fibres are the principal load-carrying entities and the matrix surrounding them keeps them in position along with acting as a load carrying member between them, protecting the fibres from the environmental damage due to elevated temperature, humidity etc. Thus it could be rightly said that fibre provides reinforcements to the matrix and hence the name **F**ibre **R**einforced **C**omposite **M**aterials (FRCM).

The fibre materials could be glass, carbon, Kevlar etc. Fibres of boron, silicon carbide, and aluminium oxide are also albeit in limited quantities. All these fibres can be incorporated in the matrix either as continuous fibres or as discontinuous fibres. The matrix material can be a polymer, a metal or a ceramic. Laminates are the most commonly used form of FRCMs in structural applications. A laminate is formed by stacking a number of thin layers of fibres embedded in matrix one after the other and then consolidating them in the desired shape. [5]

2.2 CARBON NANOTUBES

Experimental evidence of existence of carbon nanotubes came in 1990 through the works of Japanese physicist Sumio Iijima. Iijima imaged multi-walled carbon nanotubes (MWCNT) using a transmission electron microscope. Two year single walled carbon nanotubes (SWCNT) were proved to exist. MWCNTs are concentrically rolled graphene sheets with a large number of helicities and chiralities. While SWCNTs have just one rolled graphene sheet. The way the graphene sheet is rolled determines its fundamental properties. To describe the fundamental characteristics of nanotube two vectors C_h and T should be taken into account. C_h is the vector that defines the circumference on the surface of the tube connecting two equivalent carbon atoms, $C_h = n\widehat{a_1} + m\widehat{a_2}$, where $\widehat{a_1}$ and $\widehat{a_2}$ are the basis vectors of graphite and n and m vectors. n and m can also be termed as indexes and determine the chiral angle which can be expressed using the following equation;

$$\theta = tan^{-1}[\sqrt{3}\left(\frac{n}{(2m+n)}\right)] \quad (1)$$

The chiral angles classifies nanotubes into three separate classes that describes their electrical properties (Fig 1). They are described below;

- Armchair: In this case $n = m$ and $\theta = 30^0$. These nanotubes are metallic.
- Zig-zag: In this case $m = 0$ and $n > 0$, $\theta = 0^0$.
- Chiral: Here$0 < |m| < n, 0 < \theta < 30^0$. In the case of zig-zag and chiral nanotubes, these can be either semi-metals with a finite band gap or semiconductor in all cases. The band gap for the semi-metallic and semiconductor nanotubes scales approximately with the inverse of the tube diameter, thus giving a nanotube a unique electronic property.

The diameter of the nanotube is given by the following expression;

$$d_t = \sqrt{3}\left[\frac{a_{c-c}(m^2+mn+n^2)}{\pi}\right] = C_h/\pi \quad (2)$$

Where a_{c-c} is the C-C bond length (1.42 Å). [6]

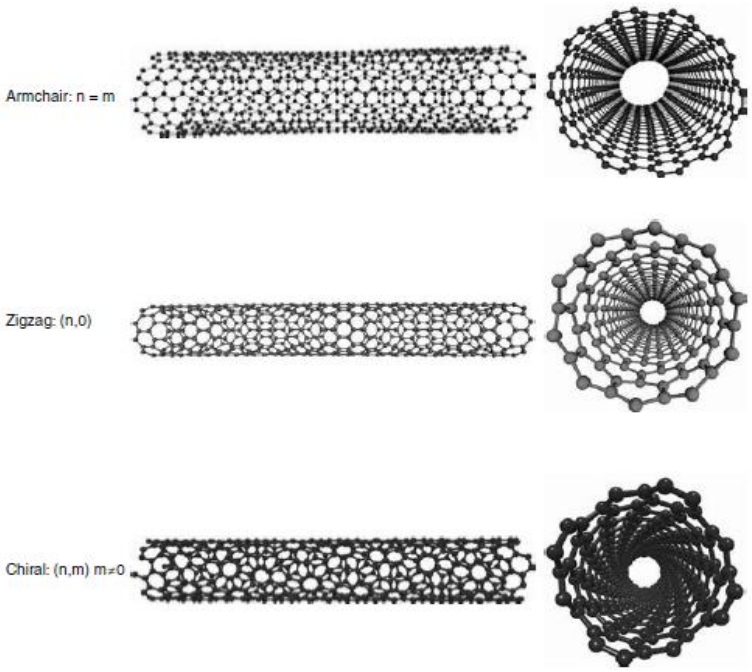

Fig 1. Three types of SWNTs identified by the integers (n,m)[6]

2.2.1 CARBON NANOTUBES MANUFACTURING PROCESS

Carbon nanotubes can be produced by many methods. One common aspect of all these methods is that they require the presence of a hot transition metal based nanoparticles and these act as seeds for growth. These particles (catalyst) are placed in contact with a gaseous carbon or hydrocarbon that deposits carbon on the catalyst surface. Depending on the diameter of the nanoparticle we can obtain either SWCNTs (single walled carbon nanotubes), or a bundle of tightly packed SWCNTs or MWCNTs (multi-walled carbon nanotubes). The spacing between the concentric tubes in MWCNTs is approximately equal to 0.34 nm. The concentric tubes are not chemically bonded, rather they are weakly coupled by van der Waals forces. This enables the tubes to slide with respect to one another without causing any structural damage. And as per literature producing MWCNTs are easier when compared to SWCNTs, this is because MWCNTs have been in R&D for longer when compared to SWCNTs. [7]

The three most important methods employed for the synthesis of nanotubes are arc discharge method, laser ablation and chemical vapour deposition (CVD). Of these the last one that is CVD

according to researches shows the promise for mass production. [8] The following section elaborates on this method.

CHEMICAL VAPOUR DEPOSITION METHOD

The source of carbon is usually methane (CH_4). This is delivered through a flow meter system. The substrates for CNTs are located within a furnace. Silicon wafer chips (SiO_2/Si) are used as substrates. Chips are made with sizes around 1-2 cm^2 by cutting and snapping wafers using a diamond cutter. These chips are placed inside a quartz tube which in turn is placed inside a furnace tightly connected and sealed to the gas flow tubes. In addition to methane the system is also infused with argon and hydrogen. Catalyst forms an important part of this process, this enables generation of CNTs on substrates. Preparation of the catalyst mixture is important and this is as follows. Iron(III) nitrate nonahydrate mixed in isopropanol is used as the catalyst . Few milligrams of the catalyst crystal is placed into a centrifuge tube and it is filled with isopropanol to its fullest capacity. The objective here is to mix the catalyst and isopropanol so that the solid particles are not visible to the naked eye. At this point the catalyst particles would have broken down into sizes matching the diameter of the nanotubes so that the nanotubes grow on these particles.

Though there are several ways in which the CVD method can be tweaked to produce long or shorter tubes, in this part of the section only the standard procedure which produces a dense growth of short CNTs covering much of the silicon wafer chip is elaborated. There are other ways to produce tailor made nanotubes (longer) which can be found in literature.

In the standard CVD procedure a concentration of 50mg/L of the catalyst is used. The catalyst can be applied on the substrate by using a syringe or by spin-coating. If syringe is to be used the catalyst is directly applied to the chip by brushing the needle against the substrate and gently squeezing out the liquid mixture. Here the liquid mixture is applied on the polished surface of the substrate and only on one side. This side would then be closest to the incoming gas. This way the nanotubes would optimistically grow in the direction of gas flow across the surface to the other side of the substrate. The nanotubes grown on silicon substrate is as shown in Fig 2. The fig shows nanoparticles deposited on the surface of nanotubes, in this case it was aerosols nanoparticles. [9]

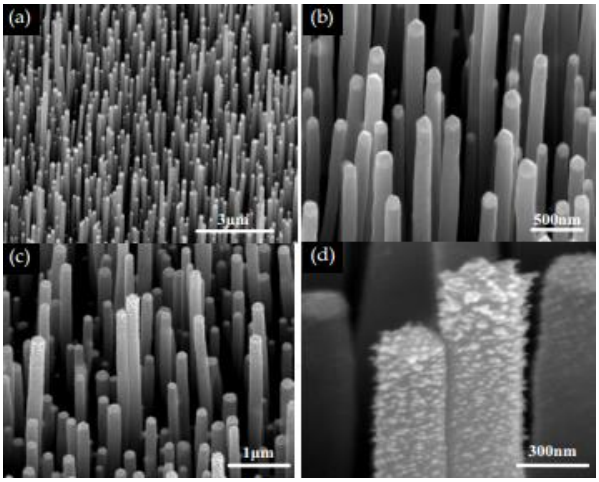

Fig 2. SEM images of as grown MWCNTs on a silicon substrate at different magnifications. (d) shows the nanoparticles deposited on the surface. [9]

Spin coating is another method of application of catalyst on the surface of the substrate. The parameters that forms part of this method includes catalyst concentration along with spin speed (rpm), the duration of spinning and the number of drops of catalyst added.

Next the chips are inserted and positioned in quartz tube. It is to be ensured that the chips are placed closer to one end of the tube since the temperature is accurate in one half of the furnace than the other. [8] This is one of the method through which carbon nanotubes can be grown. The other methods namely by arc discharge and laser ablation, it is recommended to refer the literature on these processes.

2.2.2 MECHANICAL CHARACTERISTICS OF CARBON NANOTUBES

The mechanical resistance of these materials is due to its strong bonds. Since they are flexible they can be bent repeatedly up to 90^0 without breakage or damage. The mechanical properties of CNTs which includes tensile strength, low density high aspect ratio find two different applications; first, strengthening of fibres in high-performance composite materials replacing traditionally used fibres like carbon fibres, Kevlar and glass fibres. Second, as probes in scanning tunnelling microscope (STM) and atomic force microscopy (AFM). One of the challenges of using CNTs is to achieve good adhesion between the CNTs and the matrix material. This is achieved through covalent coupling. This

is achieved by introducing functional groups to the tube walls. An optimum density of functional groups has to be found in order to have a sufficient number of connections to the matrix without weakening the stability of the tubes. [6]

Researches have shown that CNTs are 100 times stronger than steel but their density is 6 times lower. [10] They have Young's Modulus of 1TPa. [7] They have a very high thermal conductivity of 6000W/mK, which implies a small amount of this material would drastically change the properties of the material, [11, 12] as was observed in our experimental work where while using acoustic test equipment, the equipment was giving unwanted signals (electrical) of the order 6kHz, which means the specimen was electrically conducting. It has been shown that CNTs are thermally stable upto 2800^0C under vacuum conditions while maintaining electrical conductivity several times higher than that of copper. [11]

CNTs also exhibit an exceptionally good diameter dependent specific surface area of upto 1300 m^2/g. These properties make CNTs a good candidate for improving the properties of the polymer and hence the composite material. [13]

2.2.3 APPICATIONS AND ADVANTAGES OF CARON NANOTUBES

CNTs has a Young's Modulus of 1TPa. This is five times larger than steel and also five times larger than high quality carbon fibres. It has also been shown through TEM images that these materials exhibit exceptional compliance which is nothing but the ability to withstand large angle bending without breakage. These properties has made CNTs an ideal reinforcing material in composites. These incorporated CNTs also provide the benefit of electromagnetic shielding and electrostatic discharge. Due to their lower cost and availability MWCNTs (multi-walled carbon nanotubes) are used widely as MWCNT-polymer composites. MWCNTs are used widely in lithium-ion batteries. It mechanically stabilises carbon electrodes for lithium-ion batteries. CNT additives around 5-10 wt% provides an improvement in the number of charge-discharge cycles before mechanical failure occurs. The nanotubes combat the material fatigue encountered during expansion (charging) and contraction (discharging) as the lithium is moved into and out of the carbon electrode. [7]

It has been shown that through repetitious sizing treatment used to modify carbon fibre surface with carbon nanotubes for improving interfacial properties of carbon fibre/epoxy laminates, an improvement of mechanical properties was noted. For instance an increase of 13.45% in inter-laminar

shear strength and 20.31% in flexural strength was noticed. [14] In another study conducted by Niels De Greef et.al, the group identified characteristic thresholds of damage development from AE data namely ε_{min} (AE threshold strain), ε_1 (first transition strain) and ε_2 (second transition strain). The latter two represents transition from one damage to another. At ε_{min} micro-debonding was observed, at ε_1 intra-yarn cracks were observed while at ε_2 onset of de-lamination could be observed. The test was conducted on two set of specimens, one set without carbon nanotubes and the other with nanotubes. The researchers reported a delay in the onset of above mentioned damage mechanisms in the case of the specimen with CNTs. All the three thresholds were increased to higher strains by 30%, 42% and 56% respectively. Also in the same study, X-ray analysis of the damaged specimen revealed 15.6% decrease in the density of transverse cracks for CNT modified composites. [15] The presence of CNTs in the matrix material also reduced the co-efficient of thermal expansion by ~32%, this was in the case of double-walled CNTs in the epoxy system. A substantial increase in fracture toughness Mode-I by over 80% was observed in the case of MWCNTs in combination with the epoxy resin modified by using a compatibilizer. [16] Sizing of glass fibres with CNTs increased the glass transition temperature by about 10%. [4] Another study found an increase in specific surface area of carbon fibres obtained by grafting MWCNTs. These MWCNT-CF (carbon fibre) exhibited good wettability due to surface roughness and capillary action. A remarkable improvement in interfacial shear strength was observed when single-fibre composite fragmentation tests were carried out (orientation and length of MWCNTs were controlled). MWCNTs with perpendicular alignment and long length showed high interfacial shear strength in epoxy composites due to better wettability and a large contact interface between the hybrids and resin. Hybrids with an optimum length (47.2 μm) of aligned MWCNTs showed an improvement of interfacial shear strength of over 175% compared to that of pristine carbon fibres. [17] The mode-I inter-laminar fracture toughness G_{Ic}, was found to be as high as 25% when MWCNTs were in the matrix material, while it was 10% in case were it was in the sizing of the glass fibres, the composite material being glass fibre reinforced composites. The former is due to localised failure mechanisms like CNTs bridging or CNTs pull-out, while the latter is attributable to increased interaction between the fibre surface and the matrix. [4]

2.2.4 CHALLENGES INVOLVED USING CNTs IN COMPOSITES

True that using CNTs improves mechanical properties of the composites, but there are many challenges that one need to address when using these materials as fillers in matrix materials or directly as reinforcements. Some of them are elaborately discussed in this section.

The large specific surface area (SSA) of CNTs leads to several challenges which can be can be summarised as follows;

- An appropriate dispersion of reinforcements in the matrix,
- A sufficient interfacial bonding,
- Receiving representative information about nano-structural influences. These observations are further elaborated below;

Two of the important dispersion techniques (there are others also) mentioned in literature are sonication and stirring. In the case of the former a pulsed ultrasound separates the CNTs within the agglomerates and hence disperses them in matrix. This method is limited to small batches of material due to reduction in the vibrational energy with increasing distance from the sonotrode. It was further reported that this method causes rupture of the CNTs caused by local energy input, thereby reducing the effective tube length.

Next the interfacial adhesion between the matrix and the fibre is also important. This enables a sufficient stress transfer from the matrix to the tubes. This interfacial bonding between the CNTs and matrix can be improved by functionalising the surface of the CNT surface. The introduction of certain chemical groups like amino-, carboxyl- etc. enables covalent bond between CNTs and epoxy, thereby improving interfacial stress transfer and hence positively affecting the dispersibility of the nanofiller (CNTs).

The third issue concerns with a whole-in-whole knowledge about the integrity of the CNTs resulting in improved mechanical and physical properties. Based on the production techniques of nanotubes like chemical vapour deposition (CVD), electric arc-discharge method, laser ablation and likewise many, the mechanical and physical properties deviate. The parameters influencing this deviation are the defect density and distribution, the curvature, the aspect ratio, the length and diameter distribution, the density and purity.

The surface area of CNTs could act as desirable interface for stress transfer. But this induces strong attractive forces between CNTs thereby leading to excessive agglomeration. The SSA (specific

surface area) of CNTs is dependent on the diameter and the number of sidewalls, the maximum being provided by SWCNTs. To minimise the SSA the SWCNTs forms aggregates of bonded and aligned CNT bundles, called nano ropes. These ropes consists of many individual tubes ranging from ten to hundreds and are difficult to separate and infiltrate with matrix. MWCNTs provide a better dispersibility owing to its larger diameter and consisting of several concentric walls. They have SSA of around 200 m^2/g. These CNTs provide smaller interface for stress transfer. Besides stress transfer between layers has to occur via inter-layer shearing to be transferred by van der Waals forces which are relatively weak. Therefore it can be said that MWCNTs are less efficient when it comes to mechanical reinforcements. DWCNTs (Double walled carbon nano-tubes) having SSA value around 600-800m^2/g, provides a good compromise between dispersibility and reinforcement potential. [13]

The process of agglomeration of CNTs mentioned in the previous paragraphs can be attributable to the active attractive forces produced by extended π-electron systems between the graphite layers of the CNT surfaces. It is these van der Waals forces of interaction combined with the large surface area of CNTs and the typically high incompatibility with polar matrices that cumulatively lead to agglomeration. [16]

Another notable finding by A.Godara et.al (A.Godara et.al 2009)[16] was the stability of the CNT in the matrix material at high temperatures. In one method of composite material production vis the hot-melt impregnation process (room temperature to impregnation temperature)-were we have prepregs (matrix material already present) manufactured, latter cut into dimensions and stacked over one another and placed in an autoclave were it is cured under certain pressure-could imbalance the dynamism of the initial dispersion process and could induce in-homogeneity in the matrix by re-agglomeration of the CNTs. In the same study, the hot-melt CNT-resin system was solid at room temperature. It was re-heated to 80^0C in order to mix the hardener. Latter the stacked prepregs are further heated at higher temperature to follow the curing cycle. Such a large variation in temperature is detrimental for the stability of the CNTs in the matrix. And it was absorbed that under low viscosity conditions the CNTs agglomerated.

Viscosity measurements were conducted on the same nFRC (n stands for nano, mentioned above) with double, multi and thin-multi walled carbon nanotubes as the filler material. It was absorbed that with increasing temperature the viscosity decrease was similar in the case of TWCNT nFRC and DWCNT nFRC. But in the case of MWCNT nFRC, there was divergence. This divergence in viscosity was attributed to agglomeration initiated at low viscosities, thus indicating smaller interaction between MWCNTs and epoxy resin. The low viscosity facilitates the agglomeration

process caused by low affinity between MWCNTs and epoxy resin and further aggravated by the continuous flow condition imparted by the measuring geometry (parallel plates of rheometer). This leads to formation of big agglomerates. Hereafter the viscosity measurement could be more or less friction measurement between the surface of the agglomerates and the plates of the measuring geometry. This leads to a diversion in the viscosity from the normal behaviour.

2.3 FAILURE MECHANISMS

The main mode of failure in layered composites is the separation along interfaces, termed as delamination. This type of failure is induced by inter-laminar tension and shear that develops due to a variety of factors which includes; free edge effects, structural discontinuities, localised disturbances during manufacturing, moisture and temperature variations, and internal failure mechanisms like matrix cracking.

The crack face is defined by a combination of three fracture modes namely Mode-*I*, Mode-*II* and Mode-*III*. Mode-*I* represents the opening mode of the crack faces, while Mode-*II* and Mode-*III* represents the sliding mode and the tearing mode respectively (fig 3).

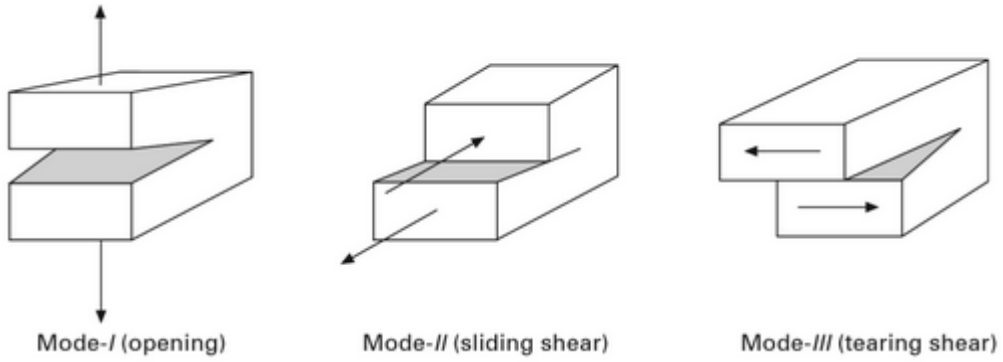

Fig 3. Three fracture modes [18]

Delamination is a crack that forms between adjacent plies. The plies on either side of the crack can have different fibre orientations. Therefore, de-lamination could be viewed as an interface crack

between two anisotropic materials. The sources of de-laminations includes material and structural dis-continuities that give rise to inter-laminar stresses. De-laminations occurs along stress-free edges due to miss-match in properties of the individual layer. This can be at ply drops where thickness must be reduced, at regions subjected to out-of-pane bending such as bending curved beams (Fig 4). All the modes of failures are prevalent when de-lamination occurs.

Although fracture mechanics principles could be utilised to characterise and predict de-lamination failures in composites laminates, but there are some short commings when using this principle. This is attributable to the fact that de-laminations are constrained to grow between composite layers. As in metals de-lamination cracks do not turn towards the opening mode immediately. The primary concern here is the necessity to characterise and analyse mixed-mode fracture involving three main modes of failure. The inter-laminar fracture toughness associated with each of the fracture modes is to be characterised and the corresponding strain energy release rates for each mode (G_I, G_{II},G_{III}) associated with the configuration and loading of interest is to be calculated to predict the de-lamination onset and growth. A generic characterisation of de-lamination growth is further complicated by damage mechanisms that occur during standardised test methods on uni-directional composite beams, like the bridging of fibres above and below the crack plane in the opening mode and micro-cracking of resin between fibres. [18]

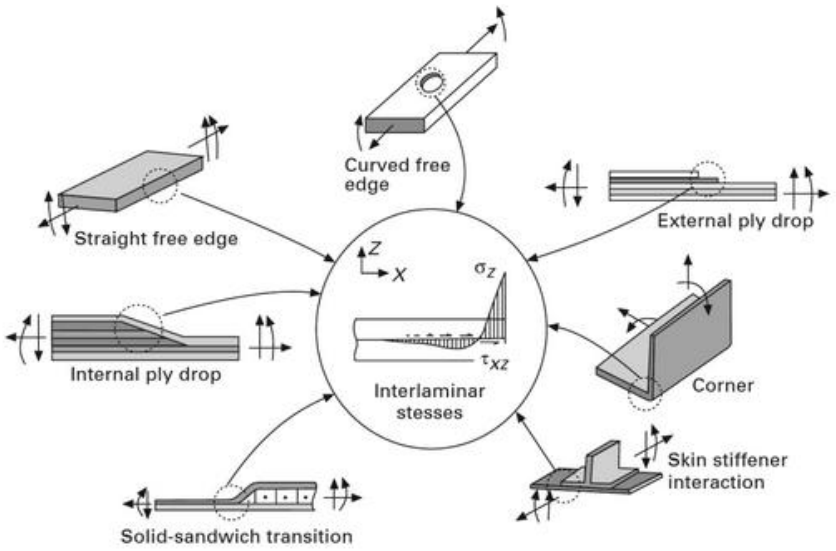

Fig 4. Sources of de-laminations at geometric and material discontinuity [18]

2.3.1 STANDARD TESTS AS PER ASTM FOR CONDUCTING EXPERIMENTS TO DETERMINE DE-LAMINATION ONSET, FRACTURE TOUGNESS AND CRACK GROWTH

American society for testing of materials (ASTM) standards has been developed for mode *I* (Double cantilever beam, DCB-ASTM 2001a, the standard intended to be used in this work), and mixed mode *I* and *II* (Mixed mode bending, MMB, ASTM-2001b) inter-laminar fracture toughness. No standards exist for pure mode-*II* and mode-*III*. But two tests has been proposed as per literature and they are "End notched flexure test for pure (ENF) mode-*II*" and the "Edge cracked torsion test (ECT) for pure mode-*III*". The inter-laminar fracture toughness is determined as a critical value of the strain energy release rate G_C, plotted as a function of mixed-mode ratio G_{II}/G. In the case of pure opening mode, G_{II}/G equals zero. Whereas in mode-*II* G_{II}/G equals unity. The toughness increases monotonically as G_{II}/G increases from zero to unity that is from pure opening mode case to pure shear mode case.

De-lamination propagation can be predicted using the following de-lamination propagation criterion. This is a power law criterion developed by Wu and Reuter;

$$\left(\frac{G_I}{G_{IIC}}\right)^m + \left(\frac{G_{II}}{G_{IIC}}\right)^n + \left(\frac{G_{III}}{G_{IIIC}}\right)^p \geq 1 \qquad (3)$$

Where *m*, *n* and *p* are empirically determined exponents for mixed-mode criterion. In the case of two-dimensional problems only the first two parts of the above equation would be evaluated. If the left hand side of the above equation equals to or exceed one then de-lamination would occur. It was found by Wu and Reuter that for two-dimensional orthotropic plates, this empirical form of the general fracture criterion is applicable when $m = 1$ and $n = 2$.

In the above expression the critical strain energy release rates for each modes of fracture are denoted by G_{IC}, G_{IIC} and G_{IIIC} respectively. G_C is the total critical strain energy release rate for a given mixed-mode condition, and G is the sum of the three strain energy release rate components. The critical values are determined through fracture toughness testing. [18]

2.3.2 STRAIN ENERGY RELEASE RATE

The strain energy release rate G, is associated with the onset and growth of delamination in composites and it is a measure of the de-lamination driving force. The G term is to be determined to measure fracture toughness G_C, to predict de-lamination. A plot of the components of G which is due to the three fracture modes, and the total $G = G_I + G_I + G_I$ are calculated as a function of the de-lamination length '*a*'. The strain energy release rates can be evaluated using the virtual crack closure technique (VCCT) in conjunction with finite element analysis.

A BRIEF ELABORATION ON VCCT: This method uses nodal displacements and nodal forces at the local elements in the vicinity of the delamination front. An example of this method for the simplest case is elaborated below.

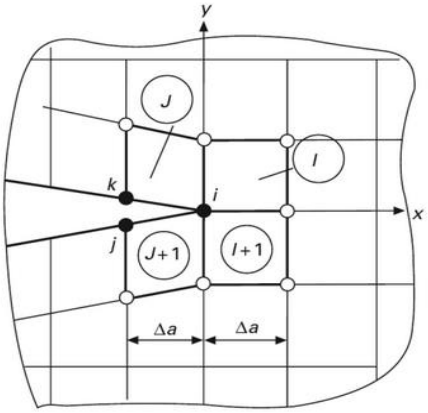

Fig 5. VCCT scheme for 4-nodal quadrilateral elements in two-dimensional analysis [18]

The figure above shows a model near a de-lamination tip in two-dimensional finite element analysis modelled with 4-noded quadrilateral elements. This technique utilises the nodal forces at the nodes at the de-lamination tip (Y_i, X_i) and the relative displacements at the nodes behind the de-lamination tip $(\Delta v_{k,j}, \Delta u_{k,j})$. The strain energy release rates are computed using the following expression;

$$G_I = \frac{1}{2\Delta a} Y_i . \Delta v_{k,j}$$

$$G_{II} = \frac{1}{2\Delta a} X_i . \Delta u_{k,j}$$

$$\Delta u_{k,j} = u_k - u_j \text{ and } \Delta v_{k,j} = v_k - v_j \quad (4)$$

Where X_i and Y_i are the nodal forces at node i in the $x-$ and $y-$ directions respectively, evaluated from elements *I and J,* and $\Delta u_{k,j}$ and $\Delta v_{k,j}$ are the relative u and v displacements between the nodes k and j, respectively. [18]

2.3.3 GENERAL OVERVIEW OF THE INFLUENCE OF CARBON NANOTUBES ON THE MECHANICAL PROPERTIES OF FIBRE REINFORCED COMPOSITES

Some of the most important use of CNTs in fibre reinforced composites is in improving properties like fracture toughness, inter-laminar shear strength and interfacial shear strength. The degree to which these properties are improved depends on a variety of factors like the way in which CNTs are integrated in the composites-like growing on fibres, mixed in the resin, added to fibre sizing, type of CNTs, surface functionalisation, toughness of base matrix etc. [15]

As explained in the previous section, de-laminations forms a constraint when composites are used especially in laminated composites. It was found that the factors contributing most to de-laminations are among others the weak fibre/matrix interface and brittle nature of the matrix resins. De-laminations in composites can be supressed by introducing through-the-thickness reinforcing elements (3D textile, stitching). But these modifications of the micro-structure of the composites do not change the intrinsic interface and matrix properties. The weak interface and low matrix toughness should be addressed to avoid the problem of de-lamination. This should be done at nanoscale, and could be done by modifying the surface of the fibres and toughening of the matrix.

It is in this context that carbon nanotubes comes could be used. Addition of CNTs in the matrix can increase the toughness of the matrix and improve the interface properties of the CNT-composites. Incorporating the CNTs in the composites can be done in two ways; either they can be dispersed in the matrix or CNTs are grown on the surface of the fibres; the delamination resistance increases due

to better interface properties of the fibre/resin system. The de-lamination resistance increases due to different mechanisms of interactions between the propagating cracks and nanotubes. [4]

Fracture characteristics of composite materials are found to be modified when nano-fillers are dispersed in the material. The nano-fillers can be for instance nanotubes, nanoclay, silica etc. For instances it was found that an improvement of fracture toughness was noticed in the case of epoxy/nanoclay composites. [19] In another paper it was found that addition of silica in the epoxy material had the effect of an increase in modulus and yield strength. Also fracture mechanics tests showed the addition of silica nanoparticles in the epoxy material up to 10 wt% brings about a considerable increase in fracture toughness and an increase in the critical crack length for the onset of crack propagation. [20]

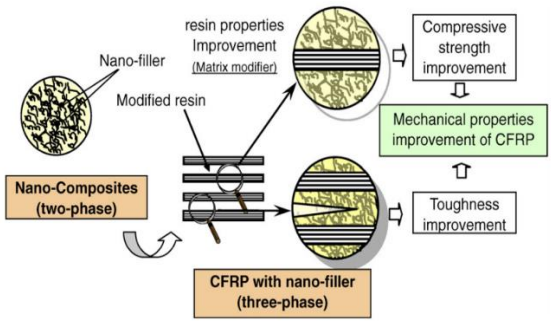

Fig 6. A typical scenario of mechanical property improvement of CFRP by incorporation of nano-fillers (nanotubes) [21]

The above mentioned literature concerns with only two-phase nano-composites i.e. carbon nanotubes-dispersed epoxy. The incorporation of nano-fillers in polymers also improves the fracture toughness, the compressive strength etc. of three-phase nano-composites (fig 6). [21] Like for instance nano-clays in the matrix material resulted in the mitigation of micro-cracking in carbon fibre reinforced plastics under cryogenic thermal cycle. [22] Likewise in another finding were organoclay was used as the nano-filler in the matrix material, the initiation and propagation values of mode I inter-laminar fracture toughness of CFRP composites increased with increasing clay concentration. It was observed in particular that with a clay content of 7 wt% the fracture toughness almost doubled. [23] Thus it can be concluded from the above findings that there is a positive change in the mechanical properties of the composites when nano-filler like nanotubes, nano-clays etc. are dispersed in the

matrix material of the fibre reinforced composite materials. But the reason of this change in the mechanical property needs to be understood. The following paragraphs elaborates on this issue.

As mentioned in the previous sections the addition of nanotubes to the resin has two effects; increasing the elastic modulus of the neat resin and toughening mechanisms such as bridging effect. The enhancement of the fracture toughness in the composites due to CNTs depends on its length. The bridging process could be either due to the CNT pull-out or CNT rupture. In either of the cases the nanotubes bridges the crack surface, thereby shielding the crack front from carrying the entire tensile load. [24]

The application of micro and nano-particles either spherical or fibrous in nature exhibit the highest effect in brittle matrix systems (e.g. thermos-setting). The most important micro-mechanical mechanisms that leads to an increased fracture toughness are listed below;

-localised in-elastic matrix deformation and void nucleation;

-particle/fibre de-bonding;

-crack deflection;

-crack pinning;

-fibre pull-out;

-crack tip blunting or crack tip deformation and;

-particle/fibre deformation or breaking at the crack tip.

The above mentioned mechanism are influenced by several parameters like volume fraction of the particles, particle size and shape, interfacial bonding etc. and are often difficult to distinguish.

The characteristics of the matrix material is also important for the reinforcing effect of the nano-fillers. The plastic zone size of the brittle epoxy resins is relatively small and when a resin is filled with nano-particles, a sufficiently large amount of them appears in the plastic zone. But in a composite containing micro-particles only a minor number of them is involved in the plastic zone deformation process. Another aspect is the growth of the process zone in front of the crack tip due to stress/strain interaction between nano-particles and matrix. This effect would be significant with nanotubes which possess very high aspect ratios.

The above described model is valid only in the context of composite containing particles in millimetre and micrometre regime. And hence their application at nano-scale would sound

overstretched. What is to be understood here is that whether a model derived from classical mechanics can explain processes that take place at nano-scale or due to nanoparticles. The answer to this question is that these models provides some assumptions which would explain the effect of nano-particles on fracture toughness. One another advantage of this model explaining the properties of micro-particle composite is that they offer the possibility to compare the influence of nano- and micro-particles, since they may give proof for the over-proportional effect of the nano-scaled reinforcements.

An important aspect of nanoparticle which concerns with their potential to toughen polymers is there high specific surface area (SSA). This parameter varies depending on the type and exact dimensions of the primary particles. Single walled carbon nanotubes exhibit a value around 1315 m^2/g. Several micro-mechanical mechanisms known to increase fracture toughness and fracture energy in a particle filled composite depends on the surface area of the reinforcing phase and the properties of the particle-matrix interface, for instance fibre particle de-bonding or fibre pull-out. [25]

RELATION BETWEEN FRACTURE ENERGY G_{Ic} AND SEPARATION OF PARTICLES S'

The theory of crack pinning developed by Lange, offers some valuable insights if applied to the nanoscale. This theory is based on the idea that, faced by an array of impenetrable obstacles, the propagating crack front is pinned and forced to bow out. By forming local semi-circular crack, the interpenetrable crack length increases until the crack front breaks away at a critical state. By using the concept of "line energy", Lange claimed more energy will be dissipated by increasing the crack length. The crack pinning also termed as crack trapping or crack front bowing is as shown in Fig 7.

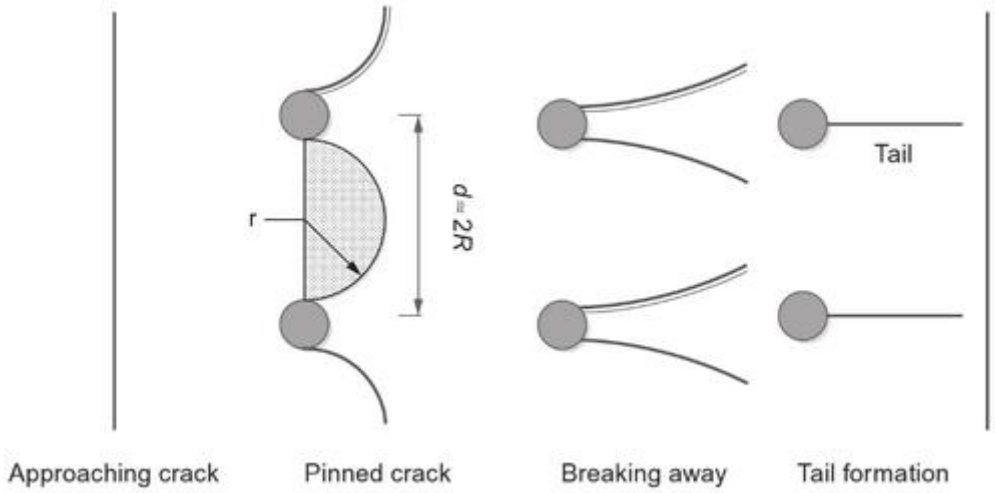

Fig 7. Formation of semi-circular secondary cracks at the pinning stage and subsequent tail formation. [26]

He showed that the bowing of the crack would lead to an increase in fracture energy and derived an equation relating the fracture energy G_{Ic} of the composite to the separation of the obstacles (particles) S';[26]

$$G_{Ic} = G_{IcM} + \frac{T_L}{S'} \qquad (5)$$

Where G_{IcM} is the fracture energy of the matrix material and T_L is the line tension of the crack tip, S' is the particle separation which can expressed by the following equation;

$$S' = \frac{2d(1-V_P)}{3V_P} \qquad (6)$$

Where V_P is the volume fraction of the filler particles, and *d* is the particle diameter.

FIBRE PULLOUT

Fibre pull out might sufficiently increase the work of fracture due to interfacial friction between the fibre and matrix. Its contribution to G_{Ic} is dependent on interfacial strength and interfacial area. The energy ΔU needed to pull out a fibre of the embedded length x is given by the following equation;

$$\Delta U = \int_0^{x_0} 2\pi r x \tau_i dx = \pi r x_0^2 \tau_i \qquad (7)$$

Where r is the radius of the fibre is, x_0 is the pull out length and τ_i is the interfacial shear strength. The integration over all fibres which are intersected by the cracks, assuming that there are N fibres per m^2, the following equation could be written down;

$$G_{pull-out} = \int_0^l \frac{N dx_0}{l} \pi r x_0^2 \tau_i \qquad (8)$$

With l being the length of the fibre. Since,

$$N = \frac{V_f}{\pi r^2} \qquad (9)$$

Where $V_f$the volume fraction of fibres is, $G_{pull-out}$ can be expressed as;

$$G_{pull-out} = \frac{V_f l^2 \tau_i}{3r} \qquad (10)$$

In the case of CNTs the value of r ranges between one and several tenth of nanometres, while the length may vary from several hundred nanometres to several millimetres. From the above equations one may notice that the high interface area of nanotube composites may lead to significant increase

in fracture work due to nanotube pull out. For the above model (describing the mechanism) to be validated, a homogeneous dispersion of nanotubes is a pre-requisite. In practise however the nanotubes get entangled and aggregated into agglomerates. Thus the pull-out model is just a rough approximation for CNT-composites. [25]

The micro-mechanical mechanism of crack bridging in a DWCNT-NH_2/Epoxy sample is as shown in Fig 8. As mentioned in previous sections this mechanism leads to an improvement in mechanical properties. The observed surface showed numerous cracks induced by thermal stress during the etching process of the nano-composites. The material was investigated by SEM and it was observed that DWCNT-NH_2 was bridging the cracks having a width of several microns. And these bridged length was 500-1000 times longer than the average diameter of these nanotubes. This bridging mechanism reduces the growth of nano-pores as well as propagation of cracks and leads to an increase in fracture toughness. And also the straightness of these CNTs as a result of bridging shows the tensed state of the nanotube-composite. The CNTs are carrying tensile loads which results in an improvement of strength, Young's Modulus and fracture toughness. [27]

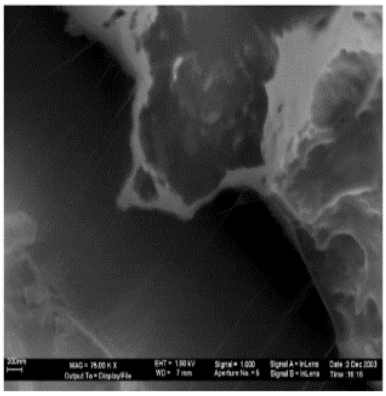

Fig 8. SEM-micrograph of a DWCNT-NH_2/epoxy sample, a crack induced by etching is bridged by double-walled CNTs. [27]

Therefore it can be concluded that the main fracture mechanical mechanisms are related to the enormous surface area of the nano-particles in general and also due to an agglomerated dispersion of filler, the main mechanisms leading to an increase in toughness can also be attributed to localised in-

elastic matrix deformation, void nucleation, crack deflection at the agglomerates [25,27], fibre pull-out and fibre bridging.

2.4 ACOUSTIC WAVES AND ACOUSTIC EMISSION TEST EQUIPMEMT FOR MONITORING CRACK GROWTH IN CARBON FIBRE REINFORCED COMPOSITES

This section would elaborate on the contributions of Joseph Kaiser who is responsible for the discovery of the "Kaiser Effect", the acoustic emission phenomena in metals, acoustic wave propagation in solids, few equations related to wave motion and the importance of Fourier transforms and wavelet transforms, types of acoustic waves and the effect of attenuation on acoustic wave propagation. Followed by this, the modal acoustic emission analysis methodology is elaborated and its use in this work is explained. Latter a brief explanation on acoustic signals registered in the equipment is given to make the reader more acquainted with the work. It is equally important to understand the feasibility of this method in the context of fibre reinforced composite materials. The first section of this part is an elaboration on this very question.

2.4.1 FEASIBITY OF ACOUSTICS IN THE CONTEXT OF MULTIPHASE COMPOSITES

A question would arise why acoustic emission (AE) test method? Crack propagation can be considered as an ultimate form of failure mechanism, which takes place in the inter-laminar zone during de-lamination. Since it can be evaluated by direct observation it could be taken as macroscopic failure activity. Microscopic behaviour such as fibre-matrix interface, micro damage is more difficult to evaluate, and it represents a major part of de-lamination.[28,29,30] To monitor microscopic events like fibre breakage, matrix cracking in composite materials, acoustic emission would be an apt tool. [28,31,32] AE is an efficient method to monitor in real time the damage growth in structural components and laboratory specimens. In loaded materials, strain-energy release due to micro-structural changes results in stress wave propagation. In composite materials many mechanisms have been confirmed to produce AE signals which includes matrix-cracking, fibre-matrix interface de-bonding, fibre breakage and de-lamination. AE deals with the detection of such waves at the surface of the material. Thus, this technique allows not only the location of the source of the emission but also helps in determination of its nature. [32] Many different authors have worked on the feasibility of using AE in

detecting flaws in composite materials. For instance S.Barré and M.L. Benzeggagh in their work reported that on working on fibre reinforced polypropylene samples the acoustic signal amplitude varies with corresponding damage mode; AE amplitudes ranging from 40 to 55 dB corresponds to matrix cracking, 60-65 dB to that of de-bonding, 65-85 dB to that of fibre pull out and 85-95 dB to that of fibre fracture. [33] In another study conducted by Ely and Hill it was shown that that the fibre breakage and longitudinal splitting occuring at the same location in unidirectional graphite/epoxy specimen, the stronger signals like high amplitude, energy, counts and long duration resulted from fibre breakage while the weaker signals like low amplitude, energy, counts and short duration resulted from longitudinal split. [34] While in another case found by Suziki et al. a correlation between failure mechanism and AE frequency in glass/polyester composite was found: for matrix cracking the frequency range was from 30-150 kHz, fibre de-bonding and pull out it was from 180 to 290 kHz, and fibre breakage it was in the range of 300 to 400 kHz. [35] In another case by Barnes and Ramirez, testing with carbon fibre reinforced composite pipes, using correlation plots of event amplitude and duration time to characterise the different modes of failure, they reported that high duration-low /intermediate amplitude-which was from 45 to 70 dB-events are associated with de-lamination and de-bonding while high amplitude-high duration events are associated with fibre fracture. [36] Thus many such finding can be cited from literature.

But a single damage mechanism can produce a wide range of AE signal parameters. The effect of large attenuations, closely occurring emission from different sources, equipment setting and large data sets leads to an overlap of the AE parameters. [37,38] Thus it can be said that multi-parameter analysis using many AE waveform parameters is required to improve the identification of damage modes (crack propagation in our work). Pattern recognition has been suggested as a suitable multi-variable technique for the classification of the AE events. If supervised pattern recognition is to be used then the number of damage mechanisms must be known in advance. On the other hand unsupervised pattern recognition is used to describe the complete methodology consisting of procedures for descriptors selection, cluster analysis and cluster validity.[32] Generated AE signal contains useful information on damage mechanism. But as mentioned in the beginning of this paragraph a single damage mechanism can produce a wide range of AE signal parameters. Each signal can be associated to a pattern composed of multiple relevant descriptors. [39,40] Then the patterns can be divided into clusters representing damage mechanisms according to their similarity by the use of multi-variable data analyses based on pattern recognition algorithms. [40] The methodology used in this work is elaborated in section 2.4.8.

2.4.2 KAISER EFFECT

"By a new reloading [of the tensile specimen] only few jumps occurred [in the photograph of the CRT] until the loading reached the former highest level of 50kg and immediately the impact of the effects [acoustic emission AE] could be observed with former vehemence."

"One important result of this testing method developed is the fact that the ex-post statements can be made about the maximum of load, which the material has endured before, without destroying the probe. Also the knowledge of the stress that had laid on the material and not the stress, which exists at the moment." [41]

The above two statements were mentioned and elaborated in the dissertation of Dr.Joseph Kaiser. To make it clearer let us consider a material that has been loaded under tension. Load levels that have been previously exerted on a material do not produce any AE activity. Which means discontinuities created in a material do not expand or move until that former stress is exceeded. [42] This effect was further studied by **Hans Maria Tensi (The Kaiser Effect and its Scientific Background)**. Tensile tests were conducted on several alloys and all revealed a similar diagram as shown in fig 9 for a soft-annealed steel specimen with 0.15%C. The maximum AE activity was noted in the elongation area of the yield strength.

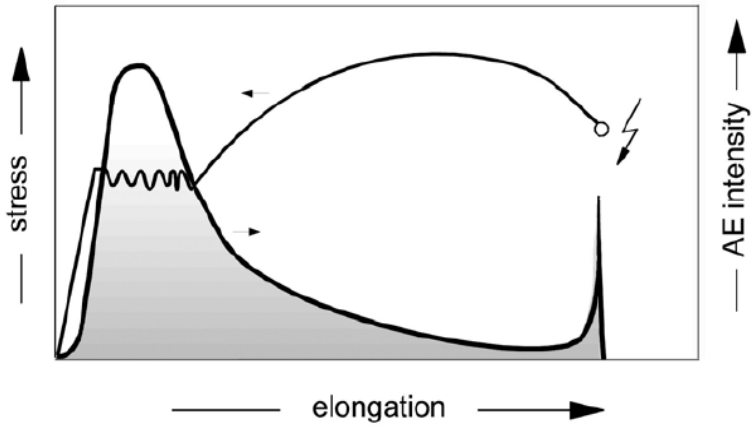

Fig 9. Stress-strain diagram and AE-strain diagram of a soft-annealed steel sample with 0.15wt% carbon [41]

Few AE activities in the Hooke's region could be attributable to faults in the experimental process. After passing the distinctive yield strength, the AE falls exponentially in the area of strain-hardening. And finally there is a peak in AE activity at the fracture point. Next we will see what happens if the load is removed and again applied to a level lower than the previously applied load levels (Refer fig 10).

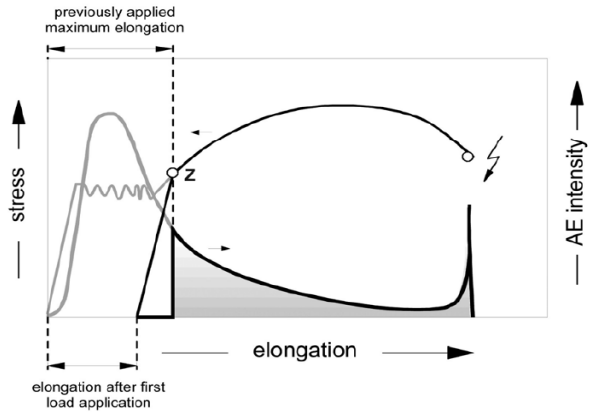

Fig 10. The Kaiser effect [41]

The figure above shows AE and stress as functions against elongation for a tensile test specimen, which has already been loaded up to point "Z". The sudden increase in AE activity upon passing the previously loaded point can be observed. [41]

2.4.3 THE ACOUSTIC EMISSION PHENOMENA IN THE CONTEXT OF METALS

Acoustic emission is the study and practical use of elastic waves generated by a material subjected to external stresses. There has been some confusions with regard to the term 'acoustic emission' for the past few decades. Strictly speaking acoustic refers to the pressure waves detected by one's ear. But elastic waves in solids are not restricted to pressure waves, but all types of vibrational modes are generated by the acoustic emission sources. Thus it could be said that acoustic emission is the generation of an elastic wave caused by the rapid change in the stress state of some region in the material. The material could be solid, liquid, gas or plasma and the external load could be applied

mechanically, thermally, magnetically etc. The stress change must be rapid enough to transmit some energy to the surrounding material and dissipate as elastic wave. On a macroscopic scale this definition includes earthquakes and thunder, while on the microscopic scale it includes the fracture of crystallites and martensitic phase transformation. The occurrence of the burst of energy is completely dependent on local conditions, the local stress field and the physical state of the region. [41] Next it would be wise to elaborate on what causes the AE phenomena. What is happening within the material that leads to AE?

It is well understood from earlier findings that the AE intensity has its maximum for an occurrence of a distinctive yield strength i.e. during extremely inhomogeneous plastic deformation. For instance it was observed that different materials with different heat treatments and significance difference in the yield strength, the maximum of AE in width and height decreases with decrease in yield elongation. This was shown in the case of carbon steel, differently heat treated aluminium alloys and that of pure aluminium (refer fig 11).

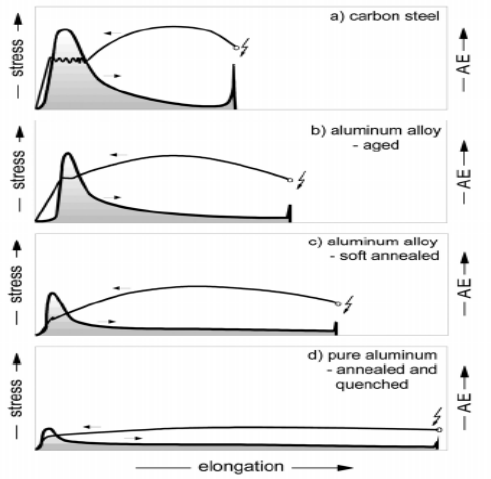

Fig 11. Differences in yield strength and AE activity of different materials and different heat treatments showing the connection of yield strength and AE. [41]

Many studies/research have shown that AE activity is strongly influenced by inhomogeneous slip of the slip dislocation. Dislocations are the only medium for plastic deformation in metallic crystals. This is validated by the model that is elaborated below (refer fig 12).

When a force is applied the dislocations slip on the slip-planes within the crystal. They distort the crystal lattice in their environment with fields of compression above and fields of tension below the slip-planes. In (a) of fig 12 the dislocations slip exactly one lattice distance 'b' when a load is applied. Homogeneously distributed impurities wouldn't disturb their movement. Taking into account the multiple dislocations, the material would deform very steadily. Next if the alloy is heat treated. The impurities would diffuse to the lower side of the dislocation, where there is a local field of stress (fig 12 b). The impurities are heterogeneously distributed near the dislocation. This would cause a release of tension and the dislocations are blocked in their mobility. The local amount of shear stress keeps increasing until the blocked dislocation is torn off and it jumps several lattice distance($n *' b'$). This causes a miniscule bump in the metal which combine to the AE.

To prove this model right flat tensile test specimens made from AlMg3-alloy were at first heat treated uniformly such that all impurity atoms were uniformly distributed within the crystal. Latter several group of specimens were differently heat treated to produce differences in elongation of the yield strength i.e. to produce inhomogeneous plastic deformation. And as expected the AE in specimens with zero elongation of the yield strength and with homogenous distribution of impurities, increased monotonously to the specimens with non-homogeneous distribution of impurities.

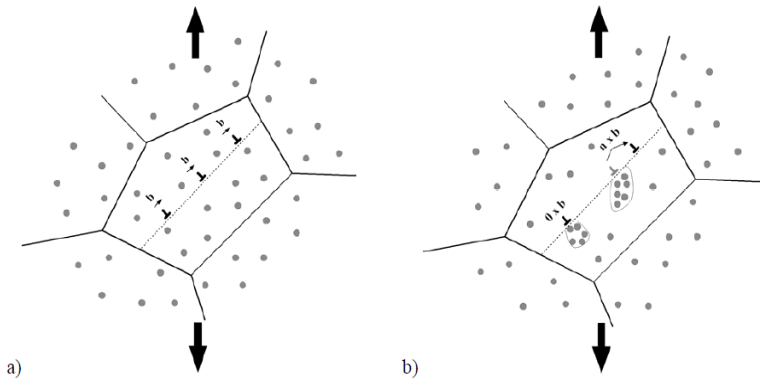

Fig 12. A) Impurities dispersed homogeneously, the dislocations are not blocked b) Impurity atoms create clusters at the dislocations and block them, by creating stress the dislocations suddenly jumps out of the Cottrell cloud. [41]

In addition to the dislocation there are certain micro-structure properties that would trigger AE. They are micro-cavities, internal cracks and fissures, inclusions which could be metallic and non-metallic phases, and external crack (fig 13).

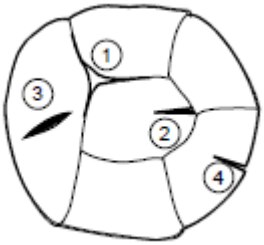

Fig 13. Microstructural phenomena leading to AE; (1) Micro-cavities (2) Internal crack and fissures (3) Inclusions and (4) External crack [41]

Micro-cavities are formed by solidification and is something that is unavoidable. Even when the casting material is post processed by either heat or mechanical treatments removal of micro-cavities is not possible without leaving other faults. These cavities are characterised by sharp notches and for small mechanical loads, local stress accumulates near the notch. Dislocation starts in these regions earlier even when the part is still in its elastic deformation phase. Latter these notches tear open and the surface of the cavities get larger. When the load is removed the exposed surfaces fold up. When re-loaded these planes are separated again. This causes rubbing noises with additional AE, even though the previous load has not been exceeded. This makes it clear, the sources that produce AE; normal dislocation reactions, reinforced dislocation reactions caused by notch-stress and repeated tearing open of notches followed by folding up of the cavity flanks.

An internal crack would cause the same AE activity as that of cavities. Inclusions could be either metallic or non-metallic. Inter-metallic inclusions have no ductility and this causes them to be brittle. They are mechanically comparable to a crack. And also they have weak connections to the interface of the lattice such that they behave like a crack. All mechanisms triggering AE elaborated above applies in this case too. An external crack is formed by leakage dislocations very often in combination with corrosion (stress corrosion where crack growth is exponential). If tensile test where to be conducted for such a specimen, it would show a blurred step in the AE-function and thus only an in-distinct Kaiser-effect. [41]

2.4.4 ACOUSTIC WAVE PROPAGATION IN SOLIDS

Acoustic wave motion is a co-operative movement of the atoms in a material extending over huge number of atoms, and hence this collective motion of atoms implies that the wavelength is longer than the distance between the atoms. As it is known that wavelength and frequency have an inverse relationship, the acoustic waves due its large wavelengths would have relatively lower frequencies.

The simplest type of an acoustic wave is a pressure wave which occurs when a shell of material around a region is suddenly compressed by disturbances in that region. This disturbance can either be positive or negative. Then the material in the shell experiences a change in density. This change in density is then passed to the next shell by coupling between the atoms. There would be a rebound of density in the first shell, usually going past the original density. This variation in density is transmitted to the next shell and hence throughout the material. The strength of coupling between the materials atoms/molecules and the density of the material determines the speed with which the disturbances propagates. The resulting wave is known as compressional wave. In a compressional wave, the average motion of the atoms parallels the wave's direction of travel. But when the material becomes more rigid, more and more modes of wave motion are possible and the averaged atomic motions are no longer parallel to the direction of propagation of wave.

The acoustic properties of material depends on its density and the long range coupling-constants between the atoms. The long-range correlations in an acoustic wave results in many atoms in a small region being displaced in the same direction from their equilibrium positions. This displacement is a local dynamic strain in the crystal; the strain's magnitude and direction are constantly changing as the atom moves. When atom motion is pseudo-oscillatory, so is the strain. An acoustic wave is an oscillating strain moving through a material. Since stress and strain are related in a material there is also an oscillating stress field. Thus an acoustic wave may be described as either a dynamic stress or strain field in a material. [42]

2.4.5 MATHEMATICAL FORMULATIONS ON WAVE MOTION AND THE IMPORTANCE OF FOURIER TRANSFORMS AND WAVELET TRANSFORMS

A wave can be depicted as a sinusoidal curve. The amplitude oscillates between positive and negative limits at a fixed rate known as frequency and the curve extends indefinitely.[42] The amplitude of a

wave as a function of time and position can be represented in several equivalent ways e.g. as sine function, cosine function, exponential of an imaginary number etc. A wave propagating in one dimension inside a material has a general form;

$$y(x,t) = A.f(kx + 2\pi\nu t) \quad (11)$$

Where y is the displacement, A is the amplitude of the wave, f is a periodic function, x is the distance along the direction of propagation, t is the time, ν is the frequency of the wave, and k is the wave vector, the reciprocal of wavelength λ, which describes how quickly the displacement varies with distance along the direction of propagation. In the simplest case f is the sinusoidal function such as sine or cosine;

$$y(x,t) = A.sin(kx + 2\pi\nu t) \quad (12)$$

Although the velocity V of ultrasonic and sonic waves in materials does not change much with frequency, the wavelength λ is inversely proportional to the frequencyν;[43]

$$V = \nu\lambda \quad (13)$$

If two waves exist in a medium simultaneously their amplitudes will add up algebraically, the sum of two waves can be written as;

$$Y = A_1 sin\omega_1 t + A_2 sin\omega_2 t \quad (14)$$

Any arbitrary transient function which does not contain a discontinuity can be represented by an infinite sum of sinusoidal curves known as Fourier series. One form of such series can be expressed as follows;

$$f(t) = \frac{A_0}{2} + \sum A_n \sin(n\omega_n t + \alpha_n) \quad (15)$$

Where A_0 and A_n are amplitudes of the sine curves, ω_n the frequencies and α_n the phases. A plot of the square of the amplitudes of the frequency components A_n in the above equation against frequency ν is known as the frequency spectrum of the wave. [42]

The wave propagation is also affected by the medium through which it propagates. The materials characteristics determines the wave velocity. The stronger the force between neighbouring atoms, the more closely coupled will be their motion. While on the other hand if the mass of the atoms are larger, more force must be applied for the same acceleration. Since a wave is a synchronised movement of large number of atoms, the density ρ governs the motion of waves rather than mass of individual atoms. [42] Therefore the following can be written down;

$$V_S = \sqrt{\frac{G}{\rho}} \quad (16)$$

Where V_S is the velocity of the wave, G the elastic constant of the material (the elastic constant can be a shear modulus in the case of transverse waves and Young's modulus in the case longitudinal waves). The elastic constant is a measure of the strength of the coupling between atoms. Another property of the material is the characteristic impedance given by the following equation;

$$Z_i = \rho v_i = \sqrt{\rho G} \quad (17)$$

The reflection and transmission of acoustic waves at an interface between two materials depends on the characteristic acoustic impedances of the two materials. [42]

Wavelet Transforms: The continuous WT of $f(t)$ is a function defined as;

$$WT_f(a,b) = \frac{1}{\sqrt{a}} \int_{\infty}^{-\infty} f(t)\varphi^*(\frac{t-b}{a})\, dt \quad (18)$$

Where a > 0 and the superscript * denotes a complex conjugation. The analysis function of the WT can be defined as;

$$\varphi_{a,b}(t) = \frac{1}{\sqrt{a}}\varphi(\frac{t-b}{a}) \quad (19)$$

Its elements are generated by shifting and scaling a basic wavelet$\varphi(t)$. The parameters a and b stands scale and shift of the basic wavelet. In time, $\varphi_{a,b}(t)$ is centred at b with a spread proportional to a. The function $\varphi_{a,b}(t)$ may be considered as a window function both in the time and frequency domain. The size of the time window is controlled by scale a. The window size could be changed in either in the frequency or time domain. This multi-resolution is a primary characteristic of wavelet analysis.

A basic wavelet satisfies the admissibility condition;

$$\int_{-\infty}^{\infty} \frac{|\widehat{\varphi(\omega)}|^2}{|\omega|} d\omega < \infty \quad (20)$$

Where $\widehat{\varphi(\omega)}$ denotes the Fourier transform of $\varphi(t)$. Though any basic wavelet could be chosen which satisfies the admissibility condition, but the Gabor function is used because it provides a better resolution in both time and domains than any other wavelets. The Gabor function can be expressed as follows

$$\varphi_g(t) = \frac{1}{\sqrt[4]{\pi}}\sqrt{\frac{\omega_0}{\gamma}}\exp(-\frac{\left(\frac{\omega_0}{\gamma}\right)^2}{2}t^2)\exp(i\omega_0 t) \quad (21)$$

And its Fourier transform as;

$$\hat{\varphi}_g(\omega) = \frac{\sqrt{2\pi}}{\sqrt[4]{\pi}}\sqrt{\frac{\gamma}{\omega_0}}\exp(-\frac{(\frac{\gamma}{\omega_0})^2}{2}(\omega-\omega_0)^2) \qquad (22)$$

Where γ and ω_0 are positive constants. But usually the Gabor function doesn't satisfy the admissibility condition if we don't set $\gamma = \pi\sqrt{\frac{2}{\ln(2)}} = 5.336$. The Gabor function can be considered as a Gaussian window function centred at $t = 0$ and it Fourier transform centred at frequency $\omega = \omega_0$. The function $\varphi_g\left(\frac{t-b}{a}\right)$ is then centred around $t = b$ and its Fourier transform $(ae^{(-ib\omega)}\hat{\varphi}_g(a\omega))$ is centred around$\omega = \frac{\omega_0}{a}$. The $WT_f(a,b)$ using the Gabor wavelet thus represents the time-frequency co-efficients of $f(t)$ around $t = b$ and $\omega = \frac{\omega_0}{a}$. [52]

Time-frequency analysis of dispersive waves: For the purpose of time-frequency analysis of dispersive waves, let us consider two harmonic waves of unit amplitude and of slightly different frequencies ω_1 an ω_2 propagating in x-direction;

$$u(x,t) = e^{-i(k_1x-w_1t)} + e^{-i(k_2x-w_2t)} \qquad (23)$$

Here k_i are wave numbers corresponding to the frequency ω_i. Let us write the following formulations;

$$\frac{k_1+k_2}{2} = k_c \qquad \frac{\omega_1+\omega_2}{2} = \omega_c$$
$$\frac{k_1-k_2}{2} = \Delta k \qquad \frac{\omega_1-\omega_2}{2} = \Delta\omega \qquad (24)$$

Using (24) we can re-write (23) as follows;

$$u(x,t) = 2\cos(\Delta kx - \Delta\omega t)e^{-i(k_cx-\omega_ct)} \qquad (25)$$

If observed carefully the above equation comprises of two parts, the first being the carrier wavelet represented by the exponential term, showing the propagation with the phase velocity $C_p = \omega_c/k_c$. The other part represents the modulated wave given by the $cosine$ term travelling with group velocity $C_g = dw/dk$ in the limit $\Delta k \to 0$. When the Gabor wavelet is used as the basic wavelet, the WT of $u(x,t)$ is given by;

$$WT_U(x,a,b) = \sqrt{a}\{e^{-i(k_1x-\omega_1t)}\varphi_g^*(a\omega_1) + e^{-i(k_2x-\omega_2t)}\varphi_g^*(a\omega_2) \quad (26)$$

The magnitude of WT can be written as;

$$|WT_U(x,a,b)| = \sqrt{a}\{\left[\hat{\varphi}_g(a\omega_1)\right]^2 + \left[\hat{\varphi}_g(a\omega_2)\right]^2 + 2\hat{\varphi}_g(a\omega_1)\hat{\varphi}_g(a\omega_2)\cos(2\Delta kx - 2\Delta\omega t)\}^{1/2} \quad (27)$$

If $\Delta\omega$ is sufficiently small such that $\hat{\varphi}_g(a\omega_1) \approx \hat{\varphi}_g(a\omega_2) \approx \hat{\varphi}_g(a\omega_c)$ we obtain;

$$|WT_U(x,a,b)| = \sqrt{2a}\left|\hat{\varphi}_g(a\omega_c)\right|\{1 + \cos(2\Delta kx - 2\Delta\omega t)\}^{1/2} \quad (28)$$

The above result indicates that the magnitude of WT takes its maximum value at $a = \omega_0/\omega_c$ and $b = \left(\frac{\Delta k}{\Delta\omega}\right)x = x/C_g$. This means the location of peak on the (a,b) plane indicates the arrival time of the group velocity C_g at frequency $\omega_c = \omega_0/a$ i.e. $f = 1/a$. [52]

Dispersion relation of plate waves:

a) 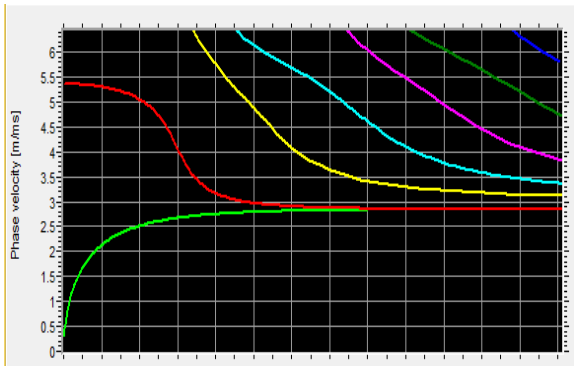

b) 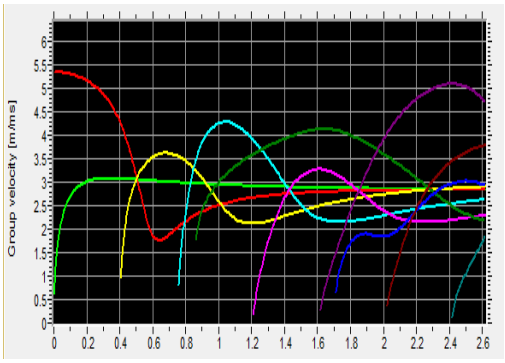

Fig 14) Dispersion curves for an aluminium plate with a thickness of 3.77mm, note that the x-axis is the frequency in MHz . a) Phase velocity dipserion curves; b) Group velocity dispersion curves. [Source: Sloved for Al using AGU-Vallen wavelet solver]

To locate the AE source the the group velocity of the considered elastic wave modes at certain frequency must be known. According to the theory of MAE (Modal Acoustic Emission), the AE signals are dispersive elastic waves. The propagation of the elastic waves in thin-walled structure exhibits multi-modes and dispersion characteristics. Figure 14 is dispersion curves for a thin aluminum plate with a thickness of 3.77mm. From 14 b it is evident that over a range of 0-400kHz, there exists only two modes and they are the anti-symmetric A0 mode and symmetric S0 mode. At 200kHz the group velocities of S0 and A0 mode are 5.4m/ms and 3.1m/ms respectively. Thus its quite simple from the dispersion curves to obtain the velocity of any mode under the concerned frequency range. [52]

2.4.6 TYPES OF ACOUSTIC WAVES

Waves travelling through an extended medium-dimensions larger than the acoustic wavelength-are called bulk waves. The two types of bulk waves are longitudinal wave and shear waves (transverse waves). [41] In the case of transverse or shear waves the displacements are perpendicular to the

direction of the travel of the waves. While in the case of the longitudinal waves the displacements are in the direction of waves. [43]

a) 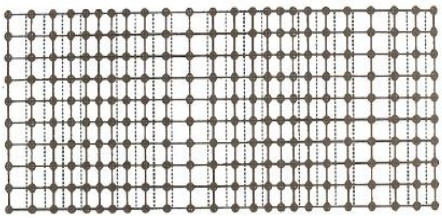 b) 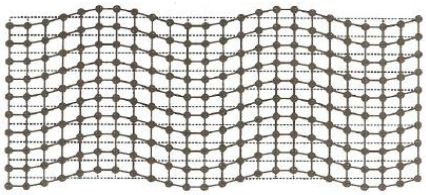

Fig 15. a) Particle motion in longitudinal or compressional waves; b) Particle motion in shear or transverse waves. [42]

Particle motion in longitudinal and shear waves is as shown above. Since the relative motion of the particles in these two cases are different the elastic constants and wave velocities differ. And hence shear velocity is slightly greater than one half of the longitudinal velocity. [42]

Apart from the bulk waves described above we have another class of vibrations collectively called as "guided waves". These waves are due to the geometrical constraints of the acoustic waves arising from the shape of the test specimen. Examples of different types of guided waves are plate waves, cylindrical waves and rod waves which are named after the different types of geometrical constraints. Two examples of the guided waves are Rayleigh waves and Lamb waves. [43]

Rayleigh waves: Surface waves can be generated on a semi-infinite half space, using a transducer with an angle beam. These waves represent an idealised limiting case where the constraints imposed by boundary conditions are at a minimum. The solutions modes of the wave equation in this case was shown by Rayleigh and included a surface travelling wave known as Rayleigh waves. Particle motion in a Rayleigh wave is as shown below.

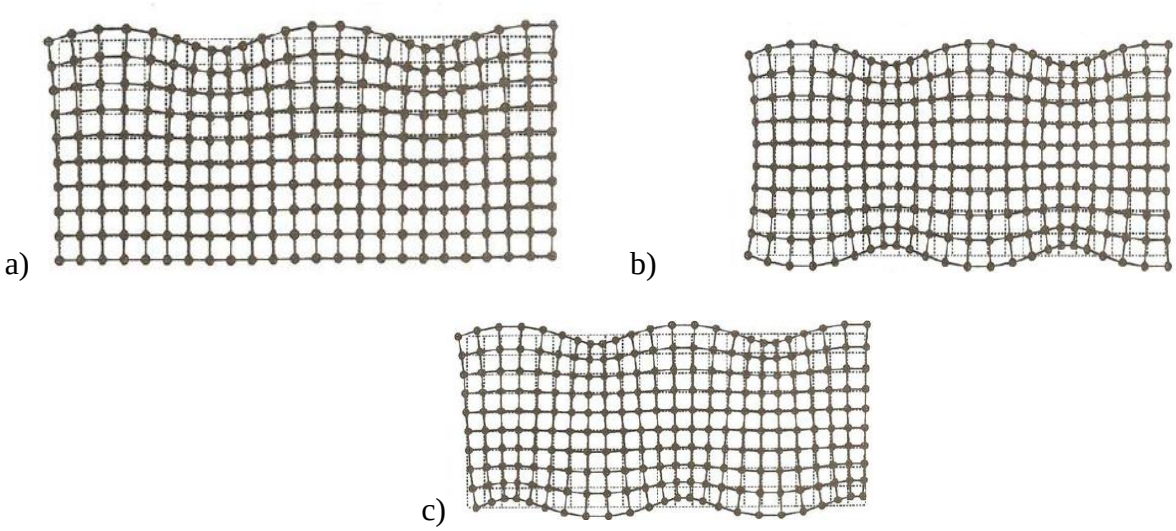

Fig 16. Particle motion in a) Rayleigh wave; b) Lamb, first symmetric mode and c) First anti-symmetric mode. [42]

Lamb waves: This is another type of guided wave and is vibration of a plate of finite thickness. The solution in this case was shown by Lamb and the surface travelling wave that is generated is known as Lamb waves. [43] A lamb wave is essentially two surface waves synchronised either symmetrically or anti-symmetrically. [42] Particle motion on the case of Lamb wave is as shown in Fig.16 b and c.

2.4.7 ATTENUATION

The passage of waves in a material is subjected to attenuation with distance and time resulting from factors like scattering of the wave energy, absorption of some of the energy by the material and divergence. If a wave is attenuated exponentially inside a material then the wave equation could be written down taking the attenuation into account;

$$y(x,t) = A_0 \sin(kx + 2\pi\nu t) e^{(-\alpha x - \beta t)} \qquad (28)$$

Here the exponential term ensures that the signal decays with both time and distance, α is the attenuation constant per unit length and β is the attenuation constant per unit time. This equation

applies only in special cases where the materials is homogeneous and in which the beam is not diverging.

If there is no divergence and the only mechanisms for decrease in intensity with distance are scattering and absorption then the above equation could be re-written as;

$$I(x) = I(0)e^{-\mu x} \tag{29}$$

Where $I(x)$ is the intensity of the wave at a distance x into the material, $I(0)$ is the intensity at $x = 0$ and μ is the attenuation coefficient. Absorption and scattering contributes to μ, where absorption can be due to damping of the acoustic vibrations in the sample caused by dislocation and other defects. Scattering can be due to grain size in the material. Since divergence is not accounted for in this equation, this equation only applies for collimated beams. [43]

2.4.8 MODAL ACOUSTIC EMISSION ANALYSIS

AE waves propagate in a structure through different modes.[48] An analysis of these modes provides some insight into the type of damage the composite material undergoes. The plate theory corroborates that the acoustic waves propagates through plates in two different modes, the symmetric mode S0 and the anti-symmetric mode A0[48] (fig 17)[49]. With reference to [48] it could be further said that, when AE waves travel in flat plates they exhibit a different behaviour attributable to the bounded surface of the structure. The waves are bounded by the surface and are subjected to wave-guide effect, thereby causing them to propagate as Lamb waves. As mentioned above these waves propagate in two distinctive modes namely, longitudinal waves, in the plane of the surface, and transverse waves, perpendicular to the surface (fig 16). The zero-order longitudinal and transverse modes exist across all frequencies and are referred to as extensional (S0) and flexural (A0) modes respectively. [54] In figure 17 we have an example of a signal representing the out-of-plane displacements from buried dipole source in aluminium plates 4.7mm thick and small and large lateral dimensions. The figure is an example of an AE signal without edge reflections and its calculated wavelet transforms (WT) magnitude as a function of frequency and time. The source for this signal was an in-plane dipole centred at a depth of 1.723 mm below the plate top surface. The signal is a representation of top-surface out-of-plane displacement at 180 mm from the epicentre of the source. The WTs were

calculated using the AGU-Vallen Wavelet which is a freeware software program (Vallen-Systeme GmbH). AGU-Vallen Wavelet was developed in collaboration between Vallen-Systeme GmbH and Aoyama Gakuin University (AGU), Tokyo, Japan. The AGU group has pioneered in the research of wavelet analysis in the field of acoustic emission. This program uses a Gabor function as the "mother" wavelet with a central frequency of 7MHz. The figure also shows the two lowest modes (S0 and A0) superimposed on the WT. The colour scale in the figure is a linear scale with red representing the highest magnitude region of the WT and pink the smallest or zero-magnitude region. It is clear form the figure, the presence of AE signal energy in the portions of both the modes. These aspects illustrates a key advantage of the WT when compared to Fast Fourier Transforms (FFT). The WT shows how the signal energy is distributed as a function of frequency, time and mode. While in the case of FFT-for the same AE signal- provides only the frequency content of the whole signal and doesn't allow to see the modal division or how the intensity of energy in frequency ranges and modes varies as a function of time. It is also evident from the same figure that the greatest concentration of energy is in the anti-symmetric mode (A0) in a frequency range of 40-80 kHz. [49]

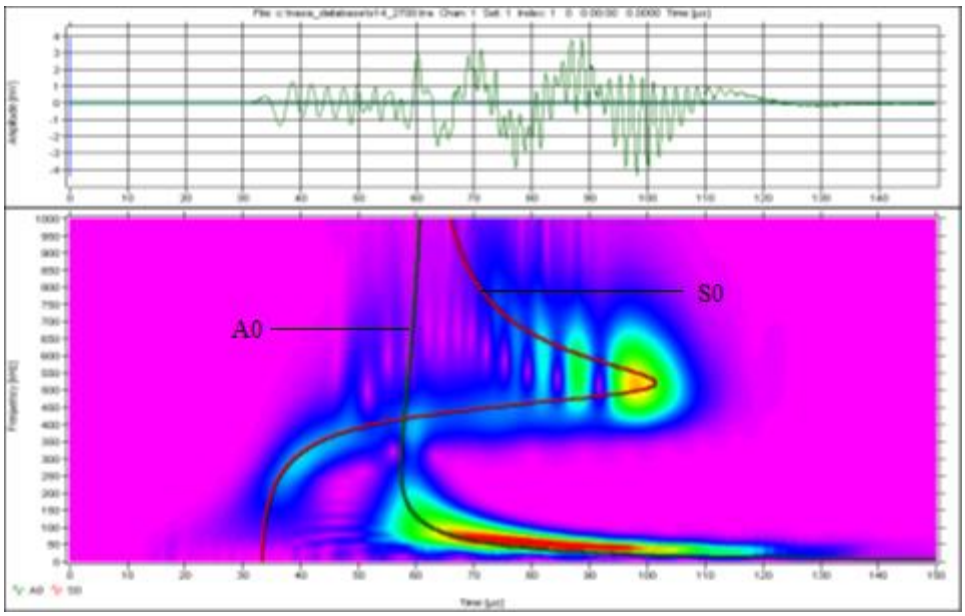

Fig 16. Calculated AE signals from an in-plane dipole source with corresponding WT with superimposed modes [49]

Studies have found that delamination in composites are largely associated with the production of mechanical displacement micro-pulses outside the plane (OP), while matrix micro-cracking and fibre breakage may produce micro-pulses inside the plane (IP). It has been proved through recent researches that A0 mode is favoured by OP excitations and S0 by the IP excitations. [49] In another study conducted by Y.Mizutani et.al, it was understood that fibre fracture was characterised by the presence of both S0 and A0 modes, with energy concentration in the S0 mode at a frequency range of 200-400kHz. Matrix cracking (transverse) when viewed in the wavelet contour was found to have a component around 300kHz. Since low frequency component were absent, signals appeared in a single mode namely S0 mode. Delamination was, like fibre fracture characterised by two modes, and the wavelet contour showed that both modes S0 and A0 had strong high frequency content. Fibre and matrix de- bonding was characterised by low frequency A0 mode. The material used in this study was carbon fibre reinforced composites subjected to point load. [50] In another study conducted by Christopher Baker et.al, the initiation and propagation of cracks in CFRC laminates were studied using modal acoustic emission analysis and waveform energies coupled with peak frequency data, the results were correlated to transverse matrix cracking. Four composites panels with different ply lay ups were used. Post test results showed that the placement of the 90^0 plies either on the surface or internally greatly influenced the modes visualised. For instance, modal AE theory could be applied to the waveforms generated from the 90^0 ply transverse cracks at different locations through-the thickness of the composite. A surface crack would excite a low frequency A0 mode because of the slight bending moment associated with an off-centre crack. An interior 90^0 ply transverse crack should excite a high frequency S0 mode since the axial-directed pressure associated with 90^0 ply transverse crack is nearer to or at the centre of the specimen. [51] Comparing the studies mentioned in [49,50,51], a complied table elaborating the kind of modes to be expected when a composite specimen undergoes failure is shown below.

FRACTURE MECHANISM	LAMB WAVE MODES	FREQUENCY RANGES	DESCRIPTION
Fibre fracture	Predominantly S0 mode along with A0 mode	S0- 300-500 kHz	Wavelet contour had both A0 and S0 mode, but usually the S0 mode prevails.
Matrix cracking	S0 and A0	S0- ~300kHz A0- ~100kHz	Surface cracks excites A0 mode while internal cracks excites S0 mode.
De-lamination	S0 and A0	S0 and A0 has higher frequency content	Both the modes usually have higher frequency content.
Fibre-matrix de-bonding	A0	Characterised by low frequency A0 mode	Characterised by low frequency A0 mode

Table 1: Modes expected from the failure mechanism of carbon fibre reinforced composites

This table would be used as a reference for further analysis on the acoustic signals obtained for the specimens used in this thesis work. This wouldn't be used as an absolute reference, since in all these tests the loads applied were either a tensile force or a bending test. While in our case we had double cantilever beam specimens and the crack opening mode was simulated. No literature specifically illustrates the kind of signal one should expect when we have this kind of loading. More about the specimens and test methods would be elaborated in the next topic (3). Specimen number 1.3 (without nanotubes) and 2.3 (with nanotubes) would be considered for the analysis. The reason for choosing these specimens is that, we initially as per standard ASTM 5528 loaded the specimen at a cross-head speed of 5mm/min upto a crack length of 5mm to see if there is unstable de-lamination growth from the insert. Latter the specimen was unloaded. It was only for these two specimens that we had the acoustic data for this initial loading, hence these specimens has to be chosen. The wavelet contours obtained would be analysed to see if it matches descriptions elaborated in the table. AGU-Vallen Wavelet solver would be used to compute the wavelet transforms.

2.4.9 ACOUSTIC EMISSION TEST EQUIPMENTS

2.4.9.1 TERMINOLOGIES INVOLVED WITH ACCOUSTIC EMISSION

AE: A transient elastic wave produced by rapid release of (elastic) energy or during certain processes.

AE-event: A physical event causing AE, e.g. crack formation.

AE-source: The physical origin of one or more AE events. This could be a crack growth step by step. Each crack growth is an AE event.

AE signals: The electrical signals of the sensor resulting from AE from a source.

Transient signal, Burst: AE signals with a clearly detectable start and end.

Hit: This is a burst detected by the AE system.

AE-activity: This is the occurrence of AE signals as a result of AE.

AE-intensity: The strength of AE events in units of energy or amplitude.

AE channel: This includes AE sensors and associated instruments for the acquisition and measurement of the AE signals measurement chain.

Multi-channel system: This includes system providing multiple AE channels, e.g. for source location, or for examining areas too large for one sensor. [44]

2.4.9.2 TRANSIENT AND CONTINOUS SIGNALS

There are two types of AE signals namely transient and continuous signals. In the case of transient AE signals, also termed as bursts, start and end points deviate clearly from background noise. But with continuous wave, we can see amplitude and frequency variations but the signal never ends. In the figure below an example of both types of AE signals are shown.

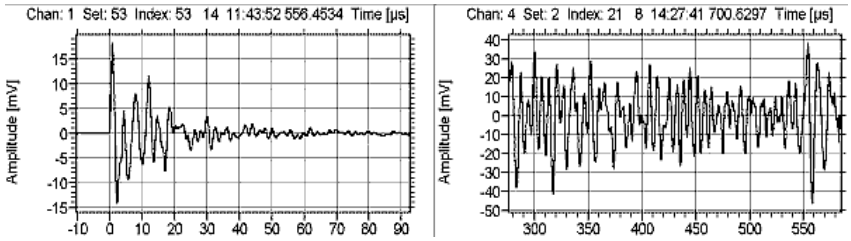

Fig 17. Transient (left) and continuous (right) AE signals [44]

The useful signal for AE testing in the case of large pressure vessels, composites etc. are the burst types signals originating from the fracture or crack growth. Continuous signals are mostly unwanted signals resulting from friction or flow noise. But even burst signals can be interfering signals, e.g. short friction noise or electrical spikes. At best the background noise is just the electronic noise of the preamplifier or the sensor. [44]

2.4.9.3 DETERMINATION OF THE ARRIVAL TIME

One of the very important tasks of an AE system is to convert the AE bursts into compact data sets and to eliminate the background noise-which is more or less continuous. For this very purpose, the AE systems uses detection thresholds. The threshold should set at the appropriate value by the user. Latter, if the AE signal exceeds the threshold in either the positive or negative direction, this means the start of a hit-detected burst.

The time at which the first threshold crossing is observed is called the "arrival time of the burst" and this is needed for location calculation. Waveforms displayed in figure 17 and 18 are produced by joining many single point called 'sample'. They correspond to single measurements at constant time intervals.

Digital systems sample the AE signal e.g. every 100ns, which means 10 million times a second. The unit of the time axes of the above diagram (figure 17) is µs, i.e. every 10 µs interval contains 100 samples. A wave packet 100 µs is made of more than 1000 samples, this shows the huge amount of memory required for a single burst. [44]

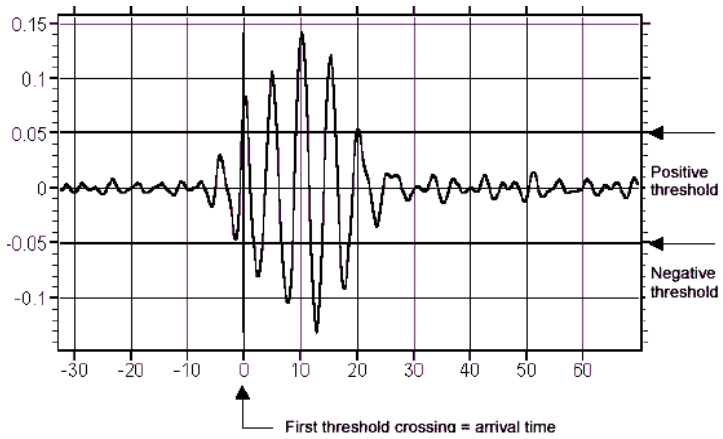

Fig 18. Determination of the arrival time [44]

2.4.9.4 AE PARAMETERS

In few cases the AE testing is based on only few bursts. In general, some hundreds or thousands of bursts are recorded for statistical evaluation. Statistical evaluation of the waveforms is quite difficult, but certain features of the waveforms could be evaluated statistically. The most important parameters of the waveform should be determined in order to compare the results of the structure under test with those of a defect-free test object and with those of a defective test object.

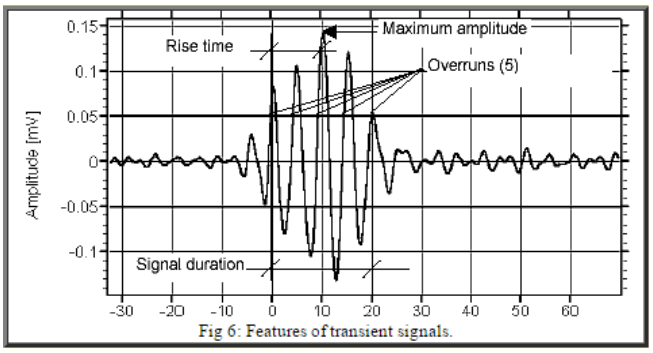

Fig 19. Features of transient signals [44]

The most commonly used features are elaborated below with reference to figure 19;

-Arrival time (absolute time of the first threshold)

-Peak amplitude

-Rise-time (time interval between the first threshold and last threshold crossing)

-Signal duration (time interval between the first and last threshold crossing)

-Number of threshold crossings (counts) of the threshold of one polarity

-Energy (integral of squared (or absolute) amplitude over time of signal duration)

-RMS (root mean square) of the continuous background noise (before the burst)

The peak amplitude is one of the most important burst features. Crack signals shows medium to high amplitudes and have durations of approximately 10μs, depending on the properties of the test object.

In most cases, bursts with less than 3 threshold crossings and durations of less than 3 μs can be regarded as unwanted signals. Most of the bursts with low amplitudes and long durations are friction noise. Very short signals may indicate electrical noise peaks, if they arrive at all channels at the same time.

With logical fibres one can separate bursts on the basis of those burst features in a flexible way and this is done carefully and important burst should not be missed.

External parameters like pressure or temperature are used as reference for the measured AE data. A parametric channel is a DC signal input, which represents the actual value of an external parameter, such as pressure, temperature etc. [44]

2.4.9.5 SENSORS-CONVERTING THE MECHANICAL WAVE INTO AN ELECTRICAL AE SIGNAL

Piezoelectric sensors have proved to be most appropriate for AE testing. They are robust and more sensitive than other sensor techniques, e.g. capacitive, electro-dynamic, or laser-optical sensors.

The sensitivity of piezoelectric sensors can reach values of upto 100V/μm. A displacement of 0.1 pm generates 100μV_{PK} then and can be well distinguished from the electrical noise (about 10 μV_{PK}).

Sensitivities of sensors are shown as frequency response diagrams (output voltage versus frequency, fig 20 b). In fig 20 b, the sensitivity is given in dB re 1V/µbar. So, -60 dB would mean an output of 1 mV_{PK} if the sensor would be excited with a sinusoidal pressure of 1 bar (peak value) of the frequency at the horizontal axis. [44]

a)

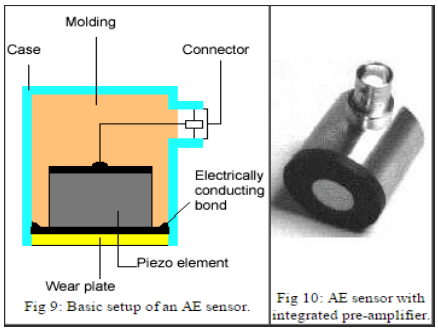

Fig 9: Basic setup of an AE sensor.

Fig 10: AE sensor with integrated pre-amplifier.

b)

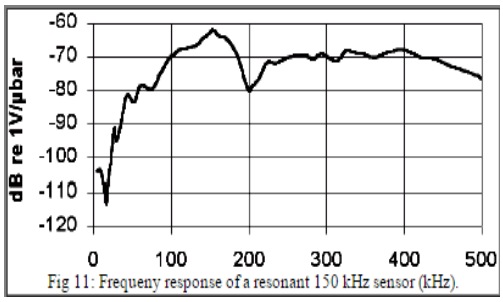

Fig 11: Frequeny response of a resonant 150 kHz sensor (kHz).

Fig 20. a) Basic setup of an AE sensor, b) Frequency response of a resonant 150 kHz sensor (kHz) [44]

3. DESIGN OF EXPERIMENTS

This chapter would deal elaborately on the material used, preparation of the composites panels, preparation of the specimens as per ASTM D 5528-01, fatigue mode-I inter-laminar crack propagation test, acoustic signal generation while the propagation of crack, determination of inter-laminar fracture toughness again in consultation with ASTM D 5528-01.

3.1 MATERIAL USED AND PREPARATION OF THE COMPOSITES PANELS

3.1.1 MATERIAL USED

The materials used in this study includes carbon fibre, an epoxy material with hardner and multi-walled carbon nano-tube (MWCNTs). The MWCNTs were procured form "FIBREMAX COMPOSITES" a Greek supplier of composite materials. The specifications of the MWCNT were; Bulk volume 4 lt; Average diameter 10-40 nm; Length 1-25 μm; Purity by weight 93% min and Specific surface area 150-250 m^2/g. The epoxy material along with the hardner was procured from "R&G Faserverbubdwerkstoffe GmbH". As per the manufacturers claim this resin system (Epoxy resin L+Hardner GL2) offers an approval by the *Germanische Lloyd* for the construction of the boats and rotor blades for wind turbines. Thus this resin system has the following properties; low viscosity, highly transparent, fully cures at 15^0C, glass transition temperature $T_g>85^0C$, Pot life of approximately 210 mins, high static and dynamic strength. The various mechanical properties of the resin system are as follows; Density 1,151 g/cm^3, tensile strength 74,8 MPa, elongation at break 4,5%, tensile modulus 3057 MPa, flexural strength 119 MPa. The Epoxy Resin L is a modified, low viscosity epoxy resin based on bisphenol A and F. Applications include among others, laminates from glass-, aramid-, and carbon fibres for wind turbine blades and boat building. Epoxy Resin L is resistant to crystallisation. The properties of the resin is further elaborated in table (2) (all details listed is as per the manufacturer's catalogue). The Hardener GL2 used in the resin system is an epoxy hardener with very low viscosity, which can be used in combination with suitable epoxy resin formulas in a wide range of applications. It is a modified cycloaliphatic polyamine free of alkyl phenol and benzyl alcohol. The properties of the hardener is further elaborated in table (3) (all details listed

are as per the manufacturer's catalogue). A 0.1 thick polyester was used as de-lamination initiator inserted in the centre plane of the laminates. Both sides of the film were coated with mould release agent to minimise adhesion between the film and the matrix material of the composite material.

PROPERTY	**VALUE**	**UNIT**
Viscosity at 25^0C	710±70	mPas
Density at 23^0C	1,15±0,01	g/cm^3
EP-Equiv. weight	178	g/Eq
Solid content	100	%
Flash point	>150	^{0}C

Table 2: Specifications of the Epoxy Resin L

PROPERTY	**VALUE**	**UNIT**
Viscosity at 25^0C	14±2	mPas
Amine index	565±10	mgKOH/g
Density at 23^0C	0,94±0,01	g/cm^3
Refractive index	1,4681±0,0001	
Appearance	Colourless, clear	
Active-H-Equiv.weight	50	g/Eq
Solid content	100	%

Table 3: Specifications for the Hardener GL 2

The fibres used in this work are carbon fibres, which are of the non-crimp type. We know that fabrics can be produced by laying several plies into a stack of required thickness. The fabrics can be a non-crimped or warp knitted type. "Non-crimp" is a term that refers to fabrics where one or multiple layers of the fibres are laid upon each other and transformed into a fabric by stitching or application of binder, such that the fibres remain straight and without substantial crimp. Non-crimp fabrics are cheaper to produce per unit mass and faster to manufacture. Such composites have potential for use in applications like production of wing skins. The fibres (commercial name: PYROFIL^{TM}TR505 15K)

were procured from "R&G Faserverbubdwerkstoffe GmbH". As per the manufacturers catalogue the fibre has the following properties; Modulus 240 GPa, tensile strength 4900 MPa, elongation at break 2%, density 1,82 g/cm^3 and areal density of 200g/m^2.

3.1.2 COMPOSITE PANEL PREPARATION

The method adopted for the preparation of the composite panel was the wet lay-up technique. This is a quite simple method and has few advantages when compared to other technique and they are; low cost tooling, wide choice of suppliers and material types, higher fibre content and longer fibre. Typical applications include wind-turbine blades, boat structures, architectural mouldings etc. We prepared two set of specimens; the first set numbering three contains no nanotubes in the matrix material, while the second set numbering three has 0.3 wt% of nanotubes in the matrix material. First we had the template cut from a cardboard with dimensions 160X120mm. This would help in cutting the fibre mat as per the template dimension from the fibre roll supplied by the manufacturer. 18 layers were cut for a single panel (we made two panels). Latter the plies/laminas were weighed. Panel 1 plies had a mass of 70.4 mg while panel 2 had a mass of 70.9 mg. The fibre weight per unit lamina area was 200 g/m^2.

Next step of the panel preparation was mixing of the matrix and hardener. The mixing ratio was 100:30 as per the manufacturer's directions. Which means we had 100 g of matrix and 30 g hardener mixed for each of the panel. The first mixture (for panel 1) was hand stirred in open air until both the epoxy and hardener mixed well. Next for the mixture of panel 2 we weighed approximately 0.39 g of multi-walled carbon nanotubes (0.3 wt%). The MWCNTs were dropped into the mixture and hand-stirred in a vacuum container until no visible agglomeration was noticed. Uniform distribution of CNTs in the matrix material forms an important part of material preparation. Ajayan et al [Ajayan et al., 1994] reported a simple method to produce aligned arrays of CNTs into the epoxy matrix. MWCNTs produced by arc-discharge method and purified in ethanol were randomly dispersed in a liquid epoxy resin by mechanical mixing with glass rod. Transmission electron microscopy (TEM) images of the thin slices cut from the composite showed that the thinner and longer nanotubes were preferentially oriented along the cutting direction, though the thicker tubes had random orientation. Most of the tubes were adhered to the polymer matrix, and the directional cutting process created shear that induced the flow of the tubes. The tubes on the surface were deformed during cutting process and were oriented unidirectionally on the newly formed surface. The weak interfacial bond

between tubes and matrix was apparent from the unbroken and straightened CNTs after cutting process. [45] Here as can be inferred a glass rod was used to mix CNTs in the matrix, but we had the CNTs mixed under vacuum condition and thereby notice the possible outcomes.

Next we had the mould cleaned with thinner and latter wax was applied on the same, wax would enable the panels to be removed without much difficulty. Appropriate markings were done on the mould so as to accurately place the laminas. Latter the mould, along with the matrix system were preheated to 50^0C. The viscosity of the matrix system reduced to some extent. Latter we prepared the panels by placing one lamina after the other and applying the matrix system after placing each layer. Excess matrix was squeezed away using a roller. After placing nine layers a polyester pre crack foil approximately 68mm long (table 4) and 0.1mm thick was placed. Latter the remaining layers were added on. Thus in total we had 18 layers per panel. The upper mould plate was placed in position and tightened. The temperature was raised to 80^0C and cured for 24 hours. The moulds were thermally insulated by placing a blanket over the moulds.

3.2 PREPARATION OF THE SPECIMEN

Specimens that were approximately 142 mm long, 24 mm and 4 mm thick were cut from the above prepared laminates according to ASTM D 5528-01. [46] The length of the de-lamination initiation was approximately 68mm. Before the actual start of the experimental work we applied white paint at both edges of the specimen to aid visual detection of the de-lamination propagation in the specimen. We used a red marker to mark lines on the paint exactly 5 mm apart to measure the length of the crack propagation. And we used plastic hinges on both top and bottom of the specimen instead of metal to insulate the sensor from the unwanted electric signals, which was a recurring problem when we used the first specimen were the hinges were made of aluminium. The plastic loading hinges were glued using an epoxy adhesive paste. The loading point was approximately 18 mm from the free end of the specimen, thus giving a nominal initial crack length of approximately 68 mm. The fibre volume fraction was calculated using the relation $V_f = \frac{Nm}{h\rho_f}$ were N is the number of plies, m the areal density, ρ_f density of fibres and h the thickness of the specimens[15]. Figure 21 shows the specimens that were used in this work. Table 4 shows detailed specimen dimensions and other details.

a)

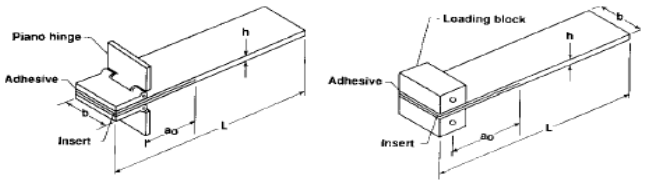

b)

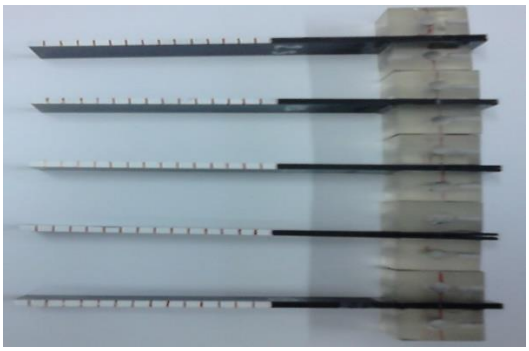

Fig 21.a) Specimen as per ASTM 5528-01, the first is the case of a piano hinge, the second is with loading blocks. b) Specimen with an edge painted white to aid visual detection of de-lamination, the black lines are 5 mm apart.

Sl. No	L1 (mm)	L2 (mm)	L3 (mm)	W (mm)	T (mm)	T1 (without foil)	Mass(g) ±0.1g	Mass(g) ±0.0001g	Mass-foil (g)	Mass-no foil (g)	Fibre Volume fraction (%)
1.1	18.75	50.08	142.81	24.98	3.82	3.72	19.7	19.6370	0.2370	19.4000	53.17
1.2	17.51	50.23	142.78	24.97	3.76	3.66	19.6	19.5500	0.2330	19.3170	53.97
1.3	18.46	50.42	142.78	25.04	3.77	3.67	19.5	19.4532	0.2380	19.2152	53.89
2.1	17.58	49.95	142.33	25.06	3.78	3.68	19.4	19.3199	0.2340	19.0859	53.75
2.2	18.28	50.03	142.22	24.88	3.78	3.68	19.5	19.4730	0.2350	19.2380	53.75
2.3	17.5	49.9	142.43	24.96	3.80	3.70	19.6	19.5626	0.2320	19.3306	53.46

Table 4: Specimen dimensions, along with the masses and fibre volume fraction. (Appendix A-2)

3.3 MODE-I INTER-LAMINAR CRACK PROPAGATION TEST

We had the specimens made as per ASTM D 5528-01. The specimens were loaded on a 50 *k*N capacity servo-drive controlled screw driven load frame. The opening forces were applied to the DCB specimen with loading blocks glued on both side of the specimen as shown in fig 28 a. The end of the DCB is opened by controlling the crosshead movement. The tests were carried out with a displacement speed of 5mm/min, while the load and delamination length were recorded. Figure 29 shows the experimental setup. Initially as per standard ASTM 5528, we loaded the specimen at a cross-head speed of 5mm/min upto a crack length of 5mm from the pre-crack to see if there is any unstable de-lamination growth from the insert. Latter the specimen was unloaded following which we loaded it again at a constant cross-head speed of 5mm/min.

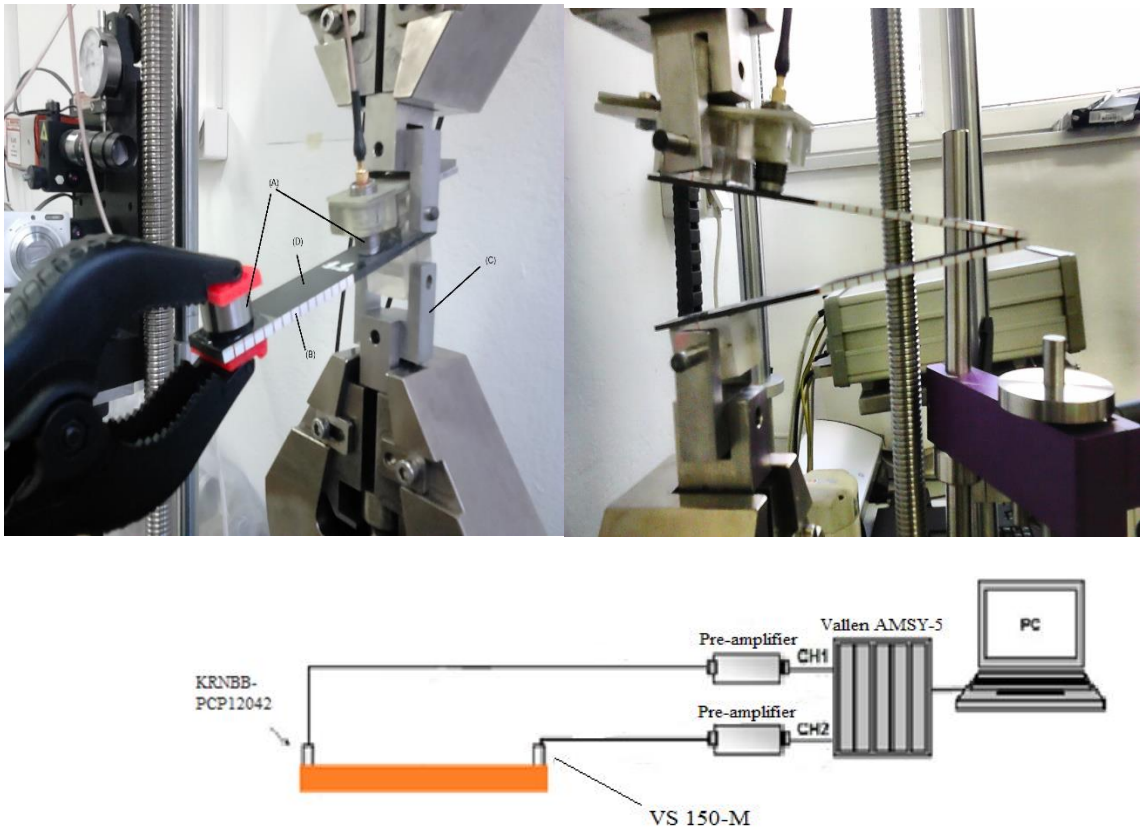

Fig 22. A) AE sensors; b) scale; c) Loading hinge; d) specimen.

Acoustic signals were captured during the loading of the DCB test specimen as shown above. A Vallen-Systeme GmbH acoustic emission measurement system AMSY-5 (Vallen-Systeme GmbH,

Icking, Germany) was used to capture and analyse the AE signals at 5 MHz sampling frequency. Two sensors namely a piezoelectric AE sensor VS150-M with a measuring range between 100 and 450 kHz and resonance at 150 kHz was mounted on the far side of the specimen and a SteveCo KRNBB-PCP12042 wide band sensor with a frequency ranging from 100kHz to 2.5MHz was mounted near to the loading blocks as shown in fig 29. Before mounting, a non-melt silicone compound for isolation and waterproofing of electronic devices (sensors) was applied at the location were the sensors were fixed. This material was provided by Sigill, Sili grass. These sensors are widely used in AE measurements and are of low cost when compared to other kind of sensors like capacitive, electro-dynamic or laser-optical sensors. Piezoelectric sensors can measure ultrasound with a sensitivity of 1V/nm as displacement sensors and a few V/(mm/s) as velocity sensors. The dynamic amplitude range of PZT sensors is around 120 dB. Another useful property of these sensors when measuring ultrasound is that these sensors measure only the dynamic events and hence automatically compensate for low-frequency motion of measuring objects that are caused by environmental vibrations. This essentially low-frequency cut-off is a consequence of the leakage of the accumulated charge. This act as a high-pass filter that determines the low frequency cut-off (compensational bandwidth) through a time constant given by the capacitance and resistance of the device [47], and also PZT sensors are insensitive to electromagnetic fields and radiation, thus enabling measurements under harsh conditions.[40] The construction of such a sensor is shown in fig 20 a, under section 2.3.7.7. The sensor also covers frequency characteristics for AE signals generated during plastic deformation and fatigue. [40] The sensors were connected to the AMSY-5 measurement system via two AEPF pre-amplifiers (Vallen-Systeme GmbH, Icking, Germany) with a gain of 40 dB. The amplitude threshold was set up at 40 dB. Vallen-Systeme provides a custom made software for analysing the wave-forms which also records the data. During loading of the specimen the process was filmed to understand the crack propagation, and also to help in the calculations of inter-laminar fracture toughness and other parameters.

3.4 DETERMINATION OF INTER-LAMINAR FRACTURE TOUGHNESS

As per the ASTM 5528-01[46] three methods are available for determination of determination inter-laminar fracture toughness and they are; **M**odified **B**eam **T**heory (MBT), **C**ompliance **C**alibration method (CC) and **M**odified **C**ompliance **C**alibration method (MCC). Since all these methods gave values not differing by more 3.1% all these methods could be used. But MBT is preferable since it

gave a more conservative value for 80% of the specimens tested. Hence in this work we would be using MBT.

The beam theory expression for strain energy release rate of any perfectly built-in double cantilever beam is given by the following expression;

$$G_I = \frac{3P\delta}{2ba} \tag{30}$$

Where P is the applied load, δ is the load point displacement, b is the specimen width, and a de-lamination length. But in practise the above equation doesn't hold good since all beams are not perfectly built in. Hence we correct this by adding an absolute value of Δ to de-lamination length thus treating the DCB, as if it contained a longer de-lamination. Δ is determined experimentally by generating least square plots of cube root of compliance, $C^{1/3}$, as a function of delamination length as shown in the figure below. The compliance is the ratio of load point displacement to that of the applied load i.e. δ/P. Therefore the graph shown below is to be obtained from the load displacements corresponding to the visually observed delamination onset on the edge and all the propagation values. Thus the above equation can be modified by incorporating | Δ |. As P reaches its critical value P_C, the crack starts propagating. The corresponding G_I value would be critical energy release rate G_{Ic} and this is a material characteristic that represents the fracture toughness of the cracked interface. Based on an energy criterion, G_{Ic} gives an estimation of the amount of energy absorbed during crack growth. [28]

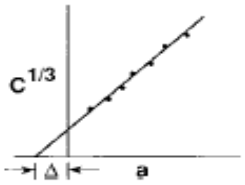

Fig 23. Modified beam theory [46]

$$G_I = \frac{3P\delta}{2b(a+|\Delta|)} \tag{31}$$

The modulus can be determined as per the following expression;

$$E_{if} = \frac{64(a+|\Delta|)^3 P}{\delta b h^3} \tag{32}$$

4 RESULTS AND DISCUSSION

This chapter would be divided into two parts. The first part would be an elaboration on the results of the mechanical performance of the composite material with and without nanotubes. The second half would deal with analysis of acoustic data for specimen number 1.3, 2.3 and occasionally other specimens when required. The wavelet transforms would be generated for these specimens, for the first few hits and would be analysed to understand the kind of damage the composite undergoes. The S0 and A0 mode would be studied using these wavelet transforms and a correlation would be made by keeping table 1 as a reference. Finally the results would be substantiated with the microscopic images captured after the experiments were conducted using a scanning electron microscope (SEM).

4.1 MECHANICAL PERFORMANCE OF THE COMPOSITE MATERIALS

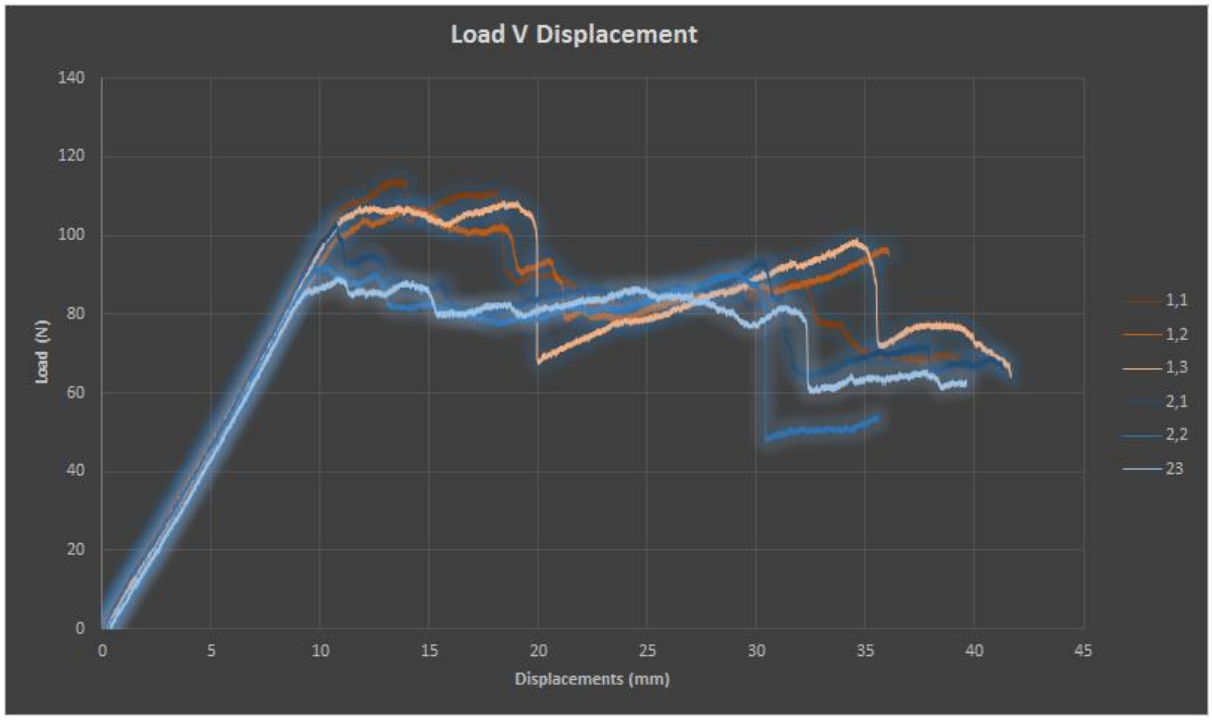

Fig 24: Load displacement curve

Figure 24 and 25 details the influence of carbon nanotubes on the mechanical performance of carbon fibre composite materials. Figure 24 is the load-displacement curve obtained while studying the mode-I inter-laminar fracture toughness of the DCB specimens. Initially there is an increase in load for all the specimens studied and the slopes are similar because same pre-crack length was used for all the specimens. This gradual increase in load is followed by a sudden decrease in load which marks the initiation of crack, this was the case with specimens without nanotubes. It was observed that after this initial drop the load increased considerably but lesser than the previously attained maximum loads in all the specimen studied. For instance in specimen 1.1 the load increased upto 113N before dropping to 103N, but latter increased to 111N. The abrupt load decrease was earlier in case of specimens without nanotubes (1.1, 1.2, and 1.3) while those with nanotubes (2.1, 2.2, and 2.3) the load decrease was found in a later stage. For instance if we take the case of specimen 2.1, though initially there was a load decrease as in all specimens but this decrease was not abrupt in those without nanotubes. After the initial negligible drop from a maximum of 98.15 N to 94 N, there was gradual decrease of load and later a gradual increase in load with intermediate negligible load drops until it reached a maximum of 92 N. From this it could be inferred that the crack growth was smooth and hence there could be fibre bridging provided by the nanotubes. This phenomena was not observed in the case of specimens 1.1, 1.2 and 1.3. In these specimens the curve looked rather unstable. But, these specimens could withstand more load before initiation of crack growth when compared to those with nanotubes. From this it could be inferred that there is considerable degradation in either the mechanical or chemical properties of the matrix material. In another study conducted in [4] and [16] there was considerable increase in load bearing capability of the material with nanotubes. Perhaps this could be attributed to a proper/homogenous dispersion of CNTs in the matrix by using a calendaring machine consisting of three rolls, which generates a high shear force by controlling the spacing between them and their speed. This helps in the exfoliation of CNTs from their pristine bundled microstructure.

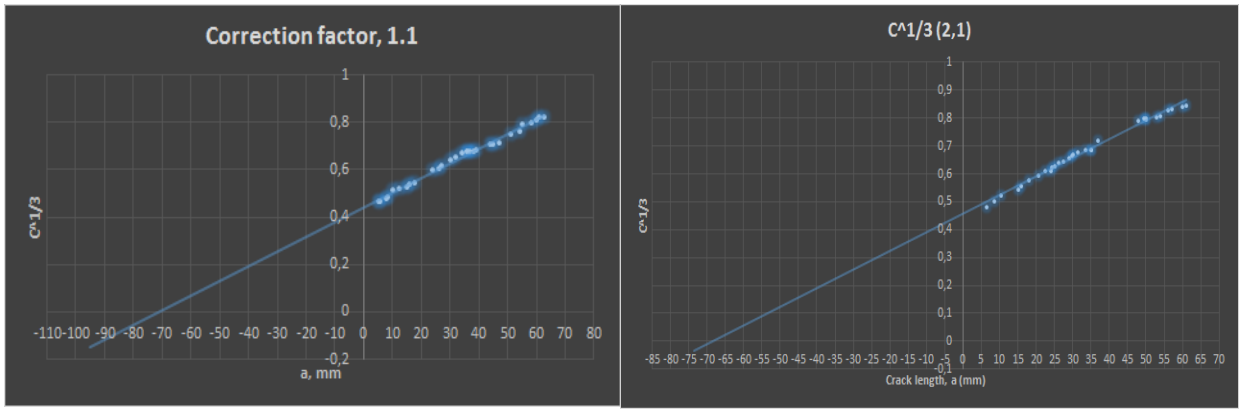

Fig 25: Correction factor for specimen 1.1 and 2.1, for 1.1 its 70 and for 2.1 its 69

Specimen	Correction factor Δ
1.1	70
1.2	72.5
1.3	72
2.1	69
2.2	62.5
2.3	65

Table 5. Correction factor

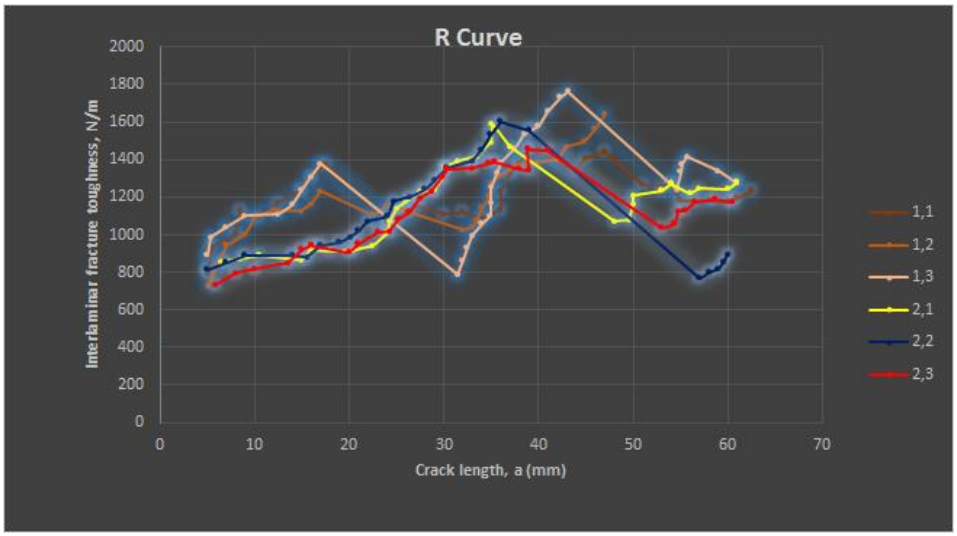

Fig 26: R-curve

Figure 26 shows the R-curve (resistance curve) which is a plot of inter-laminar fracture toughness versus the crack length. The beam compliance theory was used to calculate the inter-laminar fracture toughness G_{Ic}[46]. Table 6 elaborates on the percentage increase in G_{Ic} for crack initiation. G_{Ic} at crack initiation could be defined as the point of sudden decrease in load as shown in the load displacement curve (fig 24). The G_{Ic} was calculated using equation (31). In this equation the correction factor Δ was determined from the least square plots of the cubic root of compliance $C^{\frac{1}{3}}$ against crack length a for all the specimens. Figure 25 shows a plot of compliance versus crack length for specimens 1.1 and 2.1. The correction factor for all specimens is as shown in table 5. From the resistance curve it is evident that the G_{Ic} increases initially followed by a drop, the reason behind this resistance to de-lamination is the development of fibre bridging. From the curves it's evident that those specimens with nanotubes i.e 2.1, 2.2 and 2.3 offered the most resistance to de-lamination as is evident from the increasing inter-laminar fracture toughness. From table 6 it could be inferred that the maximum increase in G_{Ic} was for specimen 2.1 with respect all the specimens without nanotubes, while in 2.2 and 2.3 it was modest and , in few instances the G_{Ic} dropped to as low as -17.53% in the case of 2.3 with respect to 1.3. The reason for this increase in only specimen 2.1 couldn't be well understood since 2.n series were all cut from the same panel. But there was also an increase of 8.52% for 2.2 with respect to 1.1 and 12.83% for 2.2 with respect to 1.2. From these observances it could be hypothesised that some nanotubes in the matrix system may have agglomerated while some may have dispersed more uniformly. We stirred the matrix system with nanotubes in vacuum container until no visible agglomeration was observed. The more uniformly dispersed CNTs would have bridged the growing crack than the agglomerated CNTs. But this positive increase in inter-laminar fracture toughness is at the expense of reduced load bearing capacity (figure 24). But as previously mentioned using calendaring machine or any other efficient way of mixing CNTs would have produced a better results.

Specimens G_{Ic}(N/m)	2.1 (855.74)	2.2 (813.23)	2.3 (733.19)
1.1(749.37)	+14.19%	+8.52%	-2.15%
1.2(720.71)	+18.73%	+12.83%	+1.73%
1.3(889.14)	-3.75%	-8.53%	-17.53%

Table 6: Comparison of G_{Ic} increase in specimens 2.n with respect to specimens 1.n.

The G_{Ic} for crack propagation is another important aspect to be looked into. It was evident form the resistance curve that the inter-laminar toughness for propagation was higher in the case of those specimens with nanotubes. This shows considerable resistance to delamination during crack propagation probably due to fibre bridging. Among the specimens without nanotubes only 1.3 showed similar behaviour. After an initial fall the G_{Ic} tended to increase and reached values higher than the specimens with nanotubes. This was an important observation since specimens 1.1 and 1.2 showed unstable crack growth but the increase in G_{Ic} in 1.3 could be the result of effective bridging provided by the carbon fibres. These observations are partially true when compared to literature. Since in many literatures there were instances where the G_{Ic} for crack initiation and propagation was much higher than those reported here. The appropriate reasons for this increase was due to the method adopted to mix the nanotubes in the matrix like the use of calendaring machine or the use of functionalised nanotubes. For the sake of prudence, along with the modified beam theory, the modified compliance calibration method and compliance calibration method was also implemented to determine the inter-laminar fracture toughness. These methods are elaborated in appendix (A-4) and (A-5). In case of modified compliance calibration method the results obtained were in stark contrast to what we obtained using modified beam theory. While modified beam theory showed a positive result for specimens with nanotubes, but the modified compliance calibration method showed positive result in the context of specimens without nanotubes. But the percentage increase in inter-laminar fracture of specimens without nanotubes were not very large. In the case of compliance calibration the results seems to be more exaggerated like in one case the G_{Ic} at initiation was 52.64% and this was in the case of specimen 2.1 with respect to 1.2. Therefore, it is only modified beam theory that gave a more appropriate values for G_{Ic}.

Next we also calculated the modulus using equation (32). This formula is independent of the crack length, but the general trend was an increase in the modulus as the crack length increased. This was due to fibre bridging. As is evident from figure 7 (appendix A-1), the modulus for 2.n series dropped considerable when compared to 1.n series. This solidifies the assumption that the addition of CNTs degrades the material properties to some extent.

4.2 ACOUSTIC SIGNAL ANALYSIS

This section would elaborate on the classification of AE (lamb waves) events by visually examining the waveforms and wavelet contours. The wavelet contours would be generated using AGU-Vallen

Wavelet solver. The waveforms would be classified into three types. Class A will denote matrix cracking, Class B will denote fibre fracture and Class C will denote de-bonding, additionally we found two groups of waves that looked quite different from the above mentioned classes and these were groped as Class AA and Class BB. Table 1 would be used as reference for this analysis. Group velocities were determined using longitudinal velocity of 2850 m/s and a shear wave velocity of 1980 m/s. [55] The Vallen dispersion solver was used to calculate the group velocities.

An example of class A is shown below. These waveforms are characterised by slow rise time of approximately 20μs. In the study conducted in [51] it was found that surface matrix cracks would excite low frequency A0 mode, while an internal crack would excite a high frequency S0 mode. And it has been stated in the same research [51] that AE events at lower stresses are characterised by low frequency corresponding with surface ply cracking and at high stresses high frequency events are noticed, this was in the context of transverse cracking. The waveforms below (specimen 1.3-left and specimen 2.3-right) is an example of a low frequency A0 mode and therefore this waveform could be assigned to that of a surface matrix cracking. The waveform represents the first hit on sensor 2 (VS 150 M), the same is true in the case of specimen 2.3. From the figure it is clear that the highest concentration of energy is in the A0 mode at a frequency of 160 kHz for specimen 1.3 at a group velocity of 1.884 m/ms and 190 kHz for 2.3 at a group velocity of 1.905 m/ms respectively. Peak frequency analysis has also been considered as an accurate way of predicting damage mechanism in composites. Interesting results were found by researchers were it was found that matrix cracking could be attributed to low frequency while fibre breakage to high frequency. [51,53] If peak frequency analysis was to be considered then the frequency response seen in figure 27 matches with the frequency found in literature for matrix cracking. This further solidifies the conviction that this is a typical scenario of matrix cracking. But from our study we could even obtain waveforms that could be assigned to internal matrix cracking i.e. a dominant S0 mode. An example is shown below in figure 28. Here it is evident that the highest concentration of energy is in the S0 mode at a frequency of 600 kHz and the group velocity was centered about 1.539 m/ms. This waveform which was registered in sensor 1 (KRNBB-PCP12042) at precisely 13 seconds cannot be ascribed to fibre breakage because as per Y.Mizutani et.al[50], fibre breakage should excite high frequency S0 mode followed by low frequency but high amplitude A0 modes, these waves would be classed as Class B signals and elaborated next. But our results for Class A contradicts the peak frequency analysis which says that high frequency signals are generated when fibre breaks. From this it can be concluded that the high frequency response for internal matrix cracking and low frequency response for surface matrix crack

lies in the modal character of the AE waveforms, therefore peak frequency analysis cannot always point out correctly the failure mechanism within a composite material.

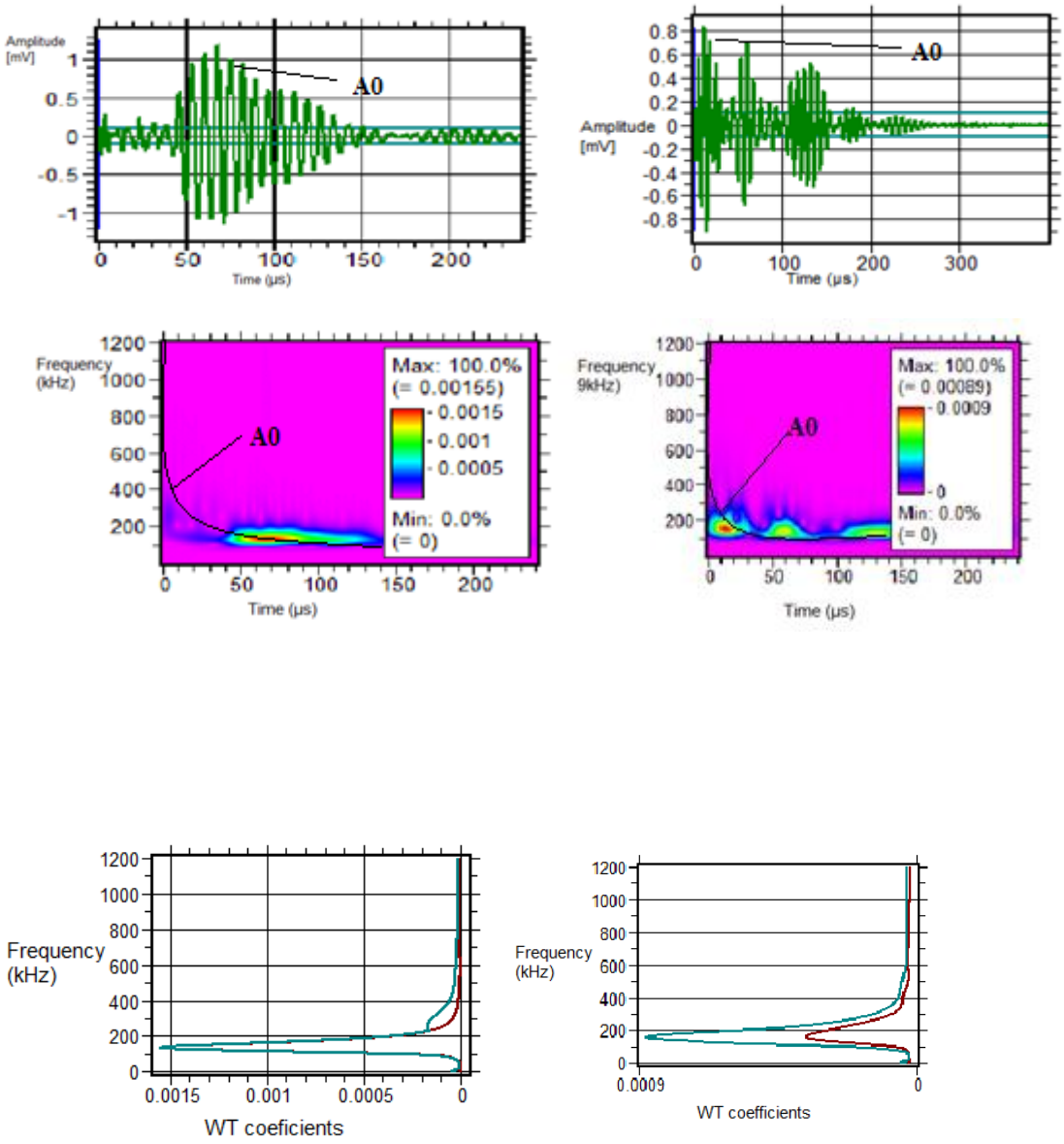

Fig 27. Waveforms, wavelet contours and frequency projections for specimen 1.3 (left) and 2.3 (right), surface matrix crack exciting low frequency A0 mode.

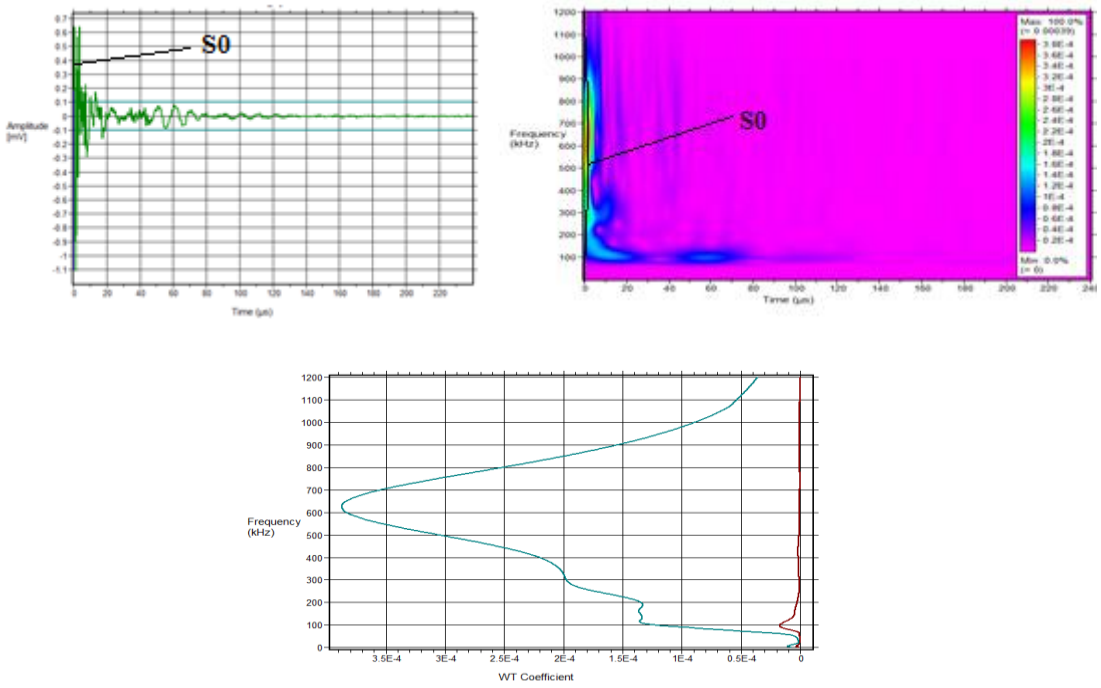

Fig 28. Waveform, wavelet contour and frequency projections for specimen 2.3, internal matrix crack exciting a high frequency S0 mode.

Class B signal here corresponds to fibre breakage. Since in this experiment we followed the ASTM 5528 standard where the crack opening mode was simulated, we don't apply any tensile force to the specimen, we don't expect many fibre breakages. But still there could be fibre breakage occasionally in the course of the experiment, those few waveforms could be analysed for fibre breakage. Y.Mizutani et.al[50] found that fibre breakage excited high frequency component initially followed by the main pulse containing low frequency with high amplitudes, which means a fibre breakage could excite both S0 and A0 modes. In another study conducted by José Martínez-Jequier et'al[48], it was found that the breakage of carbon fibre generated high frequency energy response (S0 mode) in the range of 300-500kHz. While, if the peak frequency analysis is considered the frequency range for fibre breakage lies between 400-500 kHz. [51] These observations could be used as a reference while analysing signals obtained in this experiment and predict the presence of fibre breakage in the composite material. Waveforms, wavelet contours and frequency projections (specimen 1.3 and 2.1) in the case of fibre breakage is as shown below. The waveform on the left (specimen 1.3) agrees with the waveform generated for fibre breakage in [50]. Initial high frequency component was followed by low frequency but with high amplitude. Since fibre breakage produces micro-pulses inside the

plane, the S0 mode is favoured. [48] From the figure it is evident that there is some energy concentration in the S0 mode at a frequency of 410 kHz the group velocity was cantered at 2.775 m/ms, while the highest energy concentration is in the A0 mode at a frequency of 150 kHz, but the group velocity was found to be 1.871 m/ms which is far less when compared to 2.775 m/ms, therefore this should be an A0 mode. From these observations this waveform could be assigned to fibre breakage. The same holds true for specimen 2.2 with the high frequency component at 450kHz (group velocity at 0.995 m/ms) and the low frequency component in the range of 150kHz (group velocity at 1.873 m/ms). From these observations its clearer that fibre breakage can excite both S0 and A0 modes. Peak frequency analysis can go wrong when it says that the fibre breakage excites high frequency, because as we saw in the case of class A signals were an internal matrix crack excited a high frequency response with negligible or no A0 mode. But in the case of fibre breakage both these modes are excited, with a pronounced S0 mode. But in our case the S0 mode was as not pronounced as those found in the literature because, since there the fibre were subjected to axial tensile force, eventually leading to fibre breakage. But in our case, at the most, the fibres could be subjected to bending but not breaking, this results in a lower energy content in the S0 mode. It has been hypothesised that fibre breakage produces micro-pulses inside the plane, which means the source motions are in the plane of the plate and symmetric about the mid-plane. And it has been verified that these inside-plane excitations favours S0 mode. [48] This finding along with that mentioned in [50] solidifies my understanding that the waveforms shown below could be assigned to that of fibre breakage. But we also see A0 mode accompanying the S0 when a fibre breaks. It could be hypothesised that a fibre breakage is preceded by de-bonding, as per Y.Mizutani et.al[50] findings de-bonding excites anti-symmetric flexural mode (A0). This could be the reason behind the presence of both these modes during fibre breakage. SEM images were obtained JEOL JXA-8600 super-probe. From the figure it could be seen that the fibre breakage is on a fibre that has already been de-bonded. The de-bonding of this fibre would have triggered the A0 mode and its subsequent breaking would have triggered the S0. On the right the matrix tearing could be seen clearly.

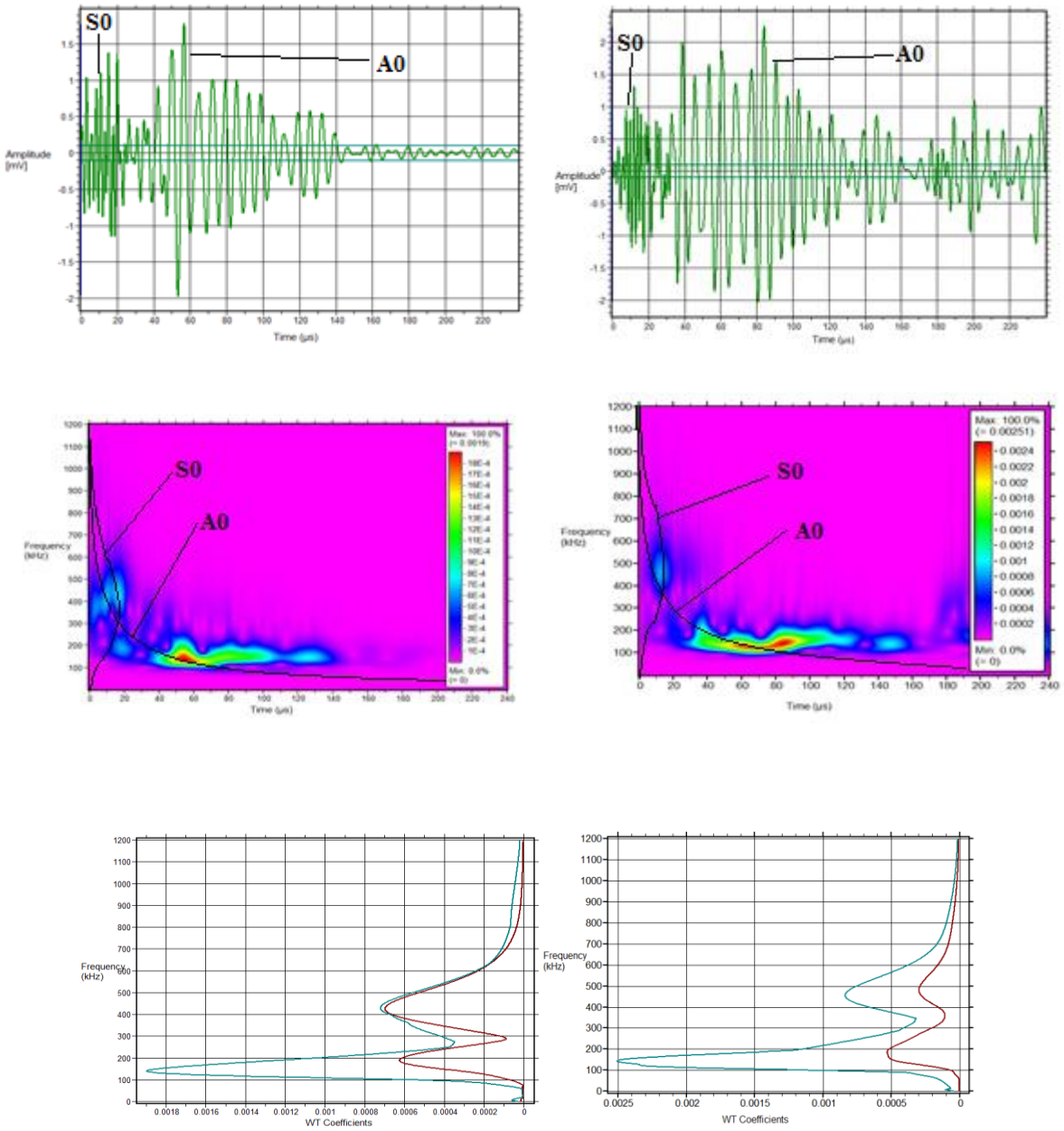

Fig 29. Waveform, wavelet contour and frequency projection for specimen 1.3 (left) and 2.2 (right), fibre fracture exciting high frequency S0 modes initially followed by low frequency high amplitude A0 mode.

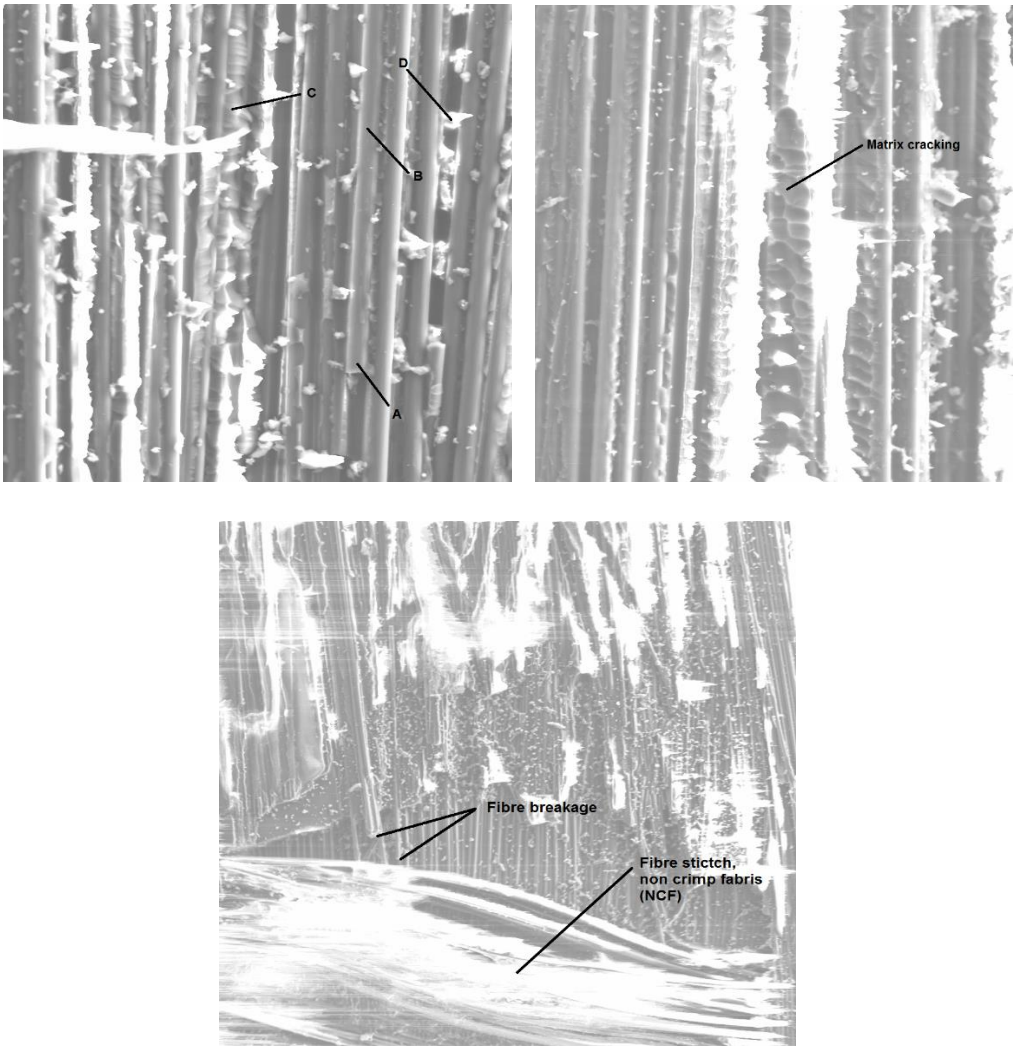

Fig 30. SEM image, on the left we have various fracture mechanisms within specimen 1.3 (a) Fibre breakage on a fibre that was de-bonded, (b) fibre de-bonding, (c) matrix cracking and (d) matrix material sticking on to the fibres, this is not a failure mechanism. On the right, we have two fibre with matrix tearing apart. Down below the fibre stitch can be seen, with broken fibres above the stich.

There was another group of signals that resembled class B signals but with stronger S0 mode lamb waves with amplitudes comparable to that of A0 mode. These were also observed in [50]. These waves would be classified as Class BB and is as shown in figure 31. Here a high energy concentration was observed in the S0 mode at a frequency hovering around 800kHz. These signals could arose confusion with regards to whether it represents fibre breakage (dominant S0 mode) or internal matrix cracking, since internal matrix crack excites S0 mode but with negligent A0 mode. But since there is a dominant A0 mode with a frequency component around 100kHz, these could be assigned to fibre

breakage. Afore mentioned hypothesis could be applied in this regard. The group velocities were found to be 1.77 m/ms for A0 mode and 1.647 m/ms in the case of S0 mode.

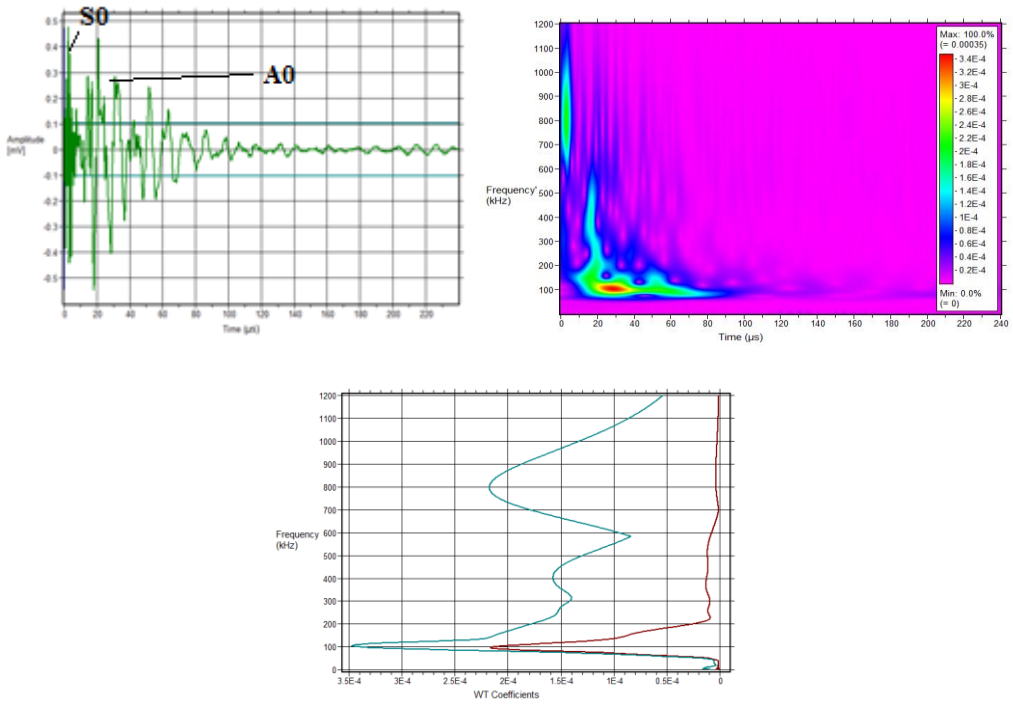

Fig 31. Waveform, wavelet contour and frequency projection for specimen 1.3.

Another set similar to Cass A signals was observed. These would be termed as Class AA (fig 32), the signal shown below was registered at five minutes and fifty eight seconds by sensor 1 (KRNBB-PCP12042). The initial arrival resembles that of class A with a group velocity of 1.766 m/ms, from the frequency these waves seems to be S0 modes, which was followed by low frequency and comparatively low amplitude A0 mode, the group velocity was centred around 1.802 m/ms. Since there is a diminished (in energy content) A0 mode, these could again be identified with matrix cracking. As per Y.Mizutani et.al[50] findings these waveforms were observed in the intermediate layers between the surface and mid-laminas.

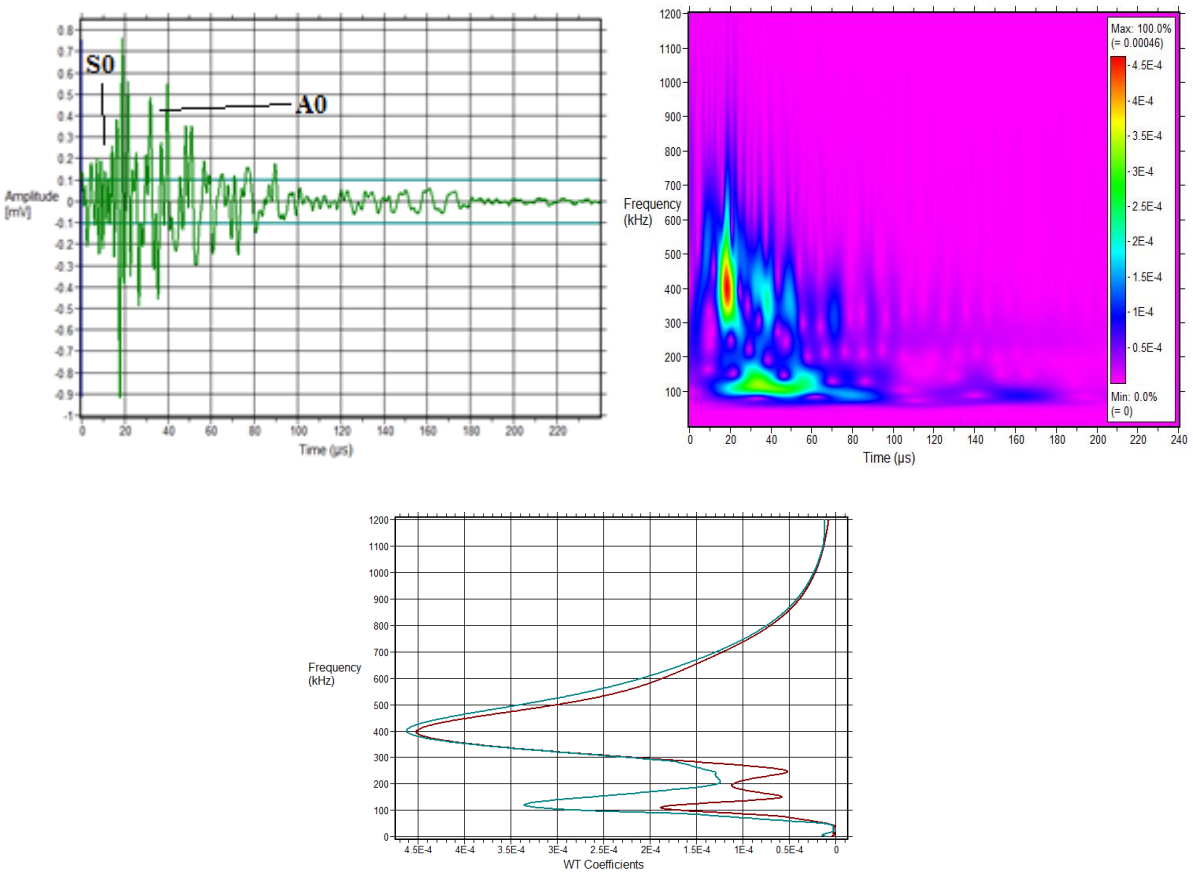

Fig 32. Waveform, wavelet transforms and frequency projection for specimen 1.2.

SEM images of failure mechanism within specimen 2.3 is shown below. In (a) one can observe a fibre on the verge of breakage. This failure should trigger S0 modes albeit with a reduced energy content. (b) is a zoomed out image of damage within the specimen. The image isn't clear enough to show clearly matrix cracking, this was due to the reduced magnification of the SEM which was 1 µm.

a)  b) 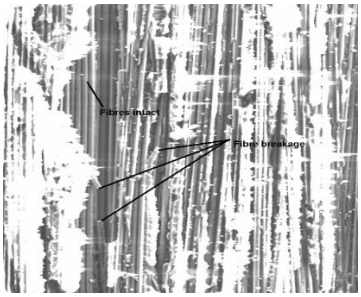

Fig 33. SEM images of fracture within specimen 2.3. a) Shows a fibre that is about to fracture, this could excite an S0 mode but with reduced energy content. b) Zoomed out image showing failure mechanisms

Another fracture mechanism observed in fibre reinforced composites is the de-bonding of fibres. Figure 30 and 33 shows de-bonding in specimen 1.3 and 2.3. Figure 33 is not clear enough because of some unforeseen situations. According to findings of Y.Mizutani et.al[50], de-bonding excited both S0 and A0 mode, with a relatively stronger low frequency A0 mode. Wavelet contours of specimen 1.3 and 2.3 were studied, and similar results were observed. In the case of both the specimens the high frequency S0 mode was followed by the A0 mode with comparatively larger amplitudes. The group velocities in both the case centred around 1.8 m/ms. There is a relationship between the de-bonding and fibre fracture as observed from the signals. In both cases there was the first S0 arrivals followed by the latter A0 modes. In the case of fibre breakage the energy content in the S0 mode was higher while the A0 could be higher or lower while in the case of de-bonding the energy content in S0 was less or negligent. Therefore it could be hypothesised that usually a de-bonding was followed by fibre breakage. When the fibre is de-bonded we see dominant A0 modes, latter if the fibre breaks we have a dominant S0 mode. Further studies needs to be conducted in this regard.

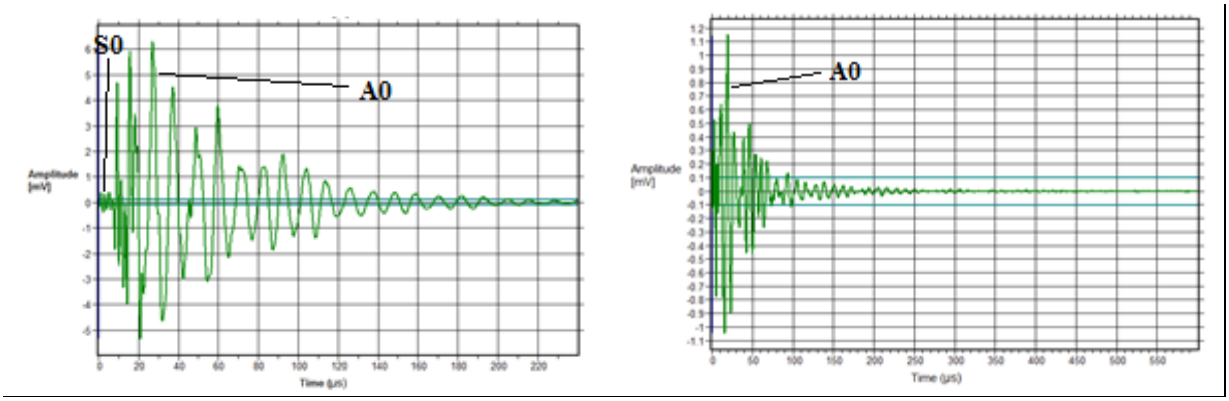

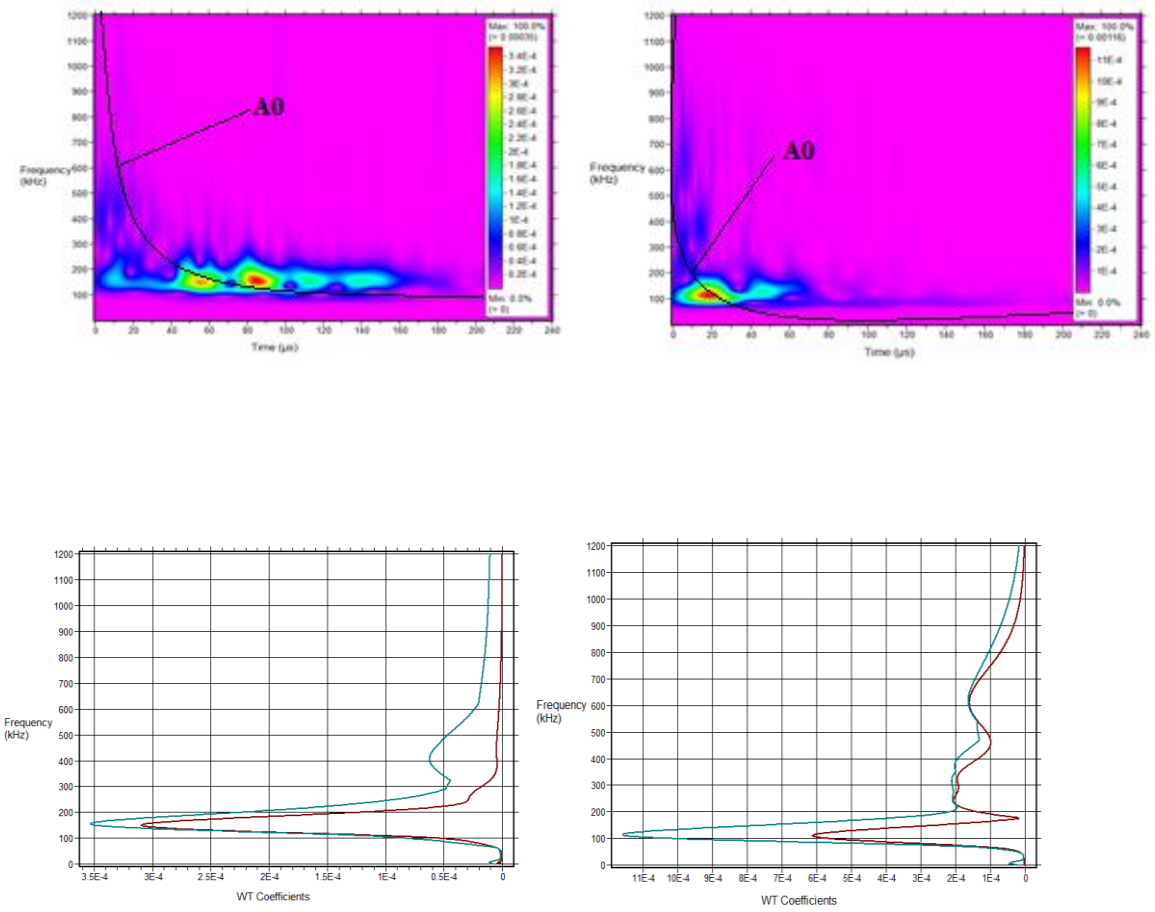

Fig 34. Waveform, wavelet contour and frequency projection for fibre/matrix de-bonding in specimens 1.3 (left) and 2.3 (right)

All the modes observed for different fracture mechanism elaborated above are detailed below in the table for different group of specimens. Note that I have classified Class AA under Class A and Class BB under Class B, since Class AA is attributable to matrix cracking and Class BB to fibre breakage respectively.

MODE	CLASS A MATRIX CRACKING			CLASS B FIBRE BREAKAGE			CLASS C FIBRE/MATRIX DE-BONDING	
	SURFACE (kHz)		INSIDE (kHz)	CLASS AA (kHz)	FIBRE FRACTURE (kHz)		CLASS BB (kHz)	FIBRE/MATRIX DE-BONDING (kHz)	
Specimen			2.3	1.2	1.3	2.2	1.3		
S0	NIL		600	400	410	500	800	NIL	
Specimen	1.3	2.3		1.2	1.3	2.2	1.3	1.3	2.3
A0	160	190	NIL	120	150	150	100	160	120

Table 7. A detailed grouping of observed signals in the specimens studied.

4.3 A GENERAL COMPARISON OF SIGNALS WITH AND WITHOUT CARBON NANOTUBES

In this section all acoustic hits from 0 to approximately 131 seconds were studied for one specimen without nanotubes and one with nanotubes. Thus we selected specimen 1.3 and 2.3. The number of hits were more for specimen 2.3 than for 1.3. To be precise there were approximately 500 hits in the above mentioned time span for specimen 2.3, while for 1.3 it was only 400. This was an important result in the context of acoustic emission signals registered for composites during their failure. The nanotubes in specimen 2.3 was contributing more hits. There could be a number of reason for such a phenomena. One reason for this increase in number of hits could be nanotube bridging the crack growth. Other reasons could be nanotubes being pulled out, and likewise many. It's quite difficult to understand the signals in the context of nanotube, i.e. signals attributable to bridging or pull out.

If we were to look into the first twenty hits lasting for approximately 15 seconds (specimen 1.3), we had signals that could be classed as the Class A signals, i.e. with slow rise time and with A0 mode dominating. This means we have a situation where the surface matrix crack is dominating of all the fracture mechanisms in this first 15 seconds interval. But, occasionally there were signals that could be classed as C signals attributable to de-bonding. There weren't any signals that could be attributable to internal matrix cracking, these signals appeared latter. But the hit registered at (fig 35) 16^{th} second could be attributable to that of an internal matrix cracking for a layer just above or below the mid-

lamina. The reason being that we have stronger S0 modes followed by A0 mode. If it were in the mid-plane we can expect a stronger S0 mode with a diminished or no A0 mode. And if it were a surface matrix crack we would get a signal with stronger A0 content in it.

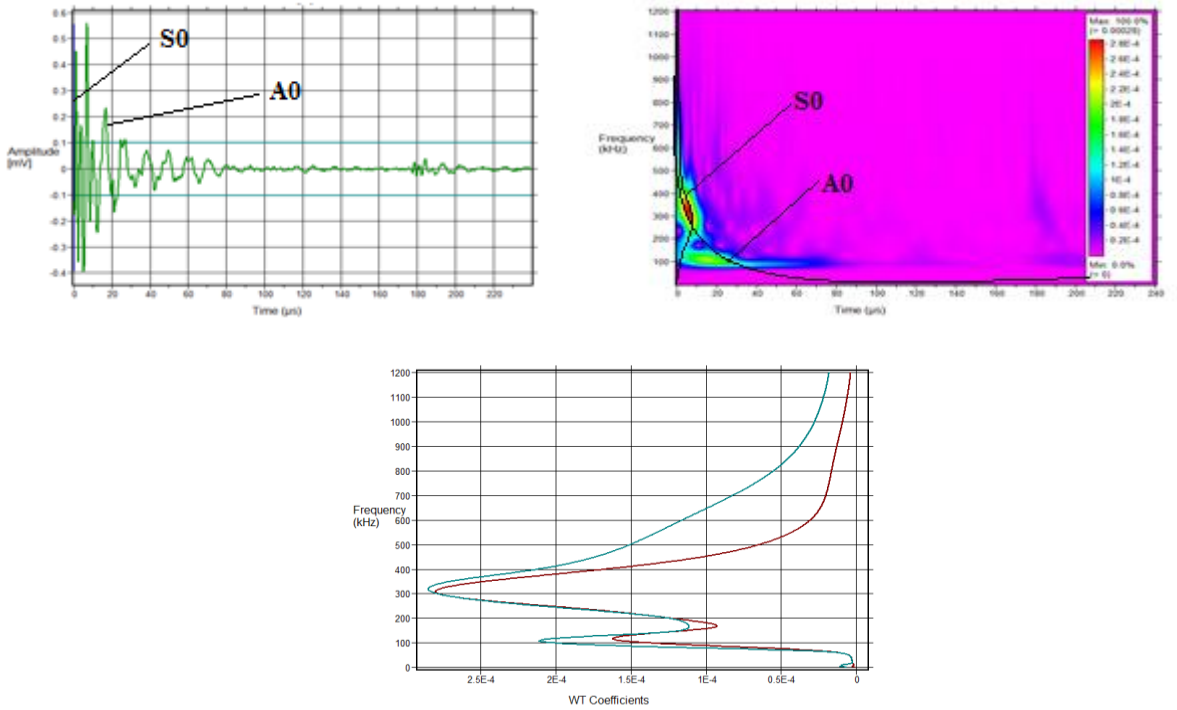

Fig 35. Waveform, wavelet contour and frequency projection for specimen 1.3 at 16 seconds

Next we considered the first 20 hits registered for specimen 2.3 which again lasted upto 15 seconds. But we noticed that the first hit was registered at 13 seconds, while in 1.3 the first hit was registered at 53 µs. Thus the 20 hits where spread over 15 seconds while in 2.3 the 20 hits were spread over approximately two seconds. This further solidifies the observation that the number of hits are larger in specimens with nanotubes in it. The possible reasons have been elaborated in the previous paragraph. The waveforms absorbed in this case was in stark contrast to the one absorbed for 1.3, where we had class A signals with slow rise time characterising surface cracks, but here we have an alternating scenario of surface cracks followed by internal matrix cracks. Figure 28 is the waveform of the second hit registered which was preceded by the hit shown in figure 27 (right). This trend continued for the rest of the hits registered upto 15 seconds. From this we could make two inferences. First the delayed crack initiation (corroborated by high inter-laminar fracture toughness), observed

from the time delay in hit registration. Second the observation that addition of nanotubes without any functionalisation could degrade the mechanical properties of the matrix material.

4.4 GENERAL ADVANTAGES OF MODAL ACOUSTIC ANALYIS OVER PEAK FREQUENCY ANALYSIS

The general advantages of acoustics in composites have been elaborated in section 2.3.1. Here the relevance of modal acoustic emission analysis over peak frequency analysis would be elaborated. Generally in many literatures it has been stated that matrix cracking excites low frequency in the range of 50-175 kHz, while fibre fracture excites a high frequency in the range of 425-500 kHz, with other failure mechanism like fibre/matrix de-bonding exciting a frequency response in the range of 200-300 kHz.[51,53] But associating a peak frequency with a particular failure cannot always be true, as elaborated in the previous sections. As one can see that high frequency S0 waves can be excited not only when fibre breaks but also when matrix cracks internally. And also fibre/matrix de-bonding as per few literature excites a frequency response in the range of 200-300 kHz. But this was not true in our case where the fibre/matrix de-bonding excited a low frequency A0 mode in the range of 100-200 kHz. In the case of peak frequency analysis one can only infer the frequency content of the entire signal but not the modal division or how the intensity of energy, particularly the frequency ranges and modes varies as a function of time. [49] This is evident from the wavelet contours generated for our waveforms. As can be seen in the case of fibre breakage, we can see the presence of both the modes, but in our case the A0 mode was dominant than the S0 mode, the reason (hypothesis) was stated. Thus, it could be said with some conviction that modal acoustic analysis presents a better idea of what really is happening within the material. While peak frequency analysis correlates peak frequencies with failure mechanism. But this method only mentions some failures at some specified frequency range which may not always be true.

But all theories have their problems so does modal acoustic emission analysis. Some of them are listed below;

1) As observed by M.A.Hamstad et.al[49], at a fixed depth (in our case the mid-plane) there was clear distinction of different fracture mode, be it inside matrix cracking, fibre fracture or de-bonding classed as signals A, B and C, there is a great likelihood of two different fracture mechanism at two different depths could have a similar wavelet contours, which is a consequence of transfer of energy between modes. This could give rise to some ambiguity in differentiating waveforms for fibre fracture

and inside matrix cracking, since both should excite a high frequency S0 mode. But by using the peak frequency analysis which specifically[51,53] states that high frequency in the range of 300-500 kHz and Y.Mizutani et.al[50] observations, we could to some extend understand which signals could be ascribed to fibre breakage. But still there could be reasons that this might prove otherwise. More research could be done in this regard.

2) Since our specimens were small we have the problem of the wavelet contours becoming quite complicated (fig 29 and 31). This was due to edge reflections [49] and this can further complicate the modal acoustic emission analysis when using smaller specimens.

5. CONCLUSIONS AND FUTURE WORK

CONCLUSIONS

The following conclusions could be drawn from this work.

- The main failure mechanism when carbon nanotubes are present in the matrix material could be attributable to fibre bridging and fibre pull out. This is confirmed by various literature surveys. Fibre bridging and pull out, positively increased the inter-laminar fracture toughness of the composite material studied.
- To validate this improvement in G_{Ic} (opening mode), experiments were conducted as per ASTM 5528. The results showed a positive increase in crack initiation values of $G_{Ic}$for those specimens with carbon nanotubes in it. The $G_{Ic}$was calculated using modified beam theory. The results showed a positive increase of 18.73% for specimen 2.1 with respect to 1.2, generally there was significant increase in 2.1 with respect to all specimens without nanotubes. It could be inferred from the R-curve that the inter-laminar fracture toughness for crack propagation was considerably higher in those specimens with nanotubes probably due to fibre bridging. For the sake of prudence we calculated the G_{Ic} using compliance calibration method and modified compliance calibration method also. It was found that modified beam theory gave a more conservative value of G_{Ic}.
- Next the AE signals were registered using two sensors, one a wideband sensor (100 kHz-2.5 MHz) while another a resonant sensor (100 kHz-450 kHz). Wavelet transforms of the signals were calculated using the solver "AGU-Vallen wavelet", latter modal acoustic emission analysis was performed to classify the signals based on the damage mechanism prevalent in the composite material during the mode-I crack opening mode. Class A & AA signals was associated with matrix cracking, Class B & BB with fibre fracture and Class C with fibre/matrix de-bonding. Information from literature, calculation of group velocities and few assumptions served as criteria based on which the signals were classified into the above mentioned classes.
- Class A was for matrix cracking, both internal and external. Energy was concentrated in the symmetric S0 mode at a frequency of 600 kHz in the case of internal matrix cracking, while in external matrix cracking energy content was in the anti-symmetric A0 mode at a frequency range of 100-200 kHz. Class AA was also associated with matrix cracking with the presence of both A0 and S0 mode.

Class B was for fibre breakage, and here both the symmetric S0 mode and anti-symmetric A0 mode was present. The energy content in the A0 mode was at a frequency of 150 kHz and in the S0 mode at a frequency range of 400-500 kHz. Class BB was also associated with fibre fracture with the presence of both A0 and S0 mode albeit with a higher amplitude in the S0 mode.

Class C was associated with fibre/matrix de-bonding, and here again there was the presence of both A0 and S0 mode, but the energy content in the S0 mode was negligible. The energy content in the A0 mode was at a frequency range of 120-160 kHz.

- From this study it can be concluded that the different frequencies, for instance in the case of matrix cracking (surface or internal) and likewise in fibre fracture which was characterised by the presence of both the modes, lie in the modal character of the AE waveforms, and thus associating a single peak frequency with a specific damage might not be an accurate way of predicting damages in a composite material.

FUTURE WORKS

In this part I would describe two area in which future works could be done in this regard. One is with respect to the nanotubes and other with respect to the AE signals. The nanotubes were introduced into the matrix material by stirring the epoxy system with a stirrer in a small vacuum chamber. While use of carbon nanotubes is limited by two issues, one is dispersibility and other effective interfacial bonding between the nanotubes and the matrix material. In the case of single-walled carbon nanotubes (SWCNTs) there is a very high possibility of agglomeration due to high specific surface area, but since we used multi-walled carbon nanotubes (MWCNTs), agglomeration is not an issue since they have less specific surface area. The main issue with MWCNTs is effective bonding with the matrix material, and this could be provided by amino-functionalisation of the MWCNTs. But before using functionalized CNTs, a high shear calendaring machine, which would enable proper dispersion. In [4] quite inter-laminar fracture toughness was obtained at crack-initiation without using any functionalised CNTs, but a calendaring machine enabled effective dispersion of CNTs. If this is not providing the necessary results we could go for an effective functionalised carbon nanotubes.

Second we could further analyse the signals. According to my co-supervisor's suggestion, different AE burst descriptors could be defined during crack propagation in composite materials. Latter in order to reduce the computational complexity and increase the performance the feature selection

method could be implemented to define a feature subset. The feature subset could be used for neural network pattern recognition of AE signals during the crack propagation in the material. A detailed description of this method is as follows;

- The first step towards characterising crack propagation in the composite material is the determination and calculation of AE descriptors for acquired AE bursts.
- These descriptors are then stacked to form a feature vector Z.
- The next step involves fuzzy C means (FCM) clustering to separate the burst characteristics for different damages involved during crack propagation like fibre breakage, matrix cracking and fibre/matrix de-bonding.
- Next a feature selection method would be introduced to select the 10-dimenaional feature subset from the 75-dimensional feature vector to improve suitability for classification.
- Latter the feature subset would be used for neural network pattern recognition of AE signals during the full span of time during crack propagation.
- Finally a classification of all input vectors and an evaluation of the proposed method to characterise the damage mechanism could be shown.

This method has been detailed in the paper titled "Wavelet packet decomposition to characterize injection molding tool damage" authored by Tomaž Kek et.al. [40]

Thus these two works are intended to be done once the thesis has been successfully submitted.

LIST OF REFERENCE

[1] Dr.Darrel R.Tenney, Dr.John G.Davis, Jr., Dr.R.Byron Pipes, Dr.Norman Johnson, et al. NASA Composite materials development: Lessons learned and future challenges. NATO Research and Technology (RTA), AVT 164-Support of composite systems, Fall-2009, Bonn

[2] P.F.Liu, J.K.Chu, Y.L.Liu, J.Y.Zheng; A study on the failure mechanisms of carbon fibre/epoxy composite laminates using acoustic emission. Materials and design 37 (2012), p. 228-235

[3] Niels De Greef, Larissa Gorbatikh, Stephan V.Lomov, Ignass Verpoest; Damage development in woven carbon fibre/epoxy composites modified with carbon nanotubes under tension in the bias direction. Composites: Part A 42 (2011), p. 1635-1644

[4] Ashish Warrier, Ajay Godara, Olivier Rochez, Luca Mezzo, Frederic Luizi, Larissa Gorbatikh, Stephan V.Lomov, Aart Willem VanVuure, Ignas Versoest; The effect of adding carbon nanotubes to glass/epoxy composites in the fibre sizing and or the matrix. Composites: Part A 41 (2010), p. 532-538

[5] P.K.Mallick, Fibre-Reinforced Composites, Materials, Manufacturing and Design; Third edition, United States of America, CRC Press, 2007, 1 p. ISBN 13:978-0-8493-4205-9

[6] Edited by Michael J.O'Connell, Carbon Nanotubes, Properties and Applications; United States of America, CRC Press, 2006, 3-8 p. ISBN 10: 0-8493-2748-2

[7] Peter Eklund, Pulickel Ajayan, Robert Blackmon, A.John Hart, Jing Kong, Bhabendra Pradhan, Apparao Rao, Andrew Rinzler. WTEC panel report on; International assessment of research and development of carbon nanotube manufacturing and application. World Technology Evaluation Centre, Inc. 4800 Roland Avenue, Baltimore, Maryland 21210

[8] Zhengtang Luo, A.T.Charlie Johnson, Alexei Matyushov; Growth of carbon nanotubes via chemical vapour deposition. With support of NSF Award no. EEC-0754741

[9]Carbon Nanotubes-Nanoparticles hybrid structure; Junhong Chen and Ganhua Lu; Internet link: < http://cdn.intechopen.com/pdfs-wm/9999.pdf>

[10] R.Guzmá de Villoria, A.Miravete, J.Cuartero, A.Chiminelli, N.Tolasana; Mechanical Properties of SWNT/epoxy composite using two different curing cycles.

[11] K.L. Kepple, G.P.Sanborn, P.A.Lacasse, K.M.Gruenberg, W.J.Ready; Improved fracture toughness of carbon fibre composite functionalized with multi walled carbon nanotube. Carbon 46 (2008) p. 2026-2033

[12] Anirudha Bagchi, Seiichi Nomura; On the effective thermal conductivity of CNT reinforced polymer composites. Composite science and technology 66 (2006) p. 1703-1712

[13] Florian H.Gojny, Malte H.G.Wichmann, Bodo Fiedler, Karl Schulte; Influence of different carbon nanotubes on the mechanical properties of epoxy matrix composites-A comparative study. Composite science and technology 65 (2005) p. 2300-2313

[14] Hongwei Yao, Xianhang Sui, Zhongbo Zhao, Zhiwei Xu, Lei Chen, Hui Deng, Ya Liu; Optimization of interfacial microstructure and mechanical properties of carbon fibre/epoxy composites via carbon nanotube sizing. Applied surface science 347 (2015) p. 583-590

[15] Niels De Greef, Larissa Gorbaikh, Ajay Godara, Luca Mezzo, Stephan V.Lomov, Ignaas Verpoest; The effect of carbon nanotubes on the damage development on in carbon fibre/epoxy composites. Carbon 49 (2011) p. 4650-4664

[16] A.Godara, L.Mezzo, F.Luizi, A.Warrier, S.V.Lomov, A.W.van Vuure, L.Gorbatikh, P.Moldenaers, I.Verpoest; Influence of carbon nanotube reinforcement on the processing and mechanical behaviour of carbon fibre/epoxy composites. Carbon 46 (2009) p. 2914-2923

[17] Peng Lv, Yi-yu Feng, Peng Zhang, Hui-min Chen, Naiqin Zhao, Wei Feng; Increasing the interfacial strength in carbon fibre/reinforced composites by controlling the orientation and length of carbon nanotubes grown on fibres. Carbon 49 (2011) p. 4665-4673

[18] Srinivasan Sridharan, Delamination behaviour in composites, United States of America, CRC Press, p 4-16 , ISBN 978-1-84569-244-5

[19] Weiping Liu, Suong V.Hoa, Martin Pugh; Fracture toughness and water uptake of high performance epoxy/nanoclay nano-composite. Composite science and technology 64 (2005) p. 2364-2373

[20] G.Ragosta, M.Abbat, P.Muslo, G.Scarinzi, L.Mascia; Epoxy-silica particulate nanocomposites: Chemical interactions, reinforcements and fracture toughness. Polymer 46 (2005) p. 10506-10516

[21] Tomohiro Yokozeki, Yutaka Iwohori, Shin Ishiwata; Matrix cracking behaviours in carbon fibre/epoxy laminates filled with cup-stacked carbon nanotubes (CSCNTs). Composites: Part A 38 (2007) p. 917-924

[22] John F.Timmerman, Brian S.Hayes, James S.Sefaris; Nanocaly reinforcement effects on the cryogenic micro-cracking of carbon fibre/epoxy composites. Composite science and technology 62 (2002) p. 1249-1258

[23] Naveed A.Siddiqui, Ricky S.C.Woo, Jang-Kyo Kim, Christopher C.K.Leung, Arshad Munir; Mode I interlaminar fracture behaviour and mechanical properties of CFRPs with nano-clay filled epoxy matrix. Composites: Part A 38 (2007) p. 449-460

[24] V.Mirjalili, P.Hubert; Effect of carbon nanotube dispersion on the fracture toughness of polymers. Internet link:

<http://iccmcentral.org/Proceedings/ICCM17proceedings/Themes/Nanocomposites/MODELLING%20&%20ANALY%20OF%20NANOCOM/E2.1%20Mirjalili.pdf>

[25] Bodo Fiedler, Florian H.Gojny, Malte H.G.Wichmann, Mathias C.M. Nolte, Karl Schulte; Fundamental aspects of nano-reinforced composites. Composite science and technology 62 (2002) p. 3115-3125

[26] Qinghua Qin, Jianqiao Ye; Toughening mechanism in composite materials; United States of America, Woodhead Publishers, p. 299, ISBN 978-1-78242-291-4

[27] F.H.Gojny, M.H.G.wichmann, U.Köpke, B.Fiedler, K.Schulte; Carbon nanotube-reinforced epoxy-composites: Enhanced stiffness and fracture toughness at low nanotube content. Composite science and technology 64 (2004) p. 2363-2371

[28] Amir Refahi Oskouei, Mehdi Ahmadi; Acoustic emission characteristics of mode I delamination in glass/polyester composites. Jouranal of composite material, Vol. 44, No.7/2010

[29] Masaki Hojo, Tadashi Ando, Mototsugu Tanaka, Taiji Adachi, Shojiro Ochiai, Yoshihiro Endo; Mode I and Mode II interlaminar fracture toughness and fatigue delamination of CF/epoxy laminates with self-same epoxy interleaf. International journal of fatigue, 28 (2006), p. 1154-1165

[30] F.Perrin, M.N. Bureau, J.Denault, J.I.Dickson; Mode I interlaminar crack propagation in continuous glass fibre/polypropylene composite: temperature and molding condition dependence. Composite science and technology 63 (2003) p. 597-607

[31] M.R'Milli, M.Moevus, N.Godin; Statistical fracture of E-glass fibres using a bundle tensile and acoustic emission monitoring. Composite science and technology 68 (2008) p. 1800-1808

[32] S.Huguet, N.Godin, R.Gaertner, L.Salmon, D.Villard; Use of acoustic emission to identify damage modes in glass fibre reinforced polyester. Composite science and technology 62 (2002) p. 1433-1444

[33] Barre.S and Benzeggagh M.L; On the use of acoustic emission to investigate damage mechanism in glass-fibre reinforced polypropylene. NDT & E International 52(3) p. 369-376

[34] T.M.Ely, E.K.Hill; Longitudinal splitting and fibre breakage characterisation in graphite/epoxy using acoustic emission data. Material evolution, 53.288-294.

[35] M.Suziki, H.Nakanishi, M.Iwamoto, E.Jinen; Application of static fracture mechanisms to fatigue fracture behaviour of class A-SMC composite. Proc 4th Japan-US Conf on composite materials 1988:297-306

[36] Barnes A.C, Ramirez G; Acoustic emission testing of carbon fibre composite offshore drilling risers. AECM-6 (Conference proceedings), San Antonio, Texas; 1998, pp. 13-22

[37] W.H.Prosser, K.E.Jackson, S.Kellas, B.T.Smith, J.M.McKeon and A.Friedman; Detection and location of transverse matrix cracks in cross-ply Gr/Ep composite using acoustic emission. ASNT Spring conference and fourth annual research symposium, pp.213-215, Las Vegas, Nevada, March 20-24, 1995

[38] William H.Prosser; Waveform analysis of AE in composites; Proceedings of the sixth international symposium on acoustic emission from composite materials, June 1998, San Antonio, pp. 661-70.

[39] Rajko Svečko, Dragan Kusić, Tomaž Kek, Andrej Sarjaš, Aleš Hančič and Janez Grum; Acoustic emission detection of macro-cracks on engraving tool steel inserts during the injection molding cycle using PZT sensors. Sensors 2013, 13, 6365-6379.

[40] Tomaž Kek, Dragan Kusić and Janez Grum; Wavelet packet decomposition to characterize injection molding tool damage. Applied Science, 2016, 6, 45; doi:10.3390/app6020045

[41] Hans Maria Tensi; The Kaiser-effect and its scientific background. J.Acoustic Emission, 22(2004).

[42] SANDIA report on "Acoustic emission non-destructive testing of structures using source location techniques" by Alan G.Beattie. SAND2013-7779, September 2016

[43] David C.Jiles; Introduction to the principles of materials evaluation, United States of America, ISBN 13:978-1-4200-0736-7

[44] Acoustic Emission Testing-Fundamentals, equipment, Application. By Hartmut Vallen. Castell-Verlag GmbH in corporation Vallen Systeme, Karl Deutsch PRÜF-UND MESSGERÄTEBAU and German society for non-destructive testing.

[45] Sreejarani K.Pillai and Suprakas Sinha Ray; Epoxy-based carbon nanotubes reinforced composites. Internet link: < http://cdn.intechopen.com/pdfs/15428.pdf>

[46] ASTM D 5528-01; Standard test method for mode I interlaminar fracture toughness of unidirectional fibre-reinforced polymer matrix composites.

[47] Požar.T, Možina.J; Detection of subnanometer ultrasonic displacements. In fundamentals of Picoscience, Sattler, K.D., ED.; CRC Press; Boca Raton, FL, USA, 2014; pp.553-578.

[48]José Martínez-Jequier, Antolino Galligo, Elisabet Suárez, Francisco Javier Juanes, Ángel Valea; Real-time damage mechanisms assessment in CFRP samples via acoustic emission Lamb wave modal analysis. Composites Part B 68 (2015) p.317-326

[49] M.A.Hamstad, A.O' Gallagher and J.Gary; A wavelet transform applied to acoustic emission signals: Part 1: Source identification. Internet link: < http://www.ndt.net/article/jae/papers/20-039.pdf>

[50] Y.Mizutani, K.Nagashima, M.Takemoto, K.Ono; Fracture mechanism characterisation of cross-ply carbon fibre composites using acoustic emission analysis. NDT & E International 33 (2000) p. 101-110

[51] Christopher Baker, Gregory N. Morscher, Vijay V. Pujar, Joseph R. Lemanski; Transverse cracking in carbon fibre reinforced polymer composites: Modal acoustic emission and peak frequency analysis. Composite science and technology 116 (2015) p. 26-32

[52] Jingpin Jiao, Cunfu He, Bin Wu, Renyuan Fei, Xiuyuan Wang; Application of wavelet transform on modal acoustic emission source location in thin plates with one sensor. International journal of pressure vessels and piping 81 (2004) p. 427-431

[53] C.R.Ramirez-Jimenez, N.Papadakis, N.Reynolds, T.H.Gan, P.Purnell, M.Pharaoh; Identification of failure modes in glass/polypropylene composites by means of the primary frequency content of the acoustic emission. Composite science and technology 64 (2004) p. 1819-1827

[54] John P. McCrory, Safaa kh. Al-Jumili, Davide Crivelli, Matthew R. Pearson, Mark J. Eaton, Carol A. Featherston, Mario Guagliano, Karen M. Holford, Rhys Pullin; Damage classification in carbon fibre composites using acoustic emission: A comparison of three techniques. Composites: Part B 68(2015) p. 424-430.

[55] Raimond Grimberg, Adriana Savin, Rozina Steigmann, Alina Bruma, Paul Doru Barsanescu, Daniel Petrica Salavastru; Determination of CFRP's mechanical properties using ultrasound methods. Internet link <http://www.ndt.net/article/Prague2009/ndtip/proceedings/Grimberg_1_Deter_10.pdf>

APPENDIXES
A-1. GRAPHS (MECHANICAL ANALYSIS)

1) SPECIMEN 1.1

Modified beam theory, a plot of cube root of compliance versus crack length to obtain the correction factor. The correction factors are listed in table 5.

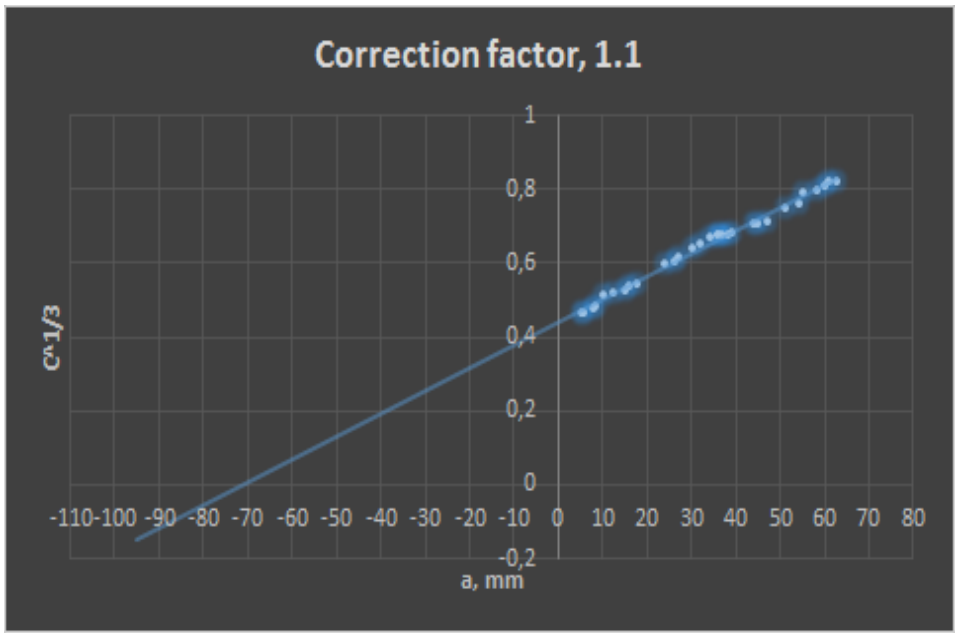

2) SPECIMEN 1.2

Modified beam theory, a plot of cube root of compliance versus crack length to obtain the correction factor. The correction factors are listed in table 5.

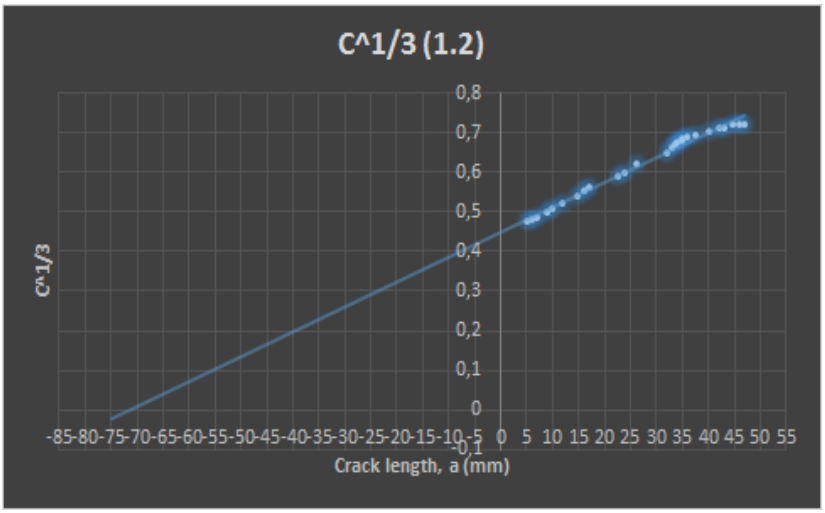

3) SPECIMEN 1.3

Modified beam theory, a plot of cube root of compliance versus crack length to obtain the correction factor. The correction factors are listed in table 5.

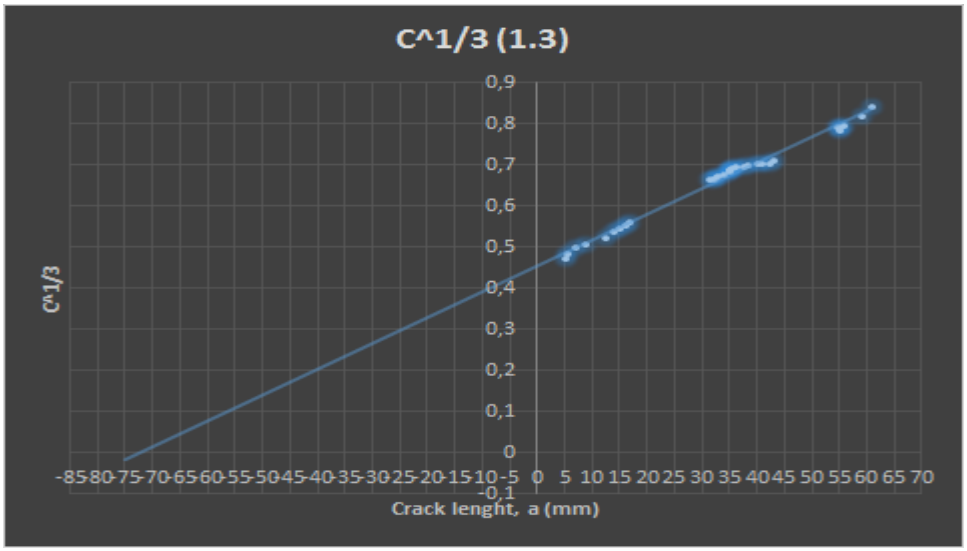

4) SPECIMEN 2.1

Modified beam theory, a plot of cube root of compliance versus crack length to obtain the correction factor. The correction factors are listed in table 5.

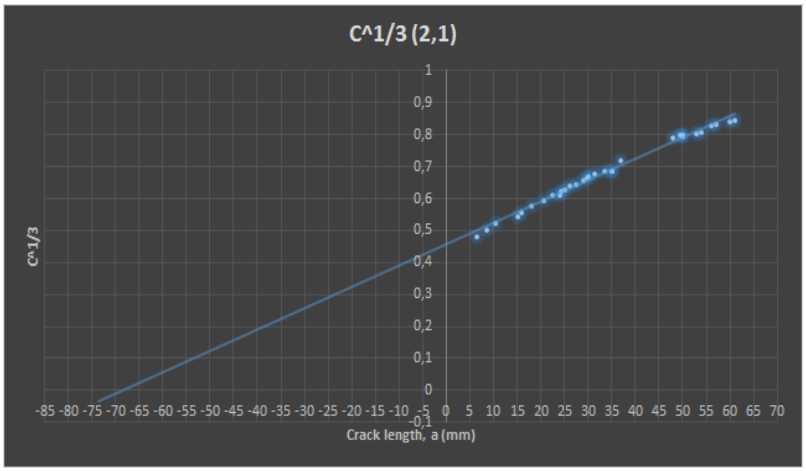

5) SPECIMEN 2.2

Modified beam theory, a plot of cube root of compliance versus crack length to obtain the correction factor. The correction factors are listed in table 5.

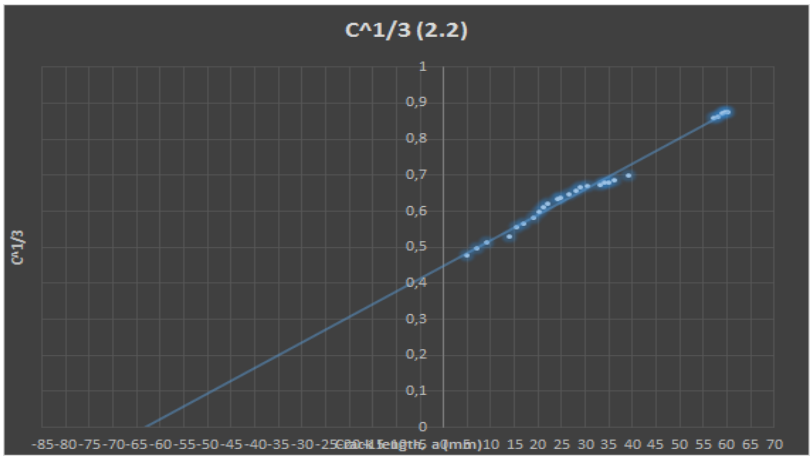

6) SPECIMEN 2.3

Modified beam theory, a plot of cube root of compliance versus crack length to obtain the correction factor. The correction factors are listed in table 5.

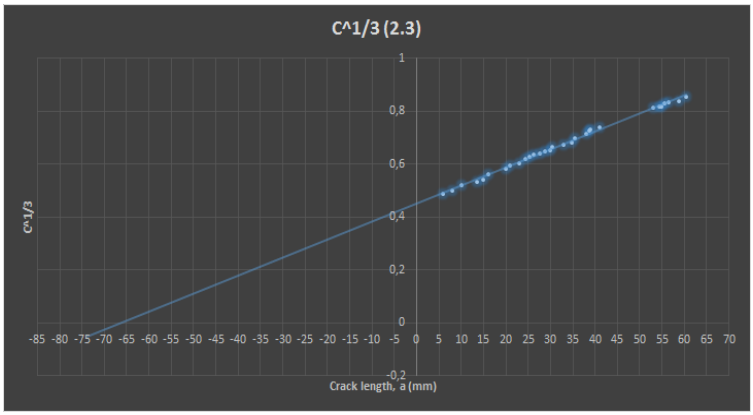

7) Plot of Young's modulus versus crack length for all specimens

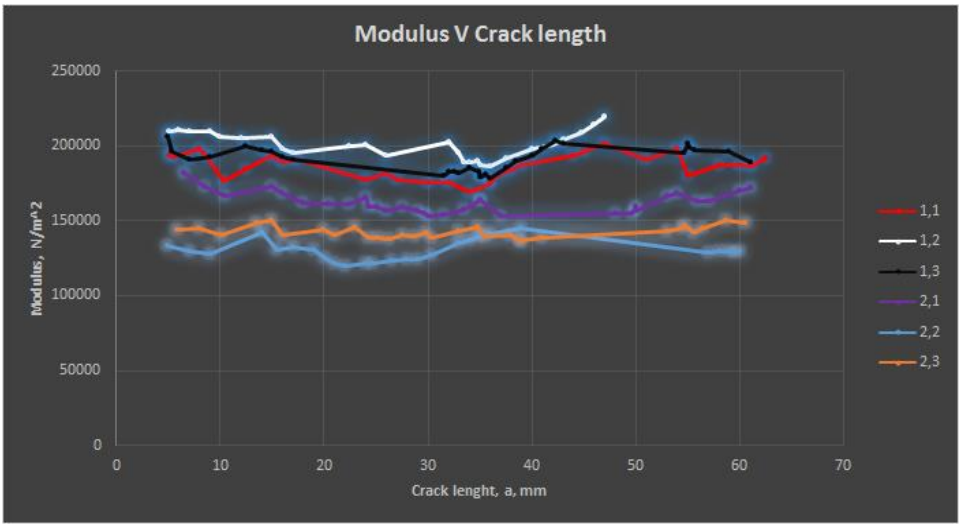

8) Plot of crack length versus displacement.

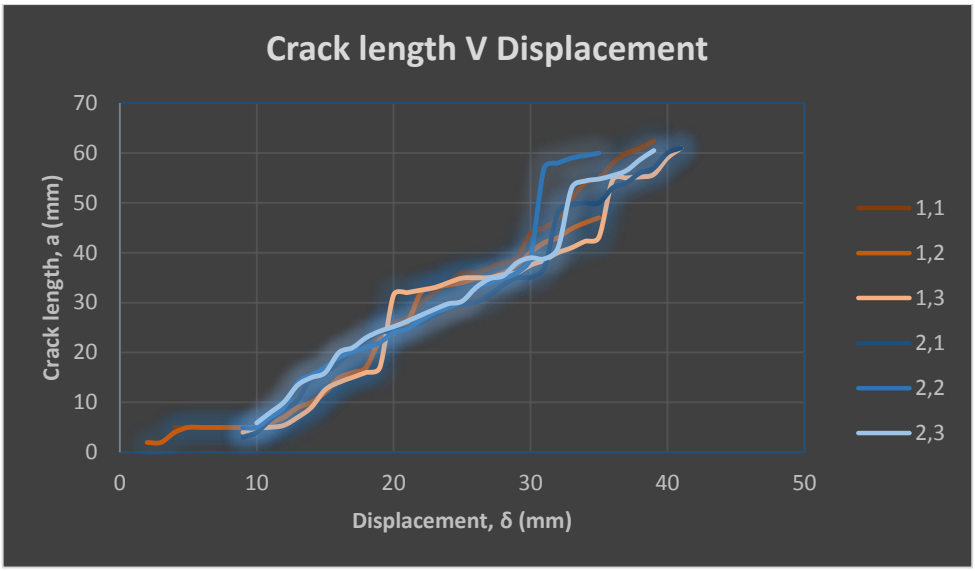

A-2. SPECIMEN DIMENIONS

The specimens were made as per ASTM 5528 standard (shown below). All dimension are in “mm”.

L1-Distance from the end of the specimen to the centre of the loading block.

L2-Distance from the centre of loading block to the end of pre-crack.

L3-Length of the specimen

W-Width of the specimen.

T-Thickness of the specimen.

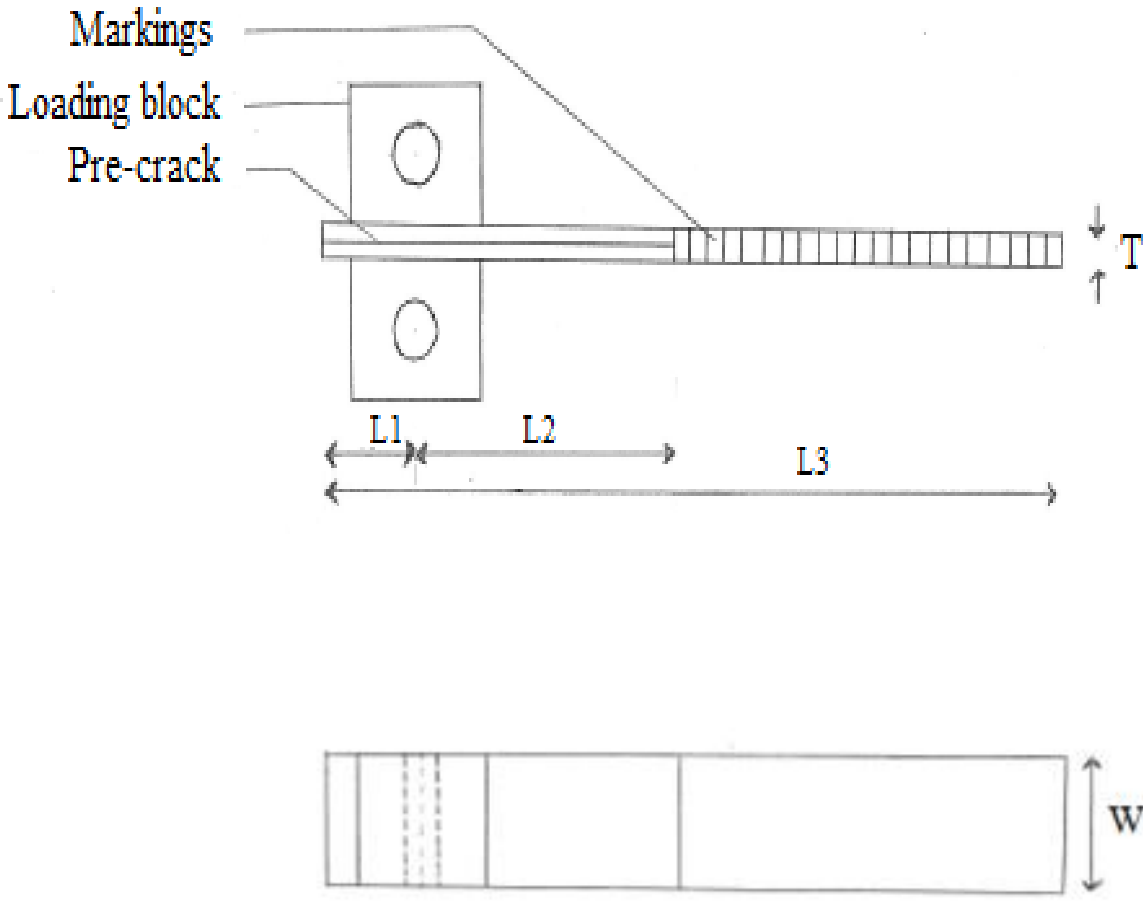

Resp. department	Technical reference	Document type		Document status		
MED		Parts Drawing		Training		
Legal owner	Created by	Title, Supplementary title	PR-00.00.001			
KTU	Sharath Peethambaran Subadra	**CARBON FIBRE REINFORCED COMPOSITE SPECIMEN**				
	Approved by		Rev.	Date	Lang.	Sheet
	Paulius Griškevičius		A	2016-05-14	En	1/1

A-3. AGU-VALLEN WAVELET SOLVER

It has been mentioned throughout the thesis about the AGU-Vallen Wavelet solver. In this section I would elaborate on how this software could be used. AGU-Vallen wavelet is a freeware software. It could be downloaded from the link http://www.vallen.de/downloads. This software was developed jointly by the Vallen-Systeme GmbH (headquartered in Germany) and Aoyama Gakuin University thus the AGU in the package name. This software uses a Gabor function as the mother wavelet with a central frequency of 7kHz. This software also allows one to determine the group velocity curves for the lowest ten modes of the infinite Lamb modes that governs the far-field wave propagation in a plate. The following paragraphs elaborates on how to the use the software.

One should keep in mind several parameters that should be selected before calculation of the wavelet transforms. Figure A-3(1) shows the setup screen for our calculations. Frequency resolution and wavelet size should be correctly selected to obtain a satisfactory resolution of the wavelet transforms.

The frequency resolution gives the frequency interval for the WT calculation. The relevance of selecting these parameters are demonstrated by figure A-3(2)a and A-3(2)b

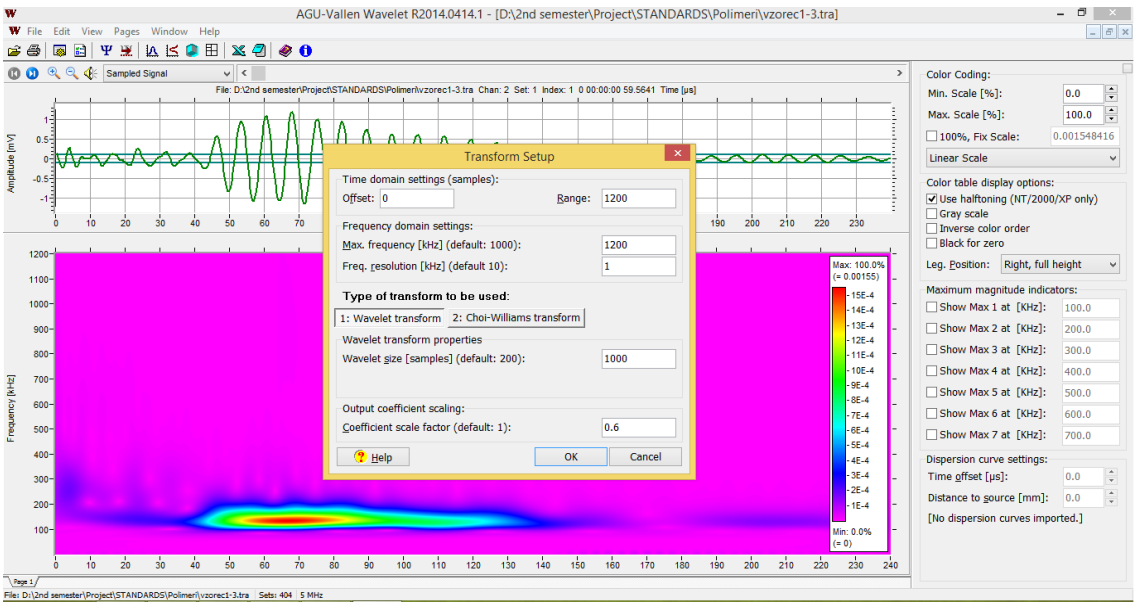

Figure A-3(1): Wavelet setup screen

Generally the solver takes a default value of 10 kHz as frequency resolution. This doesn't give a good result. Take for instance the figure shown in A-3(2)a, here the frequency resolution was 20 kHz. The 20 kHz frequency steps can be seen in the figure, but in case of A-3(2)b were we took the value as 2 kHz, we don't have the steps and hence we have a smoother result. By taking such smaller frequencies the calculation times are prolonged.

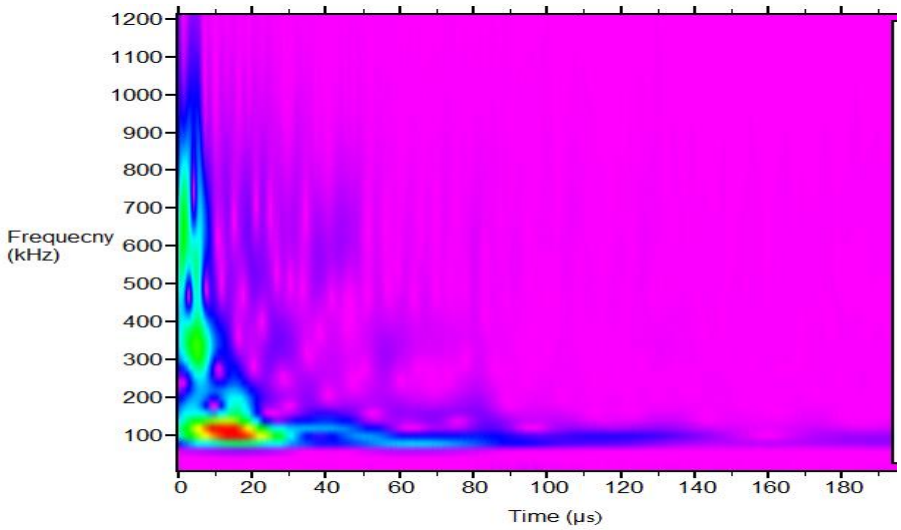

(a)

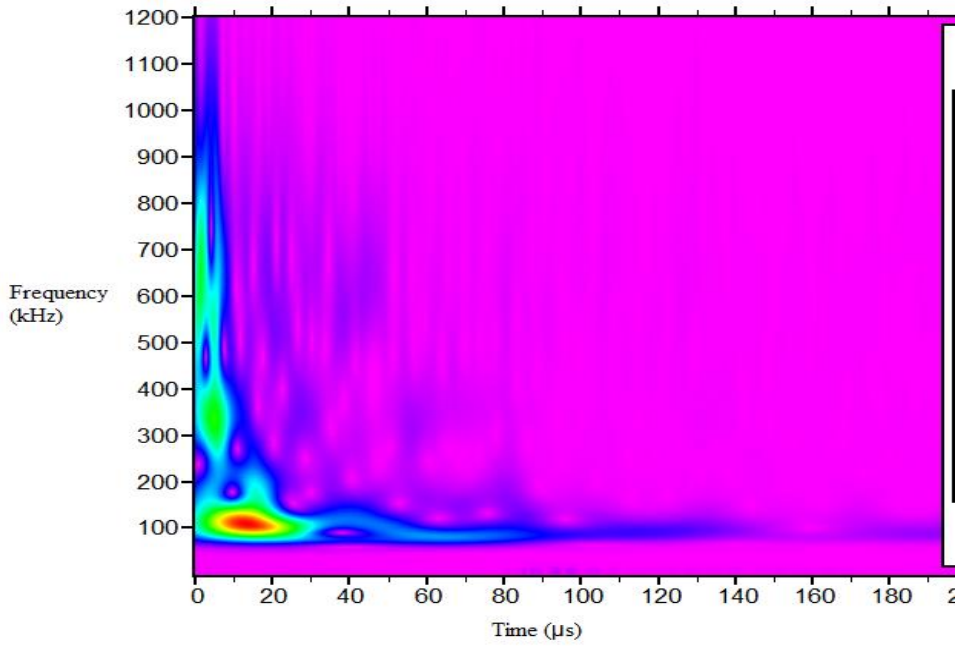

(b)

Figure A-3(2): WT results with low frequency resolution of 20 kHz (a) and high frequency resolution of 2 kHz (b).

Next the influence of wavelet size (samples) on the wavelet transforms is to be understood. The software by default takes a value of 200. Figure A-3(3)a and b shall we taken to demonstrate this. In figure A-3(3)a we considered a wavelet size of 50 with the frequency resolution being 2 kHz. One could easily distinguish the difference observed when comparing A-3(3)a and b. In fig A-(3)b also the same settings were except for wavelet size which was taken as 800. Here the wavelet transforms appeared smoother when compared to the one with 50 samples. But, this again took more time to calculate.

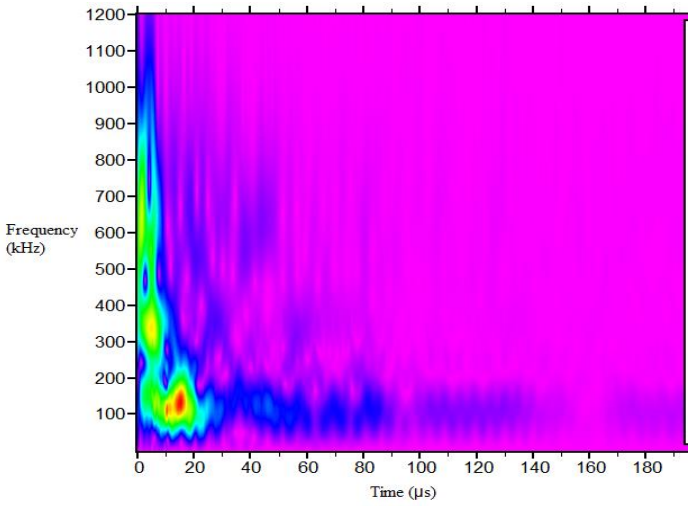

(a)

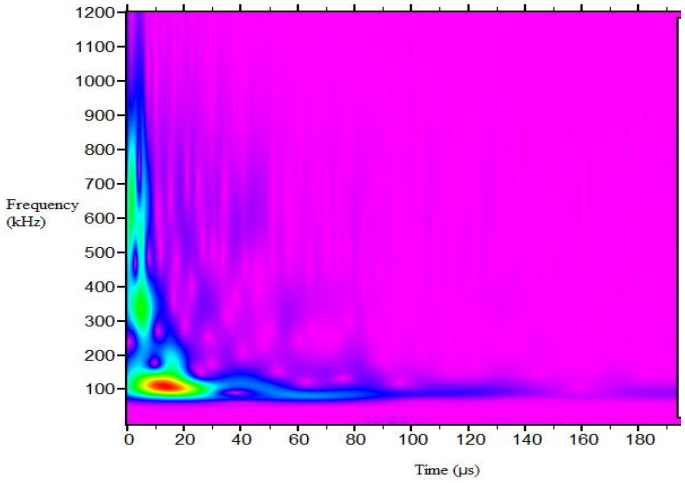

(b)

Figure A-3(3): WT result with a wavelet size of 50 (b) and with a size of 800 (b)

A-4. MODIFIED COMPLIANCE CALIBRATION METHOD

Here we are suppose to generate a least square plot of de-lamination length 'a' which is normalised by the specimen thickness 'h' i.e. a/h as function of cube root of compliance $C^{1/3}$ were $C = \delta/P$, using the visually observed de-lamination onset values and all the propagation values. The slope of this line is denoted as A_1. Latter we calculate mode-I the inter-laminar fracture toughness using the following equation;

$$G_I = \frac{3P^2C^{2/3}}{2A_1bh}$$

First we try to get the least square plot with the best fit as shown below, this was for specimen number 1.1 and 2.1 respectively;

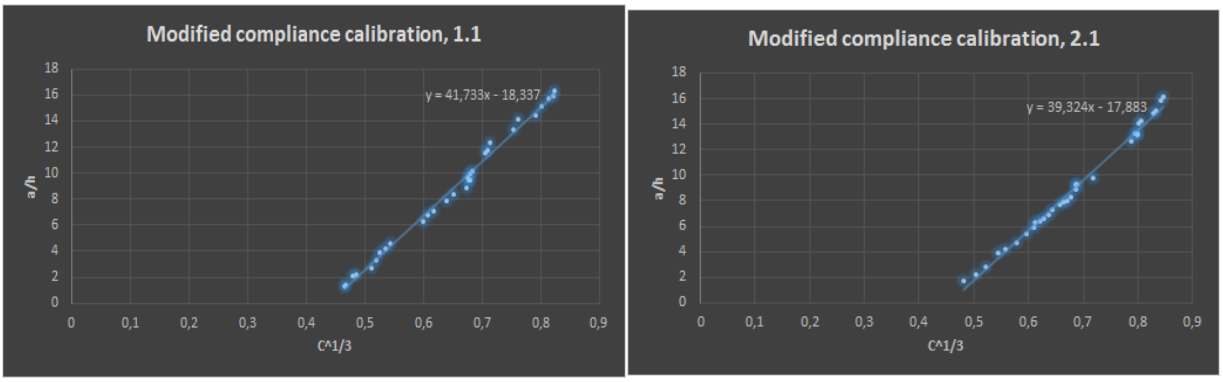

Fig A-4(1): Modified compliance calibration.

Specimens	Slope A_1
1.1	41.733
1.2	41.623
1.3	42.013
2.1	39.324
2.2	36.866
2.3	38.622

Table A-4(1): Values of the slope A_1.

Following this we calculated the inter-laminar fracture toughness and plotted it against crack length a (R-curve), to make a comparison with the curve obtained using modified beam theory.

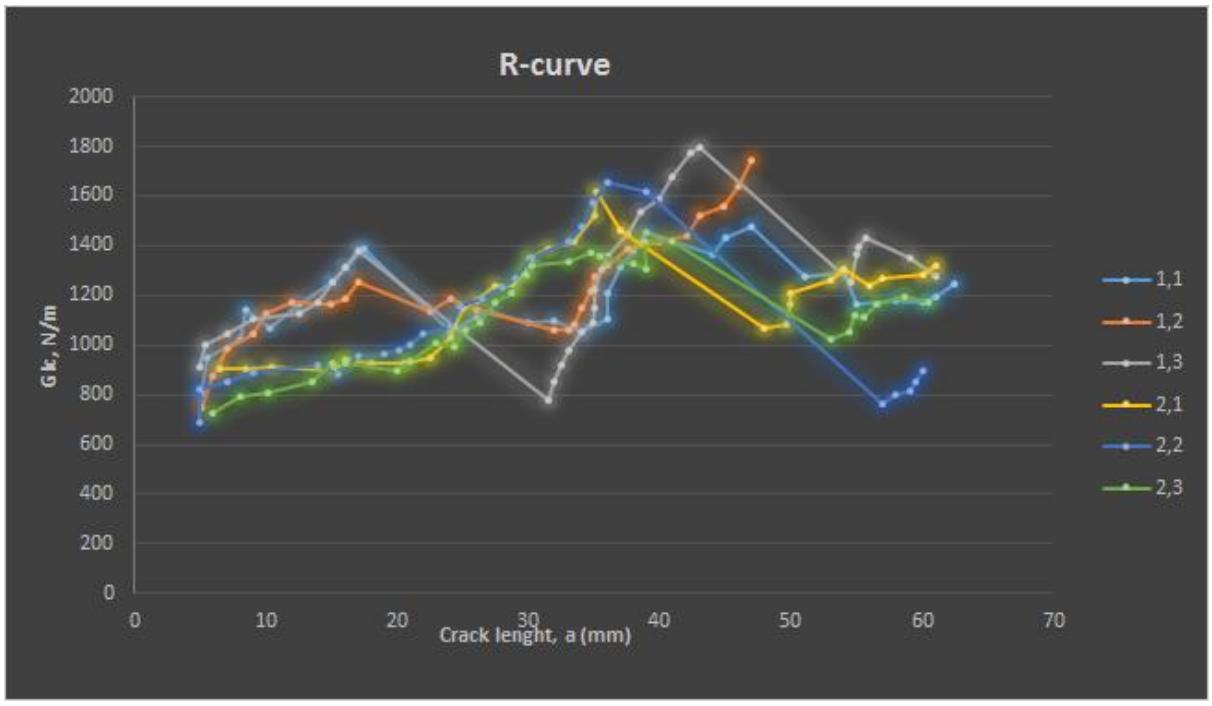

Fig A-4(2): Resistance curve obtained by modified compliance calibration method.

Specimens G_{Ic}(N/m)	2.1 (901.729)	2.2 (688.637)	2.3 (727.082)
1.1(804.476)	12.08%	-14.39%	-9.62%
1.2(751.769)	19.94%	-8.39%	-3.28%
1.3(913.723)	-1.31%	-24.63	-20.42%

Table A-4(2): Comparison of G_{Ic} increase in specimens 2.n with respect to specimens 1.n.

Clearly this is in stark contrast to what we obtained using modified beam theory. Here it seems the increase in inter-laminar fracture toughness is in the case of specimens without nanotubes. But since the standard (ASTM 5528) clearly recommend modified beam theory we could omit these results. But for the purpose of validation further experiments are recommended.

Next we even tried to obtain the mode-I inter-laminar fracture toughness using compliance calibration method for the sake of prudence.

A-5. COMPLIANCE CALIBRATION METHOD

Here again as per ASTM 5528 we are supposed to generate a least square plot of $\log(\frac{\delta_i}{P_i})$ versus $\log a_i$ using visually observed de-lamination onset values and all the propagation values. We try to fit in the best least-square fit. Calculate the exponent n which is the slope of the line so obtained i.e. $n = \frac{\Delta_y}{\Delta_x}$. And then the mode-I inter-laminar fracture toughness is obtained using the following formula;

$$G_I = \frac{nP\delta}{2ba}$$

Therefore we obtain a graph for obtaining the 'n' value and two such graphs for specimen 1.1 and 2.1 are shown below;

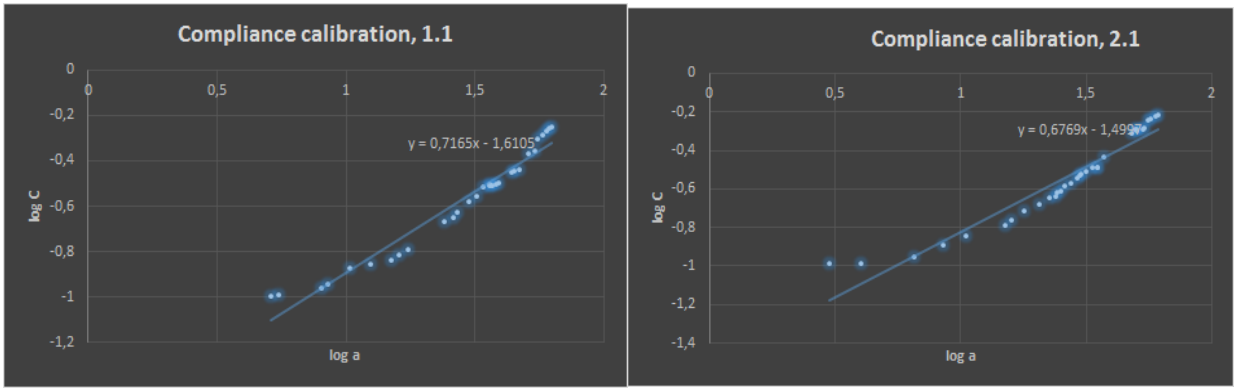

Fig A-5(1): Compliance calibration

Specimens	n
1.1	0.7165
1.2	0.6339
1.3	0.638
2.1	0.6769
2.2	0.7405
2.3	0.798

Table A-5(1): n values (slope)

Following this we calculated the inter-laminar fracture toughness and plotted it against crack length a (R-curve), to make a comparison with the curve obtained using modified beam theory and modified compliance calibration method.

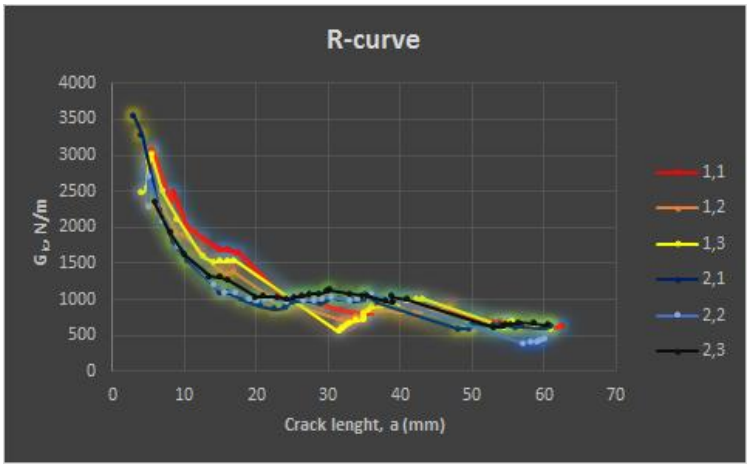

Fig A-5(1): Compliance calibration

Specimens G_{Ic}(N/m)	2.1 (3537.11)	2.2 (2709.91)	2.3 (2343.65)
1.1(3076.25)	14.98%	-11.90%	-23.81%
1.2(2317.14)	52.64%	16.95%	1.14%
1.3(2547.92)	38.82%	6.35%	-8.01%

Table A-5(2): Comparison of G_{Ic} increase in specimens 2.n with respect to specimens 1.n.

From the above comparisons it seems that these values are exaggerated in comparison with respect to modified beam theory. For instances in the case of specimen 2.1 with respect to 1.2 we have only 18.73% increase in inter-laminar fracture toughness calculated using modified beam theory. While in another case the decrease was only 2.15% for specimen 2.3 with respect to 1.1 obtained using modified beam theory, but in this method it is 23.81%. Therefore, as per the standard and as per our findings its modified beam theory that gives an appropriate value.